International Scientific-Technical and Production Journal

The Paton WELDING JOURNAL

October
2005
10

English translation of the monthly «Avtomaticheskaya Svarka» (Automatic Welding) journal published in Russian since 1948

Founders: *E.O. Paton Electric Welding Institute of the NAS of Ukraine*
International Association «Welding»

Publisher: *International Association «Welding»*

Address:
E.O. Paton Electric Welding Institute,
International Association «Welding»,
11, Bozhenko str., 03680, Kyiv, Ukraine
Tel.: (38044) 287 67 57
Fax: (38044) 528 04 86
E-mail: journal@paton.kiev.ua
http://www.nas.gov.ua/pwj

State Registration Certificate
KV 4790 of 09.01.2001

Subscriptions:
$324, 12 issues per year,
postage and packaging included.
Back issues available.

CONTENTS

SCIENTIFIC AND TECHNICAL

INDUSTRIAL

BRIEF INFORMATION

NATURE AND FEATURES OF MICRODEFORMATION IN THE ZONE OF CRACK INITIATION AND PROPAGATION IN HIGH-STRENGTH ALUMINUIM ALLOY D16AT

T.M. LABUR, A.Ya. ISHCHENKO, T.G. TARANOVA, V.A. KOSTIN and **G.M. GRIGORENKO**
E.O. Paton Electric Welding Institute, NASU, Kiev, Ukraine

Features of microdeformation of individual structural components within the zone of crack initiation and propagation in a high-strength aluminum alloy have been studied. Characteristics of crack initiation and propagation have been determined. It is shown that a proportional relationship exists between the conditions of microdeformation of metal internal structure caused by initial stresses and the resistance to crack propagation.

Keywords: *welded structures, high-strength aluminium alloy, welded joint, properties, stresses, microdeformation, structure, fracture, crack initiation and propagation*

Assessment of the actual criticality of a defect is a serious problem in operation of welded structural elements of structures. It requires a comprehensive consideration of the complex pattern of variation of stresses, structure and properties of a material and its welded joints in a local zone of stress concentration. Discontinuities of typical structural elements (undercuts, cracks, scratches, etc.), which are stress raisers, may become the site for crack initation in operation. Lowering of breaking stress under the influence of the stress raisers is possible for materials in the brittle or tough states. Crack propagation leads to an increase of the local stress in a microvolume [1–3]. The processes of crack initiation and propagation are determined by the behaviour of the material structural components. In materials with a sufficient margin of toughness at tension, fracture resistance may not change under the impact of stress raisers, this allowing them to withstand even a higher force load, than metal of the same section without a notch [4–13].

In order to understand the features of the processes of microdeformation of the structural components in the zone of crack initiation and propagation, it is necessary to determine the nature of variation of microstructural parameters and fracture properties, depending on the stress concentration level. Investigations were conducted on high-strength aluminium alloy D16AT (Al–Cu) widely applied in flying vehicle structures [7]. Kahn specimens [5] were used with different notch radii of 0.1, 0.2 and 0.9 mm. Conditions of specimens testing envisaged the loading mode from monotonic to intermittent. During the intermittent process, loading was interrupted every 200 kg and the specimens were soaked in such a mode for 2 min, thus simulating the actual conditions of stress gradient increase, which may be in place at unstable wind gusts, as well as turbulence or flutter. The selected procedure allows obtaining experimental data, representing the metal resistance to crack propagation under the conditions of off-center tension at a simultaneous action of tension and bending [5]. Here it is possible to determine strength σ_{fr}, values of specific work of crack initiation (SWCI) and propagation (SWCP), describing the main stages of fracture.

Investigations were conducted on specimens of D16AT alloy, cut out along the rolling direction with different notch radii in the tip, this allowing variation of the theoretical stress factor in a broad range: 10, 6.3 and 2.1, respectively.

During specimen testing, the load–deformation diagram was recorded, which represented the moments of crack initiation and propagation up to complete fracture, important from the practical point of view. The diagram allows quantitative evaluation of the stress intensity during deformation at off-center tension, determination of the extent of the stage of a stable metal flow, as well as the work done by the metal at the individual stages of crack propagation. Importance of analysis of the curve in the individual sections of the load–deformation diagram is obvious. They contain in the integral form the information about the metal structure state, influencing the plastic flow processes at specimen deformation, stress increase and crack formation. In this connection, the authors have improved the procedure of microdeformation determination. Fixed regions (including those with the crack) were marked out in the path of the crack propagation in individual sections of the specimen for scanning microscopy investigations. Deformation rate at testing was constant and equal to 2 mm/min ($3.30\cdot10^{-5}$ m/s). Other testing conditions met the technical requirements of GOST 25.506. Experimental results were obtained in testing five specimens using an all-purpose RU-5 machine and initial data calculation.

Level of breaking stress of the specimens was determined from the following formula:

$$\sigma_{fr} = 4P_{max}/(h - a)B,$$

SWCP — by the following formula:

$$SWCP = A_{pr}/(h - a)B,$$

where P_{max} is the maximum load; A_{pr} is the area under the curve, describing the crack propagation process; h, B is the specimen height and thickness, respectively; a is the notch depth.

Values of the crack initiation energy parameter J_c were assessed by calculation of the function of deformation energy variation, depending on crack length, using the empirical Merkle–Corten relationship [3]:

$$J_c = U\{[B(h - a_0)f(a_0 - h)]\},$$

where U is the area under the load–deformation curve; $f(a_0/h)$ is the function of the geometrical relationship of crack length a_0 and specimen size h:

$$f(a_0/h) = 2[(l + \alpha)/(l + \alpha^2)],$$

where $\alpha = \{[2a_0/(h - a_0)]^2 + 2[2a_0/(h - a_0)] + 2 - [2a_0/(h - a_0) + 1]\}^{1/2}$.

Critical stress intensity factor K_c was determined according to a linear dependence of this index on SWCP value describing the crack propagation process:

$$K_c = (4.35SWCP + 3.31)\cdot 10^{-4}.$$

Considering that in addition to phase inclusions, the matrix also participates in the crack propagation process, features of microdeformation of all the structural components were studied in each specimen. Measurements were taken in different structural zones of the specimens, namely under the notch, in the middle part and in the final fracture zone under both regular and irregular loading. For this purpose a macrosection was made on the specimen side surface. Then appropriate regions in the studied zones were registered by making imprints at 10 g load in the LECO hardness meter M-400. Base distances between the reference points were measured before and after specimen testing, and then the values of acting local deformations were calculated in relative units:

$$\Delta\varepsilon = (\varepsilon_{fr} - \varepsilon_{in})/\varepsilon_{fr},$$

where ε_{in} is the initial distance between the reference points; ε_{fr} is the distance after testing.

Structure of the marked regions was studied at different loading patterns in the initial state, after stopping at the level of 800 kg and complete fracture of the specimen. Structures in the longitudinal and transverse directions relative to the rolling direction were compared during investigations, and correlated with the analysis results, as well as fracture characteristics, obtained by fractographic analysis method. Such an integrated approach allowed not only consideration of the studied microdeformation processes along the specimen height and thickness, but also studying the metal behaviour in the crack tip.

Nature and features of microdeformation and concurrent structural changes running in the metal under the conditions of static loading, were studied using the JEOL SEM JSM-840 with a system of microanalyzers Analytic Link 860/500 and Ortek at accelerating voltage of 20 kV and electron beam current of $1\cdot10^{-10} - 1\cdot10^{-7}$ A in the secondary electron mode. Image contrast determined by the interaction of the scanning microscope electron beam with the structural components of the studied alloy, allows a qualitative evaluation of the nature of their change, depending on manifestation of plastic deformation of the specimen metal, proceeding during crack initiation and propagation. This interaction was used by the author to analyze the microdeformation mechanism, as well as cracking of different phase particles under the studied loading conditions. Calculation of experimental data and plotting of the obtained dependencies were performed using the modern computer technologies and appropriate software.

Table 1. Fracture toughness characteristics of D16AT alloy depending on the specimen notch radius and testing conditions at off-center tension

R, mm	Loading mode	σ_{fr}, MPa	K_c, MPa$\sqrt{m}$	J_c, J/cm^2	SWCP, J/cm^2
0.1	Monotonic	533	87.3	8.9	19.3
	Intermittent	513	12.5	28.1	2.1
0.2	Monotonic	588	86.4	26.7	19.1
	Intermittent	477	17.2	21.4	3.2
0.9	Monotonic	605	82.9	60.2	18.3
	Intermittent	432	35.9	14.3	7.5

As shown by the investigation results (Table 1), intermittent loading mode leads to a change of all the brittle fracture resistance indices of D16AT alloy. σ_{fr} level drops by 4 % in all the specimens with notch radius R = 0.1 mm and by 40 % for those with R = 0.9 mm. Values of the critical stress intensity factor K_c change from 2 to 7 times. However, a reverse dependence was recorded in this case. The greatest lowering is characteristic of specimens with a high level of acting stress. A similar dependence is noted also at the change of the crack initiation energy parameter J_c. Values of SWCP are even more abruptly reduced (from 2.5 to 9 times).

Based on analysis of the deformation processes and ten times measurement of microhardness, the dependence of the latter on stress acting in the specimen in the initial condition, at loading interruption (H = 800 kg) and after fracture was plotted (Figure 1). The established dependence is of a linear nature, determined by the level of stress developing as the main crack is propagating. Scatter of the alloy microhardness values (hatched region) in the initial condition is up to 30 % of the maximum level, measurement accuracy being approximately 5 %. As shown by the obtained results, increase of the load at off-centre tensile loading leads to a 2 times narrowing of the measured parameter range. The established dependence is attributable to the fact that at a low stress level there is sufficient time for the effect of deformation strengthening of the grains to be completely mani-

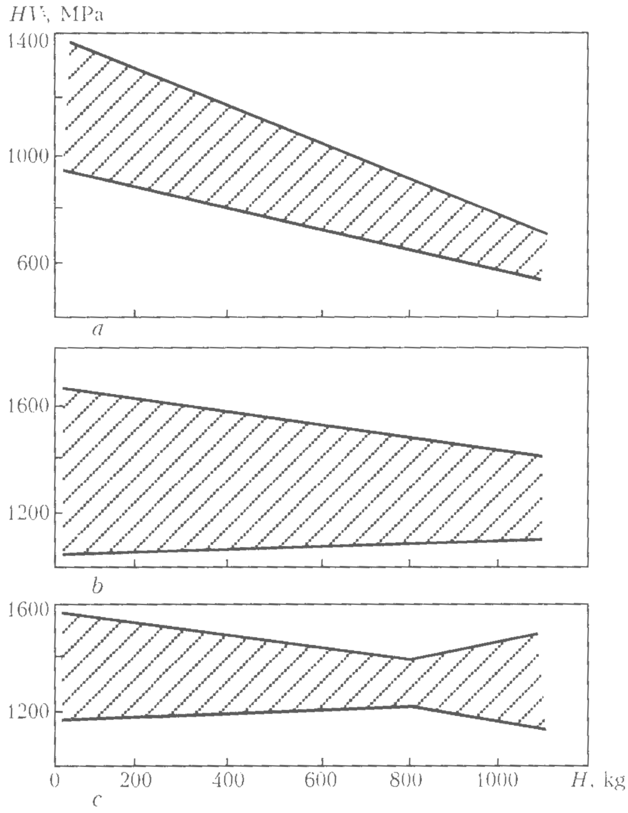

Figure 1. Microhardness variation in specimens with different notch radii at intermittent loading mode: *a* — $R = 0.1$; *b* — 0.2; *c* — 0.9 mm

fested. Location of the inclusions relative to the loading direction has an essential influence on microhardness level. Nature of microhardness variation illustrates its interrelation with the level of the stressed state in the alloy. In specimens with a sharp notch (0.1 mm) microhardness is by 15 to 20 % lower than in specimens with the notch radius of 0.2 and 0.9 mm, this leading to the conclusion about a certain interrelation of the processes of microinhomogeneous deformation and crack formation.

Methods of scanning electron microscopy were used to establish that a great number of microtears develop during the main crack formation and propagation in the adjacent regions of the studied alloy structure. Slip bands were found on the grain surface, related to initiation and subsequent coalescence of short microcracks. Their growing along the grain boundaries leads to formation of a macrocrack. At 10 mm distance from the notch fine grains were found in the alloy, having blurred boundaries and slip bands, oriented in different directions. Their study showed that a significant shear component directed along the fracture plane is acting during specimen deformation. This is exactly what influences the level of the nominal breaking stress (see Table 1). A considerable number of microtears, cracking of coarse particles located on the grain boundaries are also observed in the vicinity of the main crack mouth in the structure of samples tested with loading interruption.

Table 2. Geometrical parameters of the plastic deformation zone

Loading mode	r_y, mm	a_1, mm	a_2, mm	φ, deg
	$R = 0.1$ mm			
Monotonic	3.05	1.66	0.91	29
Intermittent	3.42	1.32	0.99	31
	$R = 0.9$ mm			
Monotonic	1.86	1.08	0.57	33
Intermittent	2.26	0.66	0.37	7

Irrespective of the notch radius and, therefore, stress concentration, traces of plastic deformation process are found in the studied specimen, this process being localized in the notch tip with formation of a specific region of the structure, namely plastic deformation zone. Its relief is indicative of the nature of resistance of the metal and its structural components to crack initiation during specimen fracture at the action of different factors on it. Therefore, geometrical dimensions of the specimen plastic zone depending on loading conditions were measured (Figure 2) when studying the features of the fracture surface.

As shown by analysis, these zones contain three characteristic regions of the relief for all the kinds of testing (see Figure 2). Extent of the plastic zone in a specimen of 0.1 mm radius (Table 2) is much greater than in a specimen with 0.9 mm radius. Plastic zone boundaries are indistinct, relief structure is non-uniform, this being indicative of the mixed mode of fracture.

Comparison of the outlined zone areas showed the dependence of zone dimensions on the stressed state level, determined by the notch radius. Zone area is increased with stress decrease. This is, probably, related to increased resistance of the metal to crack propagation at low stresses, higher rate of its propagation and reduction of critical length [7]. Structural changes in the plastic deformation zone may be used for comparative evaluation of the energy content of the crack initiation process, as the zone size is related to crack resistance by the following relationship [4]:

$$r_y = A(K_c / \sigma_{0.2})^2,$$

where r_y is the length of the plastic deformation zone; A is the energy content; K_c is the stress intensity factor; $\sigma_{0.2}$ is the studied material yield point.

Based on the study of structural changes in the plastic deformation zone, it was established (Table 2) that at intermittent nature of loading an abrupt increase of the energy content level (by 5 to 7 times) occurs in the studied alloy compared to monotonic loading. Stress accumulated at each interruption or relieving of the load in specimens with notch radius of 0.9 mm, leads to crack initiation during plastic deformation not only as a result of inclusions cracking, but also on grain boundaries (Figure 3). Grouping together, the cracks grow to critical dimensions, which may significantly lower the strength as a result of decreasing the strength of cohesion between the matrix and inclusion. No such cracking mode was registered in a specimen with 0.1 mm notch radius, where the

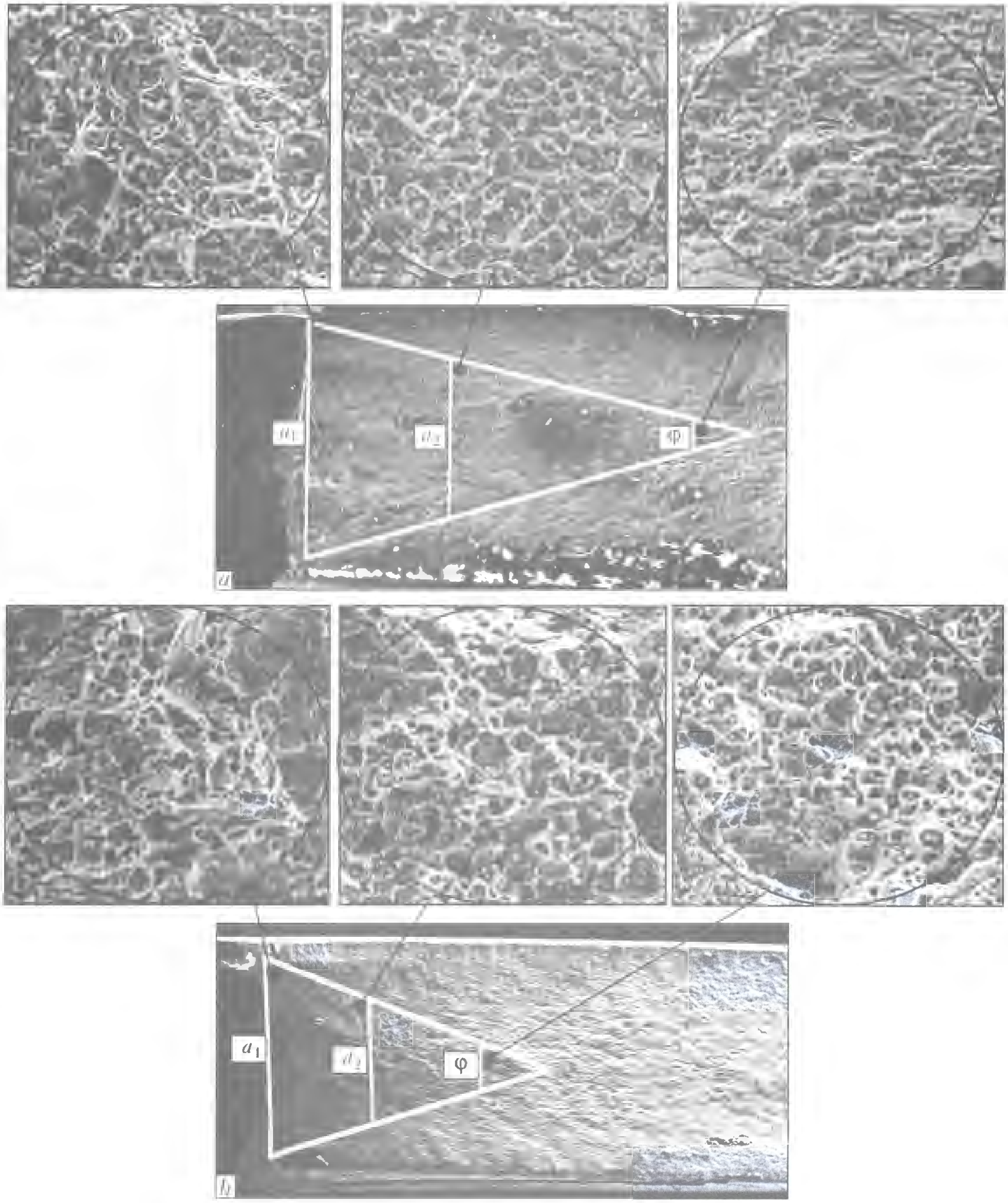

Figure 2. Plastic prefracture zone of specimens with 0.1 (*a*, *b*) and 0.9 (*c*, *d*) mm radius fractured under monotonic (*a*, *c*) and intermittent (*b*, *d*) loading mode

process of deformation localization is more pronounced.

Fractographic studies of the surface of specimen fracture during the main crack propagation showed that the fracture also contains three characteristic structural regions, similar to the case of the zone of plastic deformation under the notch. Main crack initiation and formation proceed in the first region, its stable growth is observed in the second region, and its accelerated growth up to fracture — in the third region. The first region (near the crack tip) demonstrated the presence of fine facets, which may be due to occurrence of a non-uniform plastic deformation in the specimen (Figure 4). A condition for their formation is exceeding the level of the cohesion forces in the direction normal to the matrix–inclusion phase boundary [11–13], which requires a considerable concentration of stresses in a microregion. Crack initiates in the regions where three-axial stress is the highest. If deformation is the dominant factor, fracture runs (irrespective of the existing region of triaxial stress) at such a distance from the notch, at which a critical deformation level is achieved. This is indicated by increase of the number of acting slip systems and change of their direction, as well as parallel and crossing ridges, coinciding with the direction of the main crack propagation in the fracture structure.

Region of the main crack retardation contains pits of a more round shape, which are uniformly located on the fracture surface. Brittle cracking of inclusions is observed, while the matrix is only plastically deformed, forming tearing pits of an elongated shape in

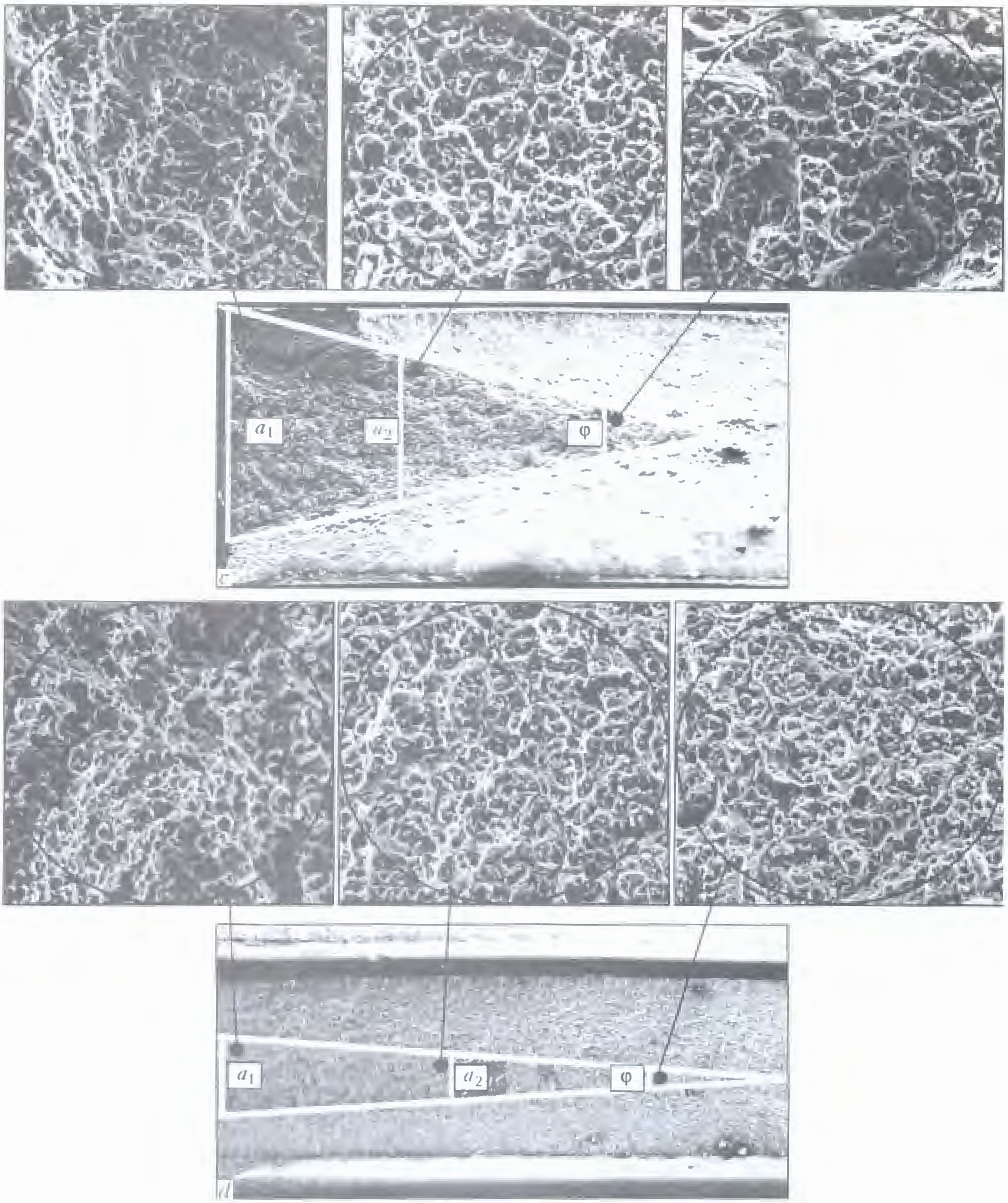

Figure 2

a narrow zone ahead of the crack front. They are equal to 10–12 μm at the plastic zone base and to 1–2 μm at the tip (see Figure 2, *a, b*). A net of small pits is found around the disperse precipitates strengthening the aluminium alloy, some fibrous thin slip lines being visible in the pit vicinity, while the majority of the inclusions is broken up. This may be indicative of the fact that pit growth proceeds as a result of slipping along many crystallographic planes. Submicrocracks form on the interfaces of the matrix and strengthening particles.

Regions of a slightly pronounced relief formed at tearing are found on the fracture surface in the zone of a stable crack growth. Ridge orientation coincides with the direction of crack propagation (Figure 4, *a, b*). Presence of such regions may be regarded as the result of the action of brittle fracture mechanism along the subgrain boundaries in the case of exceeding the level of a certain critical deformation under the conditions of a multi-axial stressed state [11, 13].

In the center of the main crack in the studied specimen, the pits become more round and are uniformly located on the fracture surface. Their size is 3 to 5 μm. In the fracture section, where the crack mouth is located, the phase inclusions are broken, and deformation bands are found on the grain boundary.

Relief of a specimen with notch radius of 0.9 mm contains non-uniformly arranged facets of different dimensions and shape (Figure 4, *b, d*) with inclusion fragments located on their bottom. Some of them have preserved the bond with the grain bulk. The fracture central part shows multi-layer tear ridges, formed at

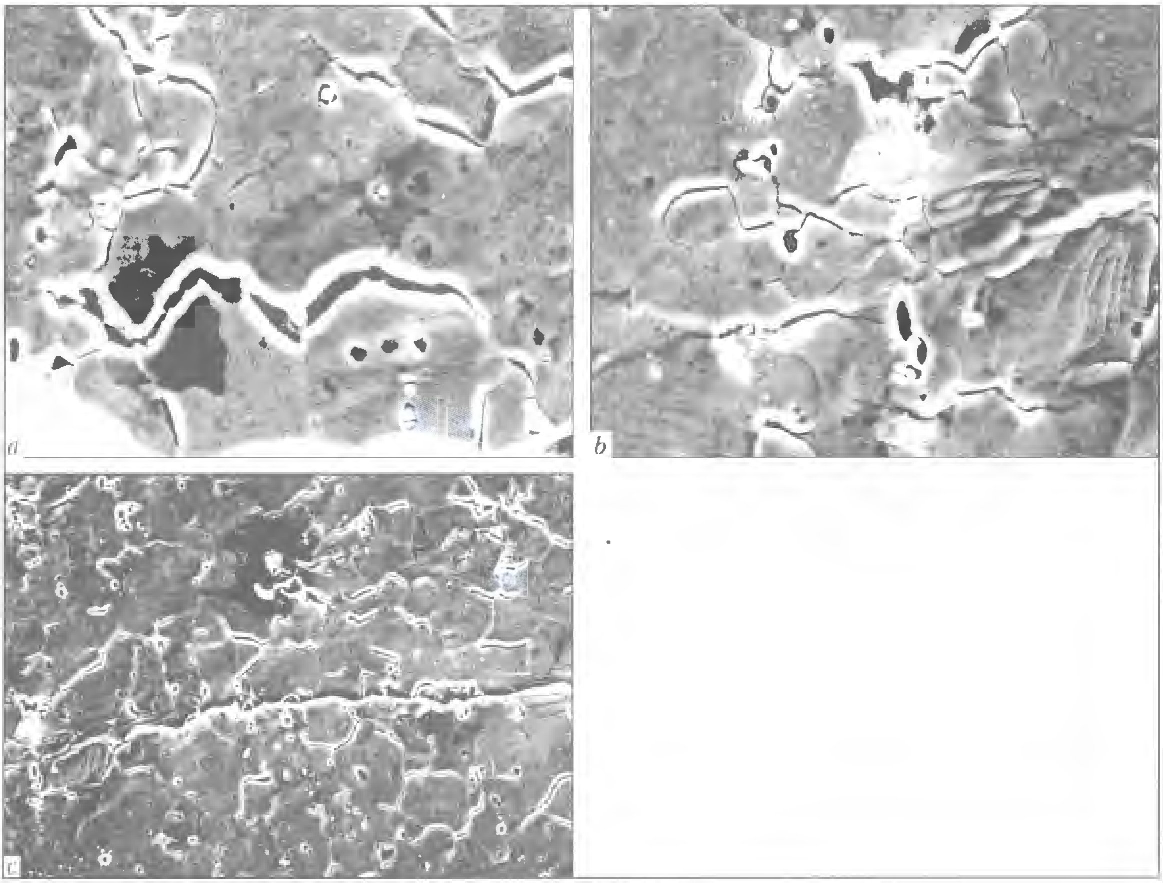

Figure 3. Microstructure of specimens with notch radius of 0.9 mm after testing by the intermittent loading mode with loading interruption in different sections of the zone of the main crack propagation (×1000) at the notch (*a*), in the central part (*b*) and in the crack mouth (*c*)

a sufficiently high ductility of the material and low level of yield stress, manifested during the slipping process. The relief in the vicinity of the main crack mouth has fine pits (1–4 μm) with broken inclusion particles.

Comparison of the fracture mode of specimens with the notch radius of 0.1 and 0.9 mm tested with load interruption showed that the dimensions of their plastic zones are close (see Table 2). In the first case, however, a mixed fracture type prevails in the fracture relief with formation of non-equiaxed pits of 2–5 μm size, the orientation of which coincides with the direction of the main crack propagation. Deformation shear terraces formed at slipping along the crystallographic planes are registered on their surface.

Different orientation of the tear ridges relative to the direction of the load application is an indication of the local stress action at microcrack initiation and discreteness of their propagation process. Particles of phases located along the grain boundaries, even though they broke up, preserved their bond with the matrix (Figure 4). Such a fracture type may be in place at critical levels of the stress intensity factor K_c, when the mechanism of crack initiation is close to the conditions of a high rate of the main crack propagation. The plastic deformation zone in a specimen with notch radius of 0.9 mm is narrow (0.66 mm) and has the length of 2.26 mm (see Table 2). Fracture surface relief simultaneously contains pits of mostly medium size (6–8 μm) and regions with deformation shear terraces. Cells have broken inclusions, limited by tear ridges. They are not well-developed, while phase precipitates are mainly broken up (see Figure 4, *b, d*). Such a fracture type is due to running of intensive plastic deformation during the main crack propagation, when the stress exceeds the level of cohesion forces of the matrix and inclusions [8, 11, 13]. Fracture surface relief near the main crack mouth incorporates microtears, formed along the grain boundaries during the process of the crack retardation.

CONCLUSIONS

1. Extent of the initial microcrack in D16AT aluminium alloy under the conditions of off-centre tension of notched specimens, simulating different loading modes in service, depends on the dimensions of brittle phase inclusions and stressed state in the concentrator tip, as well as the loading mode.

2. Plastic deformation of the metal developing at intermittent loading, increases the energy content level and cracking on grain boundaries.

3. The influence is established of the conditions of microdeformation of D16AT alloy structural components on σ_{fr}, K_c, J_c and SWCP values. It is shown that there is a proportional dependence between the conditions of metal microdeformation due to initial stress and resistance to cracking initiation and development.

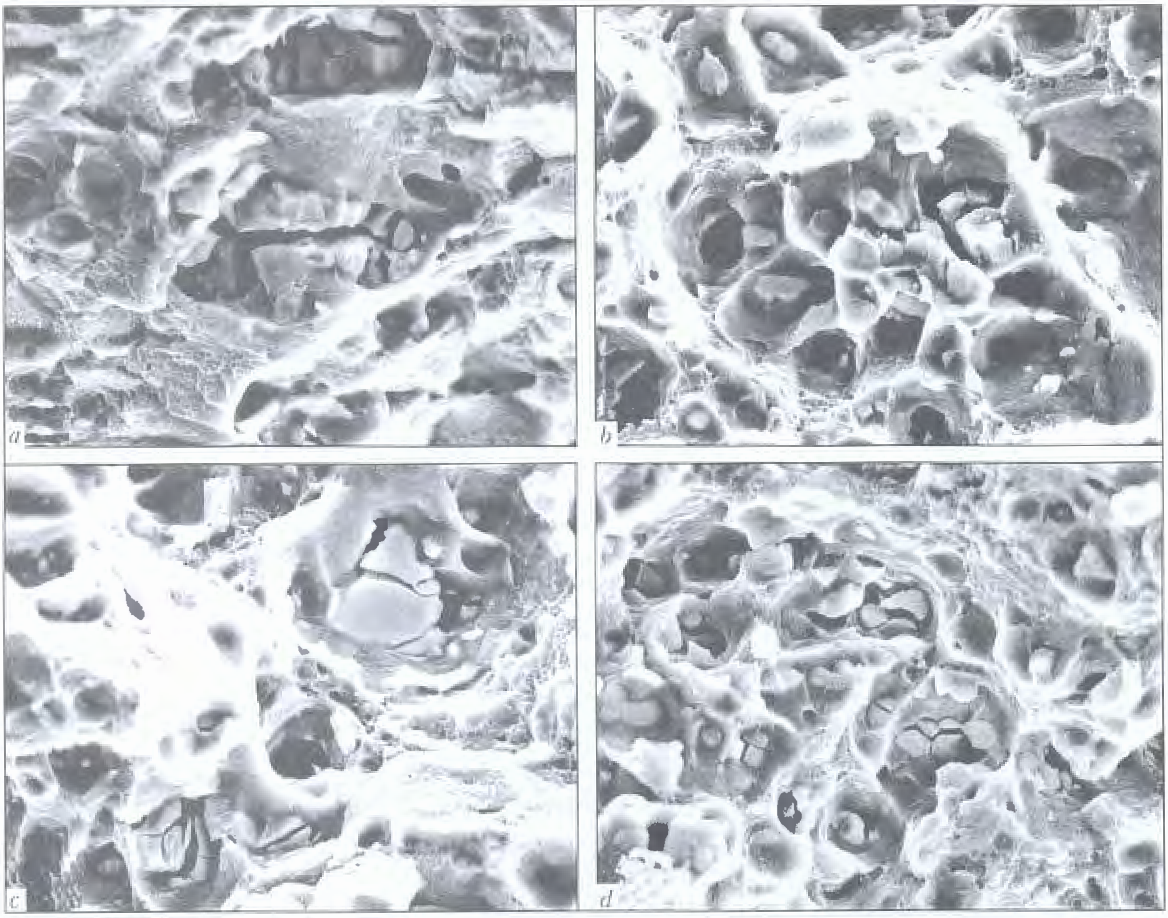

Figure 4. Fractogram of fracture surface of specimens with the radius of 0.1 (*a*, *b*) and 0.9 (*c*, *d*) mm failing in the monotonic (*a*, *c*) and intermittent (*b*, *d*) loading mode (×2000)

4. A linear dependence was derived between the microhardness of D16AT alloy and stress level at which the crack initiates. With increase of the load level the range of the measured parameters becomes 2 times narrower, which may be related to a low level of the acting stress, not limiting the deformation strengthening of the grains.

5. Lowering of microhardness level by 15 to 20 % in specimens with a sharp notch (0.1 mm), irrespective of the loading conditions, compared to specimens with the notch radius of 0.2 and 0.9 mm is indicative of metal softening, this leading to the conclusion about an interrelation between the value of microdeformation and metal resistance to microcracking at fracture.

1. Fujiwara, T. (2001) Technology of joining of light metals in aircraft and space engineering. *Keikinzoku Yosetsu*, 39(**3**), 1–11.
2. Broek, D. (1980) *Principles of fracture mechanics*. Moscow: Vysshaya Shkola.
3. Vladimirov, V.I. (1984) *Physical nature of fracture of metals*. Moscow: Metallurgiya.
4. Botvina, L.R. (1989) *Kinetics of fracture of structural materials*. Moscow: Nauka.
5. Davidenkov, N.N. (1981) *Mechanical properties of materials and methods of deformation measurement*. Vol. 2. Kiev: Naukova Dumka.
6. Ivanova, V.S., Botvina, L.R., Kudryashov, V.G. (1971) Strength and plasticity. Fracture under short-term loads. Ductile and brittle fracture. In: *Results of science and technology*. Series Materials Science and Heat Treatment. Moscow.
7. Kis, J.A., Smith, H.L., Romayi, Kh.E. et al. (1968) Fracture tests of welds. In: *Applied problems of fracture toughness*. Moscow: Mir.
8. Kishkina, S.I. (1981) *Fracture resistance of aluminium alloys*. Moscow: Metallurgiya.
9. Klevtsov, G.V. (1993) Kinetics of formation of plastic deformation zones at the crack tip in fracture of structural materials in plane-stressed state and plane deformation conditions. *Problemy Prochnosti*, **4**, 57–63.
10. Neshpor, G.S., Miklyaev, P.G., Andreev, D.A. (1980) On the possibility of unification of the procedure for determination of fracture toughness in plane-stressed state. *Zavod. Laboratoriya*, 46(**3**), 261–265.
11. Ivanova, V.S., Kudryashov, V.G., Kopelovich, B.A. et al. (1974) Fractography and fracture toughness of aluminium and titanium alloys. *Tekhnologiya Lyog. Splavov*, **3**, 65–70.
12. (1989) *Strength analysis and testing in machine-building, classification kinds of the metal fracture (rupture) surface*. Moscow: Standart.
13. Romaniv, O.N. (1981) Structural fracture mechanics as a new prospective trend in the problem of fracture of metals. *Fiziko-Khim. Mekh. Materialov*, **4**, 28–32.

INFLUENCE OF FREQUENCY PROPERTIES OF THE WELDING CIRCUIT ON CURRENT PARAMETERS IN PULSED-ARC WELDING PROCESSES

G.A. TSYBULKIN
E.O. Paton Electric Welding Institute, NASU, Kiev, Ukraine

Results of analysis and modeling of frequency characteristics of welding circuit in pulsed-arc welding processes are given. Three different approaches to implementation of these processes are considered, namely through modulation of output voltage of the welding current source, exciting torch vibrations, and pulsed feed of electrode wire. It is shown that the working range of welding current pulses strongly depends on the approach employed.

Keywords: *arc welding, pulsed-arc processes, consumable electrode, amplitude-frequency characteristics*

Considerable achievements in the field of power semiconductor engineering, computer technologies and welding process robotisation, lead to a significantly greater interest in consumable-electrode pulsed-arc welding, which, as is known [1], was proposed for the first time at the E.O. Paton Electric Welding Institute in 1964. As indicated by publications [2–14], intensive research and development of this welding process are conducted chiefly in the three main directions: development of pulsed sources, providing broad capabilities of program control of the amplitude, duration and frequency of welding current pulses [2, 3]; development of the methods and special mechanisms to perform a pulsed feed of electrode wire and so-called vibration of the welding torch [4–10]; investigation and development of adaptive methods and algorithms of automatic control of pulsed-arc welding processes [11–16].

One of the complex engineering problems arising, in particular, in development of welding equipment, is related to the fact, that so far application of program-controlled pulsed feed of electrode wire or welding torch vibration does not allow a considerable increase of welding current pulse frequency, and, therefore, a noticeable increase of the effectiveness of automatic control of metal melting and transfer in pulsed-arc welding.

On the other hand, solving the problem of increasing the pulse frequency may run into difficulties, unrelated to the above engineering problems, but due to frequency limitations of the welding circuit proper as a dynamic system. As far as we know from publications, this issue is not yet well-studied.

The objective of this study is investigation of the influence of frequency properties of the welding contour on current parameters in pulsed-arc processes of consumable-electrode automatic arc welding in all the studied approaches to its implementation.

Mathematical model. In keeping with [10, 17, 18] let us write a system of equations based on a simplified diagram of the welding circuit shown in Figure 1, *a*:

$$\begin{cases} L\dfrac{di}{dt} + Ri = u_s - u_a, \\ u_a = u_0 + El, \\ l = H - h \quad (0 < l < l_{th}), \\ h = \displaystyle\int_0^t (v_e - v_m)dt, \ v_m = Mi, \end{cases} \qquad (1)$$

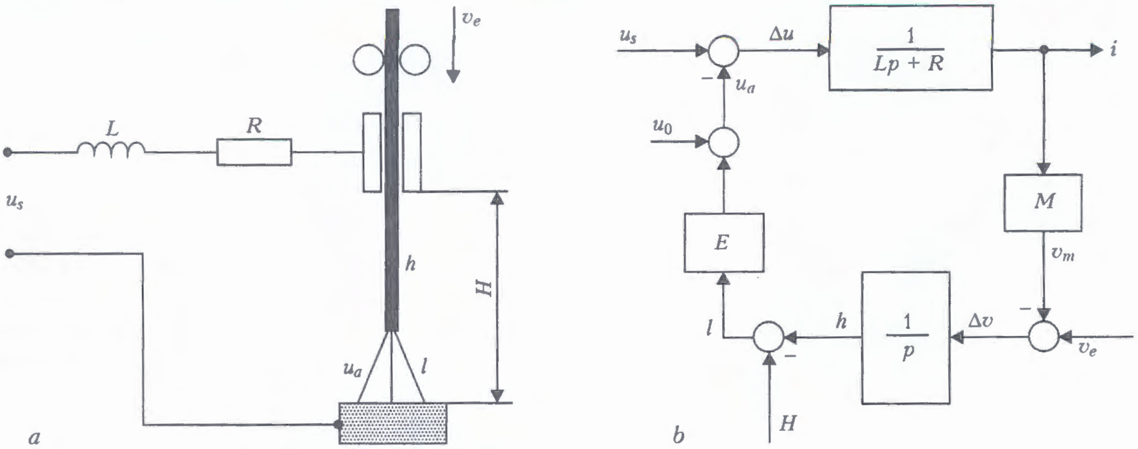

Figure 1. Equivalent (*a*) and block (*b*) diagrams of welding circuit (for explanation see the text)

where L, R are the inductance and equivalent resistance of the welding circuit, respectively; $u_s = u_s(t, i)$ is the voltage on the output terminals of the welding current source, dependent on welding current i and time t; $u_a = u_a(i, l)$ is the arc voltage, which is the function of i and arc gap length l; $u_0 = u_0(i)$ is the total voltage drop in the near-electrode regions of the arc gap; E is the electric field intensity in the arc column; $H = H(t)$ is the distance between the edge of the current-conducting nozzle and free surface of the weld pool; $h = h(t)$ is the electrode extension; l_{th} is the threshold value of arc length, at which it is extinguished; $v_e = v_e(t)$ is the rate of consumable electrode feed relative to the current-conducting nozzle; $v_m = v_m(t)$ is the electrode melting rate; $M \equiv \partial v_m / \partial i$ is the slope of the electrode melting characteristic at rated values of welding current i_{rat} and electrode extension h_{rat}.

System of equations (1) did not include the parameters, characterizing, in particular, electrode metal transfer through the arc gap and motion of the weld pool free surface in the direction of the axial line of electrode extension. Influence of these and other small parameters on the dynamics of the arc welding process may be ignored.

For visual representation and convenience of further consideration, let us use the traditional graphic interpretation of the system of equations (1) in the form of a block-diagram shown in Figure 1, *b*.

As is seen from this diagram, in terms of the theory of automatic control, the welding circuit is a closed system with a negative feedback. Electrode feed rate $v_e(t)$, distance between the current-conducting nozzle edge and free surface of weld pool $H(t)$ and voltage at output terminals of welding current source $u_s(t)$, both individually and in certain combinations can act as controlling or disturbing actions.

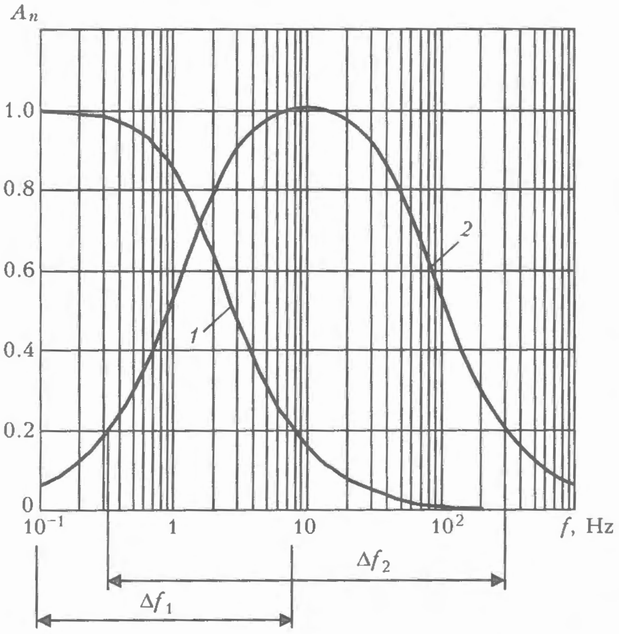

Figure 2. Standardized AFC: *1* — $A_{1n}(f)$; *2* — $A_{2n}(f)$ and $A_{3n}(f)$

As we are eventually interested in the frequency properties of the considered system, let us immediately move over to the graphoanalytical characteristics, and based on the block-diagram (see Figure 1, *b*) let us write the expressions for transfer functions from its inputs v_e, u_s and H to output i (here p denotes Laplace operator):

$$W_1(p) = \frac{i(p)}{v_e(p)} = \frac{M^{-1}}{T_e T_s p^2 + T_s p + 1};$$
$$W_2(p) = \frac{i(p)}{v_s(p)} = \frac{EM^{-1}p}{T_e T_s p^2 + T_s p + 1}; \qquad (2)$$
$$W_3(p) = \frac{i(p)}{H(p)} = \frac{M^{-1}p}{T_e T_s p^2 + T_s p + 1},$$

where T_e and T_s are the time constants determined by the ratios

$$T_e = \frac{L}{R}, \quad T_s = \frac{R}{EM}.$$

Let us note that at $T_s \geq 4T_e$ the welding circuit relative to the setting action $v_e(t)$ is equivalent to the aperiodic link of the second order, and relative to actions $u_s(t)$ and $H(t)$ to the successively connected aperiodic and differentiating links. Let us consider their amplitude-frequency characteristics $A_k(f) = |W_k(j2\pi f)|$, where $k = 1, 2, 3$; $j = \sqrt{-1}$; and f is the frequency of the harmonic action.

Amplitude-frequency characteristics (AFC). ACF of the welding circuit can be plotted directly by the following formulas:

$$A_1(f) = \frac{M^{-1}}{\sqrt{(1 - 4\pi^2 T_e T_s f^2)^2 + (2\pi T_s f)^2}};$$
$$A_2(f) = \frac{2\pi (EM)^{-1} f}{\sqrt{(1 - 4\pi^2 T_e T_s f^2)^2 + (2\pi T_s f)^2}}; \qquad (3)$$
$$A_3(f) = \frac{2\pi M^{-1} f}{\sqrt{(1 - 4\pi^2 T_e T_s f^2)^2 + (2\pi T_s f)^2}},$$

which are derived by the known procedure after substitution into expressions (2) of the false variable $j2\pi f$ instead of p operator [19].

For convenience of comparison, Figure 2 gives the graphs of normed AFC $A_{1n}(f)$, $A_{2n}(f)$ and $A_{3n}(f)$ plotted by formulas (3), where $A_{1kn}(f) = A_k(f) / \max\limits_f A_k(f)$. Contour parameters included into these formulas, were assumed to have the following values: $E = 2.5$ V/mm; $M = 0.67$ mm/(A·s); $T_s = 0.1$ s; $T_e = 2.4 \cdot 10^{-3}$ s. Values of the above parameters are taken from studies [20, 21] for the case of argon-arc welding by consumable electrode wire Sv-08G2S of 1 mm diameter. As was anticipated, $A_{2n}(f)$ and $A_{3n}(f)$ curves completely coincide and essentially have the shape of a band filter AFC, while $A_{1n}(f)$ curve is the AFC of a low-frequency filter.

Let us single out in Figure 2 the so-called working ranges of frequencies Δf_1 and $\Delta f_2 = \Delta f_3$, within which

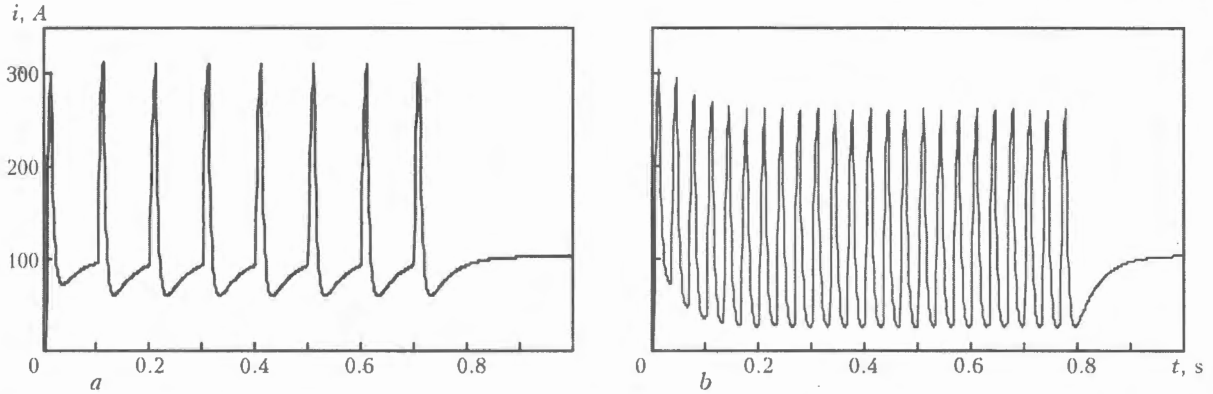

Figure 3. Welding current pulses formed using modulation of current source output voltage at $\tau = 0.01$ s: *a* — $f_{\text{pulse}} = 10$; *b* — 30 Hz

the values of functions $A_{kn}(f)$ do not go beyond the desirable amplitude tolerance, equal, for instance, to 0.2. This means that on the upper limit of the above ranges the amplitude of the harmonically changing welding current $i = i(t, f)$ becomes 5 times smaller than its maximum value, which it reaches at the same input action at the frequency $f_{\max k} = \arg\max_{f} A_k(f)$.

At further increase of frequency f the amplitude of welding current fluctuation rather quickly and asymptotically approaches zero (see Figure 2).

Comparison of working ranges shows that Δf_1 value is essentially lower than Δf_2, and is equal to just 8 Hz at these parameters. It becomes obvious that pulsed feed of electrode wire with a frequency exceeding 8 Hz in our case, is low effective, as outside of the working band Δf_1 the welding circuit acting as a low-frequency filter, will «suppress» the welding current pulses.

The situation is different, when the pulses are formed using a welding current source or by periodic variation of distance between the current-conducting nozzle and free surface of the weld pool. In this case the working frequency range is broad enough, and is equal to $\Delta f_2 = 300$ Hz at the same 0.2 level (see Figure 2).

Analysis of frequency characteristics shows that rather rigid restrictions due to the dynamic properties of the contour, are imposed on the pulse frequency only at pulsed feed of the electrode wire. In two other cases considered, these restrictions are minor.

Simulation results. In order to perform an experimental check-up of the degree of the influence of welding circuit frequency properties on the welding current pulse parameters, its dynamics was simulated in a computer. The experiment was conducted by finding a numerical solution of a system of equations (1) for three cases: u_s = var; H = const; v_e = const; H = var, u_s = const, v_e = const; v_e = var, H = const, u_s = const. In this case, the same parameters of the welding circuit were used, as at AFC calculation. Input actions were assigned in the form of the following algorithms:

$$u_s = 21(1 + z)\ [\text{V}];$$
$$H = 17 - 3z\ [\text{mm}];$$
$$v_e = 70(1 + z)\ [\text{mm/s}],$$

where

$$z = \begin{cases} 1, & nT \le t \le nT + \tau, \\ 0, & nT + \tau < t < (n + 1)T,\ n = 0, 1, 2, 3, \ldots\ ; \end{cases}$$

$T = 1/f_{\text{pulse}}$; f_{pulse} is the pulse repetition rate; τ is their duration.

Results of simulation at $f_{\text{pulse}} = 10$ and 30 Hz and $\tau = 0.01$ s are presented in Figures 3–5. Comparison of the obtained results showed that the pulses, formed with modulation of the output voltage of welding current source (Figure 3), have a quite large amplitude, which will change only slightly within the bandwidth with increase of f_{pulse}. This is true to a smaller degree for current pulses, caused by welding torch vibration (Figure 4). As regards the case when the welding current pulses are generated at pulsed feed of the consumable electrode, then, as is seen from Figure 5, their amplitude is small, and the pulses proper are of a considerably distorted shape.

It is clear that outside the Δf_1 bandwidth (see Figure 2) welding current pulses are suppressed by the welding circuit the stronger, the higher is their repetition rate. Then it would be quite natural to

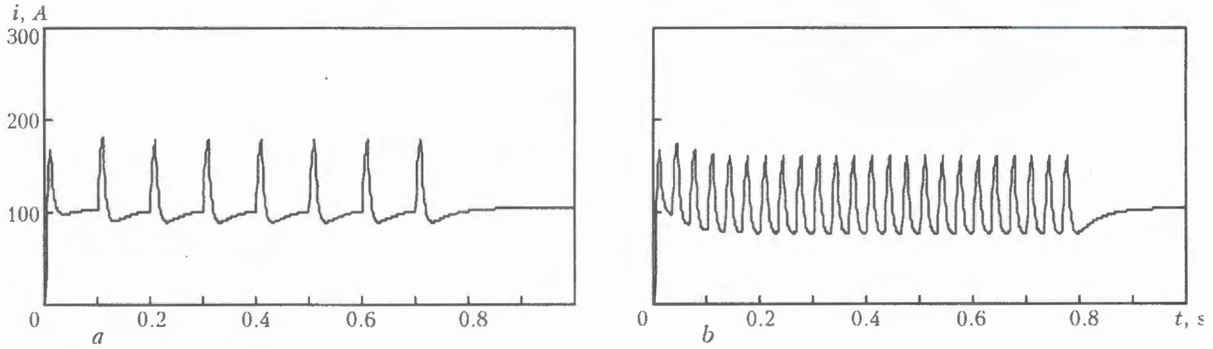

Figure 4. Welding current pulses caused by torch vibration (*a*, *b* are the same as in Figure 3)

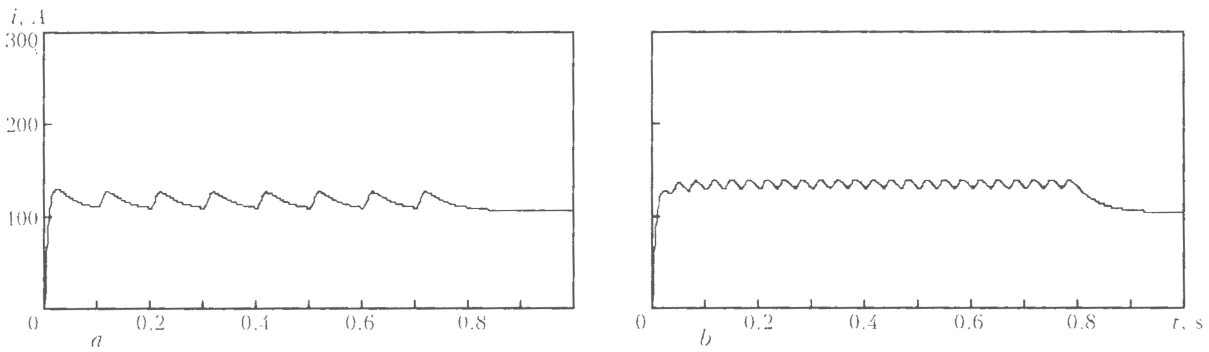

Figure 5. Welding current pulses generated at pulsed feed of consumable electrode (*a*, *b* are the same as in Figure 3)

anticipate a considerable increase of pulse amplitude in the case, if their frequency is selected from the inside of the working range Δf_1. It turned out to be not quite so. Figure 6, *a* presents the results of simulation of the considered process at $f_{\text{pulse}} = 2$ Hz. Comparison of Figure 6, *a* with Figure 5, *a* shows only a slight increase of pulse amplitude.

This fact can have a quite simple explanation, if we consider the relationship

$$\Delta l = -\Delta v \tau, \qquad (4)$$

written on the basis of the last two equations of system (1) after their differentiating at H = const and then transition to finite increments. From (4) it is seen that change of arc length to Δl is proportional not only to difference of rates $\Delta v = v_e - v_m$, which results from the pulsed electrode feed, but also to a product of this difference by pulse duration. At very small τ values, Δl value will, obviously, be also quite small. Therefore, welding current pulse amplitude will also be small. Increase of pulse duration at the same Δv value should lead to increase of pulse amplitude. This is exactly the effect observed as a result of simulation (Figure 6, *b*).

At rather large τ values, commensurate with the welding circuit time constant T_s, Δv difference can no longer be regarded as a constant value, as in the case of small τ values. Because of negative feedback on electrode melting rate (the known self-regulation effect), Δv value will decrease exponentially, and during time $\Delta t \approx 3T_s$ it will become practically zero. In keeping with (4), Δl value will also be zero, and the amplitude of welding current pulses, actually stops growing, starting from this moment of time (Figure 6, *c*).

This makes it clear that the pulse amplitude reaches its maximum importance at $\tau \approx 3T_s$ and pulse repetition rate equal to 2, i.e. $\tau = T/2 = 1/2f_{\text{pulse}}$. Therefore, the optimum frequency of electrode wire feed is

$$f_{\text{opt}} \approx 1/6T_s. \qquad (5)$$

Conducted research leads to the conclusion that frequency properties of the welding circuit as a dynamic system depend not only on its parameters, but also on the system input u_s, H, or v that the pulse

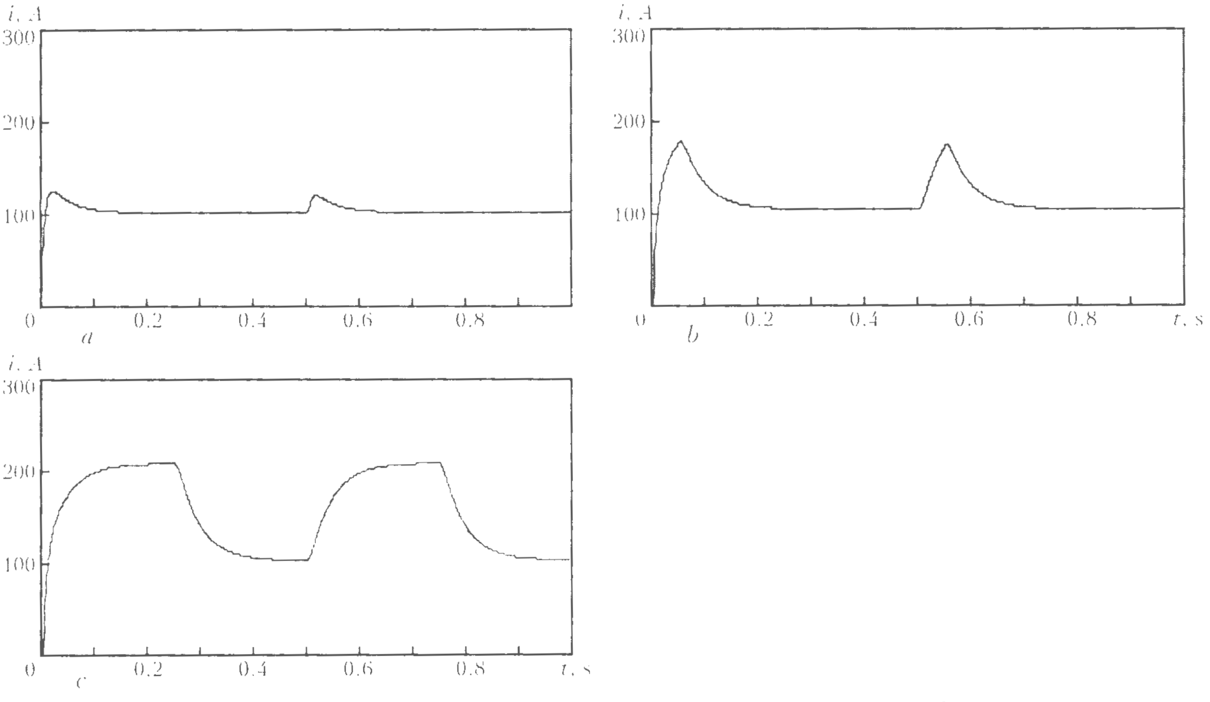

Figure 6. Dependence of amplitude *i* of welding current on duration τ of electrode wire feed pulses at $f_{\text{pulse}} = 2$ Hz: *a* – $\tau = 0.001$; *b* – 0.10; *c* – 0.25 s

actions come to. In this case, when the above action is set by modulation of output voltage of welding current source or periodic variation of distance H between the current-conducting nozzle edge and free surface of the weld pool, the range of working frequency values is quite wide (hundreds of hertz). Now in the case of welding current pulse formation due to pulsed feed of electrode wire, the range of working frequency values is rather limited (units of hertz).

1. Paton, B.E., Potapievsky, A.G., Podola, N.V. (1964) Consumable-electrode pulse-arc welding with programmable control of the process. *Avtomatich. Svarka*, **1**, 1–6.
2. Lebedev, V.K. (1995) Trends of development of arc welding power sources. *Ibid.*, **5**, 3–6.
3. Loos, A.V., Lukutin, A.V., Saraev, Yu.N. (1998) *Power sources for pulsed electric technological processes*. Tomsk: TPI.
4. Paton, B.E., Voropaj, N.M., Buchinsky, V.N. et al. (1977) Control of arc welding process by programming of electrode wire feed rate. *Avtomatich. Svarka*, **1**, 1–5.
5. Voropaj, N.M., Saveliev, O.N., Semergeev, S.S. (1980) Electromagnetic mechanisms of pulsed electrode wire feed. *Ibid.*, **1**, 46–49.
6. Voropaj, N.M. (1996) Parameters and technological possibilities of arc welding with pulsed feed of electrode and filler wire. *Ibid.*, **10**, 3–9.
7. Lebedev, V.A., Moshkin, V.F., Pichak, V.G. (1996) New mechanisms of electrode wire pulsed feed. *Ibid.*, **5**, 39–44.
8. Paton, B.E., Lebedev, V.A., Pichak, V.G. et al. (2002) Analysis of technical and technological possibilities of electrode wire pulsed feed in the processes of arc welding and surfacing. *Svarochn. Proizvodstvo*, **2**, 24–31.
9. Ushio, M., Liu, W., Mao, W. (1995) An experimental investigation of dynamic behavior of arc sensor in GMA welding in short-circuit transfer mode. *Transact. of JWRI*, 24(**1**), 25–31.
10. Mao, W., Sadek, A.A., Ushio, M. (1997) Measurement of dynamic characteristics of arc sensor in GMA welding in dip transfer mode. *Ibid.*, 26(**1**), 9–19.
11. Paton, B.E., Shejko, P.P. (1967) Automatic control of consumable-electrode pulse-arc welding process. *Avtomatich. Svarka*, **1**, 3–8.
12. Paton, B.E., Lebedev, A.V. (1988) Control of melting and transfer of metal in CO_2 welding. *Ibid.*, **11**, 15–18.
13. Saraev, Yu.N. (2002) Adaptive methods of mechanized pulsed-arc welding in main pipeline construction. *Svarochn. Proizvodstvo*, **1**, 4–11.
14. Paton, B.E., Shejko, P.P., Zhernosekov, A.M. et al. (2003) Stabilization of the process of consumable electrode pulsed-arc welding. *The Paton Welding J.*, **8**, 2–5.
15. Dyurgerov, N.G., Sagirov, D.Kh. (2004) Determination of arc properties in pulse processes. *Svarochn. Proizvodstvo*, **4**, 14–18.
16. Shejko, P.P., Zhernosekov, A.M., Shimanovsky, Yu.O. (2004) Consumable-electrode pulsed-arc welding with automatic stabilization of mode parameters. *The Paton Welding J.*, **1**, 7–10.
17. Tsybulkin, G.A. (1994) Construction of mathematical models in problems of adaptive control of arc welding. *Avtomatich. Svarka*, **1**, 24–27.
18. Tsybulkin, G.A. (2002) To the question of GMAW stability. *The Paton Welding J.*, **5**, 14–16.
19. Pervozvansky, A.A. (1986) *Course of automatic control theory*. Moscow: Nauka.
20. Lenivkin, V.A., Dyurgerov, N.G., Sagirov, Kh.N. (1989) *Technological properties of shielded-gas welding arc*. Moscow: Mashinostroenie.
21. Tsybulkin, G.A. (2002) About the influence of electric field fluctuations in arc column on arc welding process stability. *The Paton Welding J.*, **6**, 38–39.

TIG WELDING OF TITANIUM AND ITS ALLOYS IN ARGON ATMOSPHERE USING FLUX-CORED FILLER WIRE (TIG-FW)

TIG-FW welding is performed with flux-cored filler wire of the PPT grade using modern standard TIG welding equipment and commercial DC power supplies. This welding method provides welds on metal 5 to 16 mm thick in one pass without groove preparation.

In addition to technological advantages, the use of the flux-cored filler wire for TIG welding of titanium guarantees the pore-free welds, which leads to improvement of fatigue resistance of welded joints.

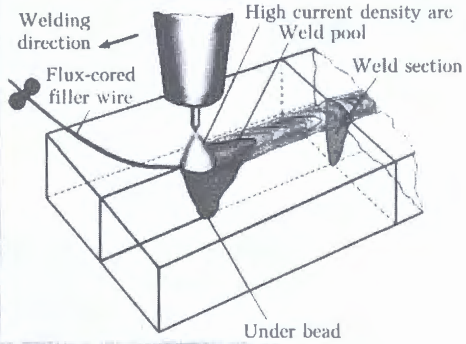

Welding flow diagram

Typical part welded by the TIG-FW method

Application. The TIG-FW welding method is indicated for making butt, overlap, T- and plug joints in titanium and titanium alloys. Consumption of flux-cored filler wire per metre of the weld is 1.2–1.5 m.

Proposals for co-operation. Transfer of the developed technology on a contract base.

DETERMINATION OF RESIDUAL STRESSES IN THE WWER VESSELS AFTER MULTI-RUN WELDING, SURFACING AND HIGH-TEMPERATURE TEMPERING

B.Z. MARGOLIN, A.Ya. VAROVIN and V.I. KOSTYLYOV
Central Research Institute of Structural Materials «Prometej», St.-Petersburg, Russia

Calculations of residual stresses formed after welding, surfacing and tempering have been made for bodies of the water-moderated (WWER) type reactors. The calculation procedure is based on solutions of temperature and non-isothermal elastoplastic problems obtained using the finite elements method. α-Fe ↔ γ-Fe transformations and creep have been allowed for in solving the deformation problem. The investigations conducted show that the α-Fe ↔ γ-Fe ransformation does have an effect on the distribution of residual stresses depending upon the conditions, under which this effect can be substantial, and under which it can be ignored.

Keywords: *arc welding, surfacing, tempering, nuclear reactor, residual stresses, embrittlement, relaxation of stresses, calculation*

It is noted in many studies devoted to evaluation of the strength of the reactor vessels [1–7] that the calculations should take into account the residual stresses caused by the welding and surfacing. Analysis of the effect of residual stresses on resistance of the vessels to the brittle failure carried out by the specialists from different countries underlies the IAEA special guidelines [8] where the necessity to consider the residual welding stresses is envisaged.

Nonetheless, a level of residual stresses and a nature of their distribution are still viewed in the calculations arbitrarily without their dependence on the peculiarities of welding, surfacing and tempering technology. For example, for the girth welds it is assumed that distribution of both circumferential and axial stresses may be described by one and the same expression of the following form:

$$\sigma^{\text{res}}(x) = \sigma^{\text{res}}_{\max} \cos\left(\frac{2\pi x}{S}\right), \qquad (1)$$

where S is the thickness of the vessel wall; x is the coordinate by the radius of the shell; $\sigma^{\text{res}}_{\max}$ has a constant value irrespective of the temperature variations and tempering duration. Besides, the distribution of residual stresses caused by the surfacing is usually assumed as follows: they approach the yield point in the surfacing and zero in the HAZ and the parent metal.

This work presents the results of the calculations of residual stresses caused by welding, surfaces and postweld tempering for vessels of the WWER-440/230 (reactors without anticorrosion surfacing), WWER-440/213 and WWER-1000 (reactors with surfacing). The studies are carried out for the girth welds in the active zone of the vessel (welds No.4) where the neutron flow is maximal and where the embrittlement of the materials proceeds more intensively as compared to other parts of the reactor vessel. Therefore, this zone is the weakest in terms of brittle failure and here the residual stresses have their most essential effect.

The calculation procedure is based on the solution of temperature and non-isothermal elastoplastic (for welding and surfacing) and elastic-tough-plastic (for postweld tempering) problems by the finite element method (FEM) [9–11].

Peculiarities of the solution algorithm of the strain problem. The basic equations for solution of the strain problem are based on the theory of flow [9–11]. Let us present only those dependences that consider creep and structural transformations.

Formulation of the yield condition with and without considering creep. Residual stresses arising in the process of welding and surfacing were determined by the solution of the non-isothermal elastoplastic problem using the Prandtl model (ideal elastoplastic body) and the Mises condition of yield in the following form:

$$\sigma_{\text{eq}} = \Phi(T), \qquad (2)$$

where $\Phi(T) \equiv \sigma_y(T)$ is the function describing the surface; σ_y is the yield point.

For estimation of the redistribution of the residual stresses in postweld tempering the elastoplastic problem was solved with regard to creep. Its solution was performed as the solution of the elastoplastic problem using the model of isotropic strengthening. In this case it is assumed that strain–stress curves depend on the Odquist parameter $\kappa = \int d\varepsilon^{\text{p}}_{\text{eq}}$ ($d\varepsilon^{\text{p}}_{\text{eq}}$ is the intensity of plastic strain growth), rate of the intensity of plastic

---

[*] By the materials of the presentation at the 2nd International Conference «Mathematical Modelling and Information Technologies in Welding and Related Processes» (Katsiveli, Crimea, September 13–17, 2004).

strain growth ξ^p_{eq} and temperature T while the yield condition is formulated as

$$\sigma_{eq} = \Phi(\kappa, \xi^p_{eq}, T), \tag{3}$$

where $\Phi(\kappa, \xi^p_{eq}, T)$ is the function describing the yield surface.

$\Phi(\kappa, \xi^p_{eq})$ for this temperature is determined on the basis of the experimental data on stress relaxation [10]. According to [12, 13] the stress relaxation at a certain temperature may T be described by the equation

$$\frac{\sigma}{\sigma_0} = \exp(-k\tau^p), \tag{4}$$

where σ is the current stress at the moment τ; σ_0 is the initial value of stress at $\tau = 0$; k and p are the constants of the material.

The condition $\varepsilon^c + \varepsilon^e = \text{const}$ (ε^c is the creep flow; ε^e is the elastic strain) is valid at stress relaxation. Using this condition and the equation (4) we obtain

$$\xi^c = \frac{kp}{E}\sigma\tau^{p-1}, \tag{5}$$

where ξ^c is the creep flow velocity; E is the elasticity module. Assuming that under uniaxial loading $\varepsilon^c_{eq} = \frac{2(1+\mu)}{3}\varepsilon^c$, $\varepsilon^c_{eq} = \kappa$ and $\sigma_{eq} = \sigma$, from equations (4) and (5) we obtain

$$\xi^c_{eq} = \frac{2(1+\mu)}{3E}kp\sigma_{eq}\left[\frac{1}{k}\ln\left(1+\frac{3E\kappa}{2(1+\mu)\sigma_{eq}}\right)\right]^{\frac{p-1}{p}}, \tag{6}$$

where μ is the Poisson coefficient.

The equation (6) may be presented in the compact form $\sigma_{eq} = \varphi(\kappa, \xi^c_{eq})$ at $\sigma_{eq} < \sigma_y$.

In the general case the creep for the model of the ideal elastoplastic body may be presented as follows:

$$\Phi(\kappa, \sigma^p_{eq}) = \begin{cases}\varphi(\kappa, \xi^c_{eq}), \text{ if } \sigma_{eq} < \sigma_y,\\ \sigma_y, \text{ if } \sigma_{eq} \ge \sigma_y.\end{cases} \tag{7}$$

Schematization of mechanical and thermal physical properties regarding α-Fe ↔ γ-Fe *transformation*. It is known that γ-Fe → α-Fe transformation may have an essential effect on the residual stresses, the effect being greater the lower being the temperature of transformation during cooling [9, 14]. For steel of low strength γ-Fe → α-Fe transformation proceeds within the 600–800 °C temperature range, and in this case its effect may be neglected. For hull steels the temperature of the beginning and the end of the γ-Fe → α-Fe transformation varies from 450–550 to 260–360 °C depending on the cooling velocity. Welding of the hull reactor steels is carried out with preheating, which decreases the cooling velocity and γ-Fe → α-Fe transformation in this case proceeds within the 450–350 °C temperature range. At these temperatures the γ-Fe → α-Fe transformation may have an effect on the residual stresses.

Residual stresses created in this structure under these welding conditions are determined by the properties of the material depending not only on the chemical composition but also on its structural state. The latter may change in the process of the thermal cycle. Therefore, at different moments of time it is necessary to use different combination of properties for describing the behaviour of the given material. In view of the effect of the α-Fe ↔ γ-Fe transformation on the residual stresses the most important is to take into account the changes in the nature of the dependences $\sigma_y(T)$ and $\varepsilon^T(T)$ (ε^T is the temperature strain) under the changes of the structural state of the materials.

If in the thermal cycle $T_{\max} > T_{A_{c1}}$, then α-Fe ↔ γ-Fe transformation will proceed in the material. It is noteworthy that cooling rates in welding are rather high, therefore it is necessary to consider both circumstances. First, the interval of the γ-Fe → α-Fe transformation and dependence $\varepsilon^T(T)$ essentially change under cooling. Second, the dependence $\sigma_y(T)$ essentially changes under hardening. In the subsequent thermal cycle when a certain heating temperature of the hardened material is achieved the oversaturated solution of carbon decomposes into α-Fe with decomposition of the residual austenite. Hence, a specific volume of the material, i.e. the dependence $\varepsilon^T(T)$, changes. Then carbides grow and coagulate at higher temperatures. This phenomenon is accompanied by a loss of strength by the material, i.e. by a change of the $\sigma_y(T)$ dependence.

We have described the algorithm for calculation of the residual stresses with regard to the changes of $\sigma_y(T)$ and $\varepsilon^T(T)$ caused by the α-Fe ↔ γ-Fe transformation. Three variants of the dependence of the properties of the materials on the temperature are presented in Figure 1: in the tempered and hardened states and under fast cooling from the austenite state.

It is assumed that under heating of the hardened material (curve *3*) an abrupt change of the specific volume proceeds at $T = T_1$, while loss of strength proceeds at $T = T_{\text{tem}}$. Thus, if the hardened material is heated up to $T \ge T_1$, then further both in heating and in cooling $\varepsilon^T(T)$ will correspond to the behaviour of the tempered material. Similarly, after heating of the hardened material to $T \ge T_{\text{tem}}$, $\sigma_y(T)$ will correspond to the tempered condition. Curves *1* and *3* in Figure 1 for $\varepsilon^T(T)$ coincide at $T \ge T_1$, while for $\sigma_y(T)$ — at $T \ge T_{\text{tem}}$. Therefore, curves *3* correspond to the dependences $\varepsilon^T(T)$ and $\sigma_y(T)$ for initially hardened material within the whole temperature range. The heat calculations showed that by the beginning of the next run the material in the zone of the previous run has enough time to cool down to the temperatures approaching the temperatures of the preheating, i.e. to $T < T_1$. Therefore, the next bead is deposited either on the hardened (curves *3*) or tempered (curves *1*) material. Hence, there is no need to consider rather complicated case when the repeated heating starts from the moment of cooling to $T_1 < T < T_4$ at the previous cycle. Regarding the above the following

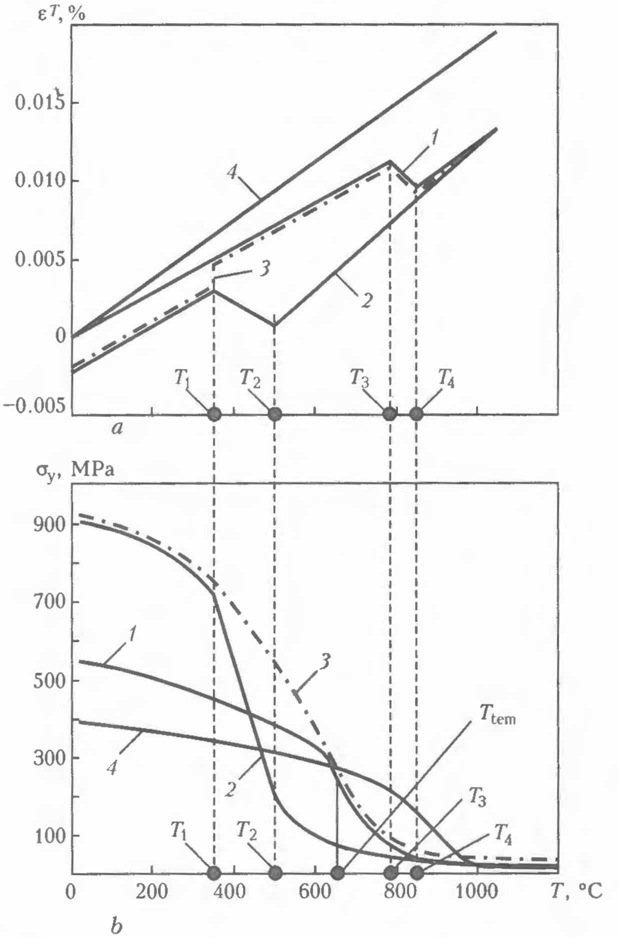

Figure 1. Dependence of temperature strain (*a*) and yield point (*b*) on temperature of heating and cooling for the parent and weld metal (*1–3*) and austenite deposit (*4*): T_1 and T_2 are the temperatures of end and beginning of the γ-Fe → α-Fe transformation in cooling, respectively; T_3 and T_4 are the temperatures of beginning and end of α-Fe → γ-Fe transformation in heating, respectively; T_{tem} is the temperature approaching the temperature of tempering

scheme of the material state in the current thermal cycle is proposed.

1. *The initial state of the material is tempered*.

- heating stage to $T = T_{max}$: curves *1* are used for $\sigma_y(T)$ and $\varepsilon^T(T)$;
- cooling stage from $T = T_{max}$: curves *1* are used for σ_y and ε^T at $T_{max} \le T_4$, curves *2* are used at $T_{max} > T_4$.

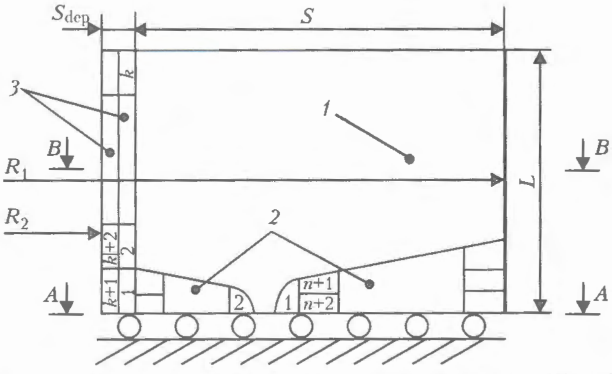

Figure 2. Design scheme of reactor vessel part in the zone of girth weld No.4, and a scheme of the groove filling: *1* — parent metal; *2* — weld metal; *3* — deposit metal; *n* — number of welding run; *k* — number of surfacing run (other designations see in the text)

2. *State of the material after the previous thermal cycle is hardened*.

- heating stage to $T = T_{max}$: curves *3* are used for σ_y and ε^T at $T < T_1$, curves *1* are used at $T > T_{tem}$; curve *1* is used for ε^T at $T_1 < T < T_{tem}$ and curve *3* is used for σ_y;
- cooling stage from $T = T_{max}$: curves *1* or *3* are used for σ_y and ε^T at $T_{max} < T_4$, i.e. curves that correspond to the state at $T = T_{max}$; at $T_{max} > T_4$ curves *2* are used.

This algorithm allows tracing a change of the state and properties of the material at every point during subsequent thermal cycles in multi-run welding.

It is noteworthy that curves *1* weakly depend on the heating rate while curves *2* may strongly depend on the cooling rate. Cooling rate of the HAZ material is within 3–6 °C/s and according to the results of the experimental studies a difference between curves $\varepsilon^T(T)$ for steels 15Kh2MFA and 15Kh2NMFA (parent metal for WWER-440 and WWER-1000 reactor vessels, respectively) is almost inconsiderable at such rates. For example, a difference of T_2 values does not exceed in this case 30 °C, so the temperature range of γ-Fe → α-Fe transformation is basically the same for these steels. Regarding the above it was assumed in the calculations that steels 15Kh2MFA and 15Kh2NMFA and their welds have identical dependences for $\varepsilon^T(T)$. A difference in the yield point σ_y of these materials does not exceed 10 %, so for $\sigma_y(T)$ similar dependences may be assumed. The austenite material of surfacing is not exposed to α-Fe → γ-Fe transformation, therefore, the dependences $\sigma_y(T)$ and $\varepsilon^T(T)$ coincide for it in heating and cooling.

Other characteristics necessary for solution of the heat problem (temperature dependence of specific heat conduction and specific heat capacity) and strain problem (temperature dependence of the Young modulus) are presented in [10].

Calculation of the fields of residual stresses. *The object of study*. Design scheme of a part of the reactor vessel in the zone of the girth weld and a sequence of runs in welding and surfacing (surfacing was not considered for WWER-440/230) is shown in Figure 2. Groove geometry is shown in Figure 3. The following dimensions of the vessels were assumed: R_1 = = 1770 mm, R_2 = 1920 mm for WWER-440/230 and WWER-440/213; R_1 = 2070 mm, R_2 = 2270 mm for WWER-1000. To avoid the edge effect the height of the cylinder L was assumed to be equal to $2\sqrt{R_2S}$.

Welding and surfacing of the vessels were carried out with preheating whose temperature for WWER-440 was 220 °C before welding and 150 °C before surfacing, and for WWER-1000 — 150 and 100 °C, respectively. Tempering was carried out after welding and surfacing: T_{tem} = 670 °C for WWER-440 and T_{tem} = 650 °C for WWER-1000. Duration of tempering varied within 10–50 h.

Calculation procedure. Simulation of every run in welding and surfacing was carried out by diving the whole process into small time steps ($\tau - \Delta\tau$, τ), solution

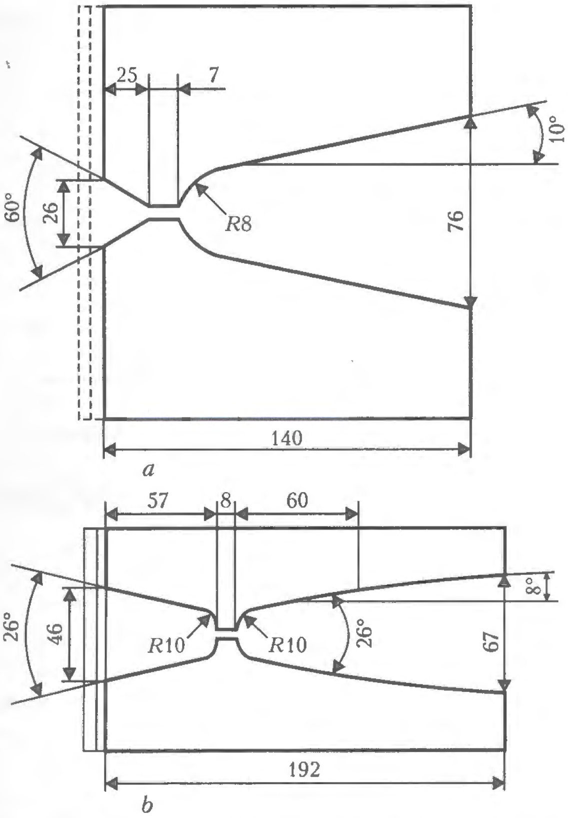

Figure 3. Groove geometry of weld No.4 for WWER-440 (*a*) and WWER-1000 (*b*)

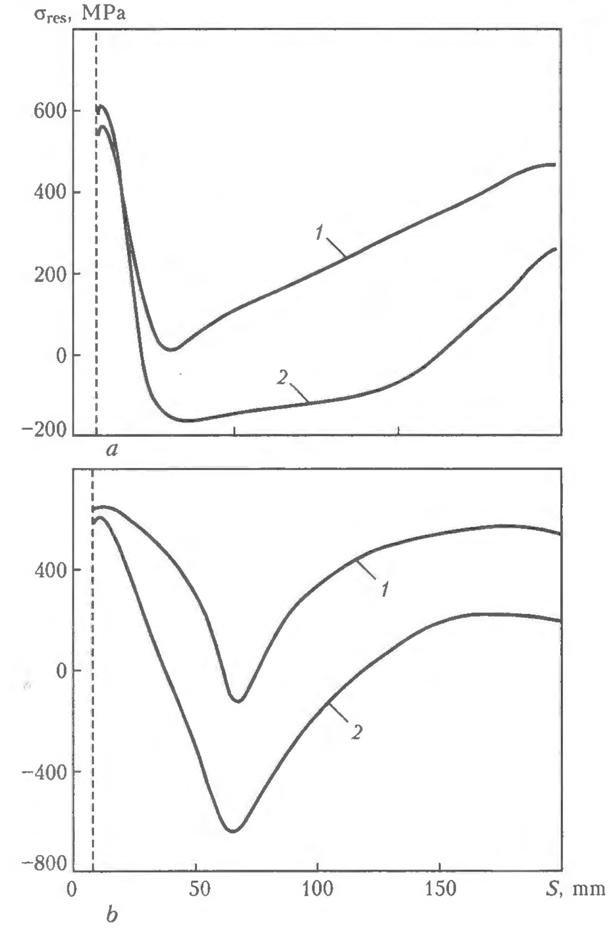

Figure 4. Distribution of residual circumferential (*1*) and axial (*2*) stresses in the section *A–A* (see Figure 2) after making of the weld No.4 for WWER-440/213, WWER-440/230 (*a*) and WWER-1000 (*b*)

of the heat problem and determination of the temperature field at every step [10]. Knowing the field temperatures at the beginning and at the end of the step ($\tau-\Delta T$, τ) it is possible to determine the field of temperature strains $\Delta\varepsilon^T$, which is the initial information for solution of the elastoplastic problem for the step of time ($\tau-\Delta\tau$, τ).

Postweld tempering was simulated as follows. Fields of residual plastic strains after welding and surfacing were the input data for solution of the elastoplastic problem regarding creep. Inelastic strain in the parent and weld metal was considered in this problem as instant plastic strain and/or creep strain, while inelastic strain in the deposited metal was considered only as instant plastic strain. All calculations were carried out in the axisymmetric formulation. Creep parameters according to (4) and [10] were assumed as $k = 0.90$, $p = 0.16$ for $T = 650$ °C and $k = 1.18$, $p = 0.14$ for $T = 670$ °C.

Calculation results. As it is seen from the presented results circumferential and axial stresses are distributed in the weld metal heterogeneously up to the sign reverse (Figures 4–7). After welding maximal tensile stresses are created in the weld near the inner and outer surfaces of the vessel, maximal compression stresses — in the zone of the weld root; values of residual stresses achieve the yield point. After surfacing and tempering maximal values of the tensile stresses in the weld and parent metal are distributed in the zone of transition to the deposit, circumferential residual stresses in all zones are at the level of axial ones. Maximal tensile stresses act on the inner and outer surface of the vessel without surfacing (WWER-440/230).

After tempering a considerable relaxation of tensile stresses in the parent and weld metal takes place. Tensile stresses in the deposit almost do not change and approach the yield point within the whole section by thickness. Maximal tensile stresses in the weld and parent metal are determined mainly both by the temperature and by the tempering duration (Figure 8). Different distribution of the residual stresses by the wall section is determined by such factors as a different shape of the weld No.4 for WWER-440 and WWER-1000, the presence of deposit for WWER-440/213 and WWER-1000 and its absence for WWER-440/230, different temperatures of tempering for WWER-440 and WWER-1000.

Thus, a distribution of axial and circumferential residual stresses in the section of the welds cannot be described by the expression (1). Safety of vessels is evaluated by the brittle failure criterion for postulated defects with depth not more than 1/4 of the vessel wall thickness. Therefore, it is enough to approximate the obtained distribution of the residual stresses for different vessels of the WWER type within 1/4 of the wall thickness [15]. The following dependences are proposed to describe the axial and circumferential residual stresses in the *A–A* section of the weld for

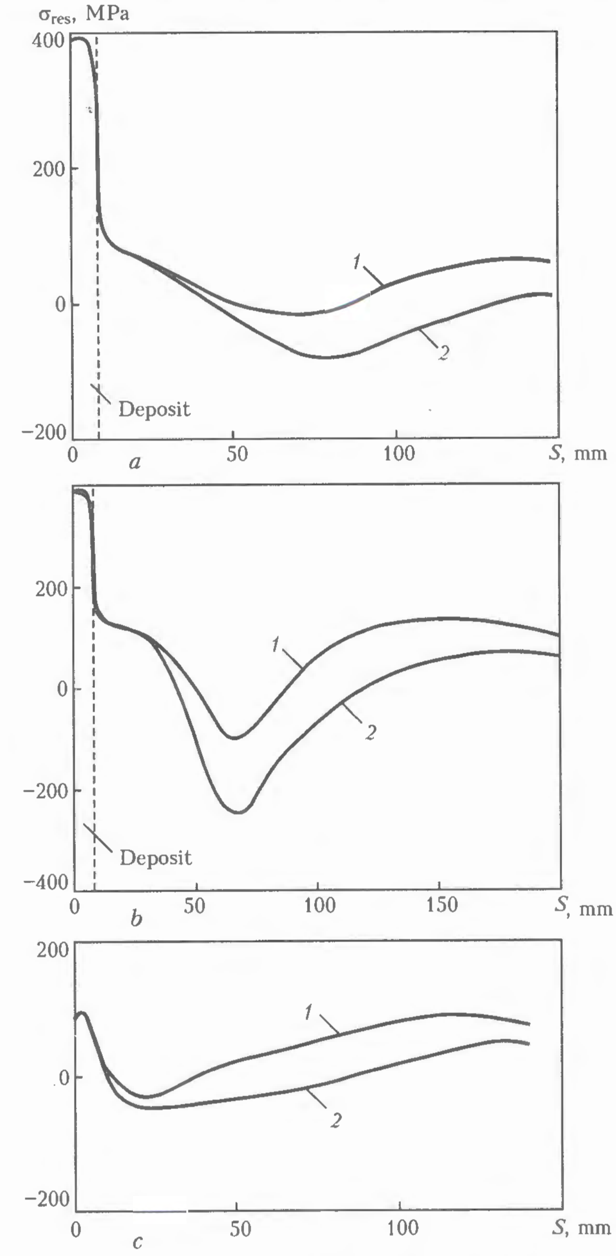

Figure 5. Distribution of residual circumferential (*1*) and axial (*2*) stresses in section *A–A* (see Figure 2) after making the weld No.4, surfacing and tempering (10 h) for WWER-440/213 (*a*), WWER-1000 (*b*) and after making the weld No.4 and tempering (10 h) for WWER-440/230 (*c*)

vessels with surfacing (WWER-440/213 and WWER-1000):

$$\begin{cases}\sigma^{res}(x)=\sigma^{res}_{dep} \text{ at } x<S_{dep},\\ \sigma^{res}(x)=\sigma^{res}_{max}(a_0+a_1\hat{x}+a_2\hat{x}^2+a_3\hat{x}^3+a_4\hat{x}^4) \text{ at } S_{dep}\le x\le 0.25S,\end{cases} \qquad (8)$$

where $\hat{x}=x-S_{dep}$; x is the coordinate by the thickness of the vessel wall, starting from its inner surface, mm; S_{dep} is the deposit thickness; S is the thickness of the vessel wall.

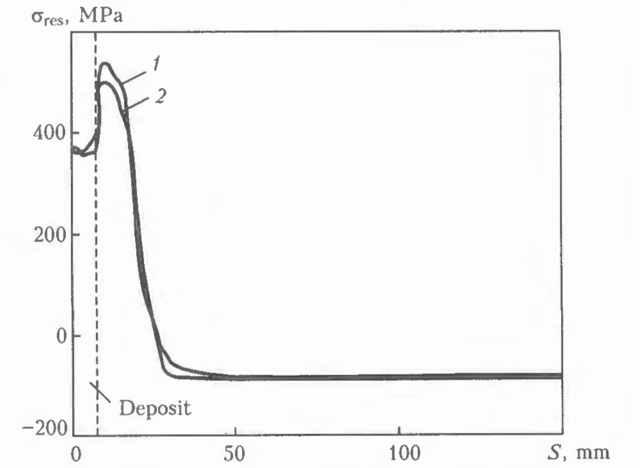

Figure 6. Distribution of residual circumferential (*1*) and axial (*2*) stresses after surfacing in section *B–B* (see Figure 2) outside the zone of weld No.4 for WWER-440/213

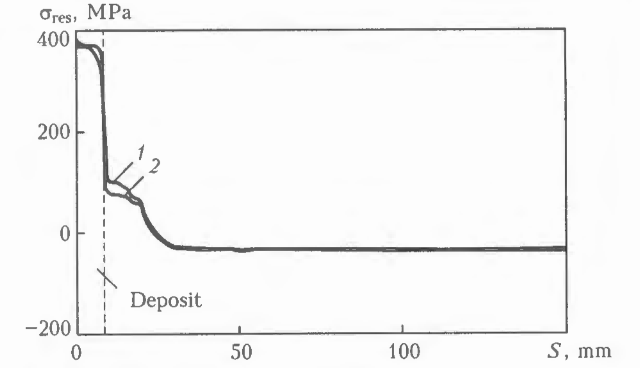

Figure 7. Distribution of residual circumferential (*1*) and axial (*2*) stresses after surfacing in section *B–B* (see Figure 2) outside the zone of weld No.4 and tempering (10 h) for WWER-440/213

Value of stresses σ^{res}_{dep} and σ^{res}_{max} used in (8) are shown in Figure 8 as the functions of the temperature and duration of tempering. Coefficients a_i in (8) are presented in the Table. The results presented in the work [10] may be used to describe a distribution of residual stresses caused by surfacing in the vessel wall outside the weld:

$$\begin{cases}\text{at } t(x)\le S_{dep},\ \sigma^{res}(x)=\sigma^{res}_{dep},\\ \text{at } S_{dep}\le x\le 2.5S,\ \sigma^{res}(x)=\sigma^{res}_{max},\\ \text{at } t(x)>2.5S_{dep},\\ \sigma^{res}(x)=\sigma^{res}_{max}-2\sigma^{res}_{max}(x-2.5S_{dep})/S_{dep}, \text{ if } \sigma^{res}(x)>\sigma_{com},\\ \sigma^{res}(x)=\sigma_{com}, \text{ if } \sigma^{res}(x)\le\sigma_{com},\end{cases} \qquad (9)$$

where σ_{com} is the uniform compression stress determined from the equilibrium equations.

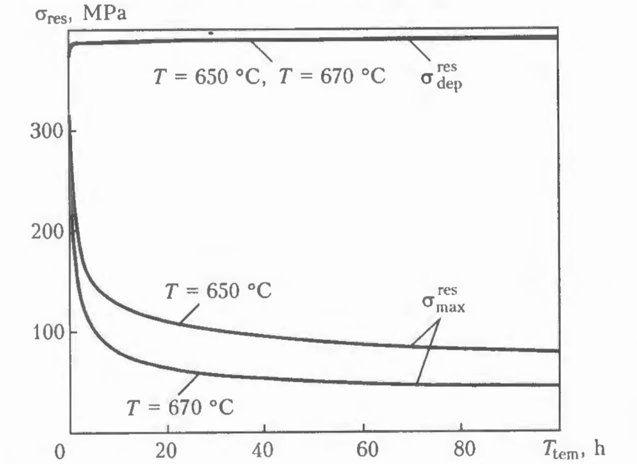

Figure 8. Dependence of residual stresses on duration and temperature of tempering

Values of coefficients a_i for calculation of residual axial σ_{zz}^{res} and circumferential $\sigma_{\theta\theta}^{res}$ stresses (MPa) by the equations (8) and (10)

Coefficient a_i	WWER-440/213		WWER-440/230		WWER-1000	
	$\sigma_{zz}^{res}\cdot 10^{-6}$	$\sigma_{\theta\theta}^{res}\cdot 10^{-6}$	$\sigma_{zz}^{res}\cdot 10^{-6}$	$\sigma_{\theta\theta}^{res}\cdot 10^{-6}$	$\sigma_{zz}^{res}\cdot 10^{-6}$	$\sigma_{\theta\theta}^{res}\cdot 10^{-6}$
a_0	1	1	1	1	1	1
a_1	+9225	−1650	−11087	+1321	−11962	−1831
a_2	−1775	−1062	−8637	−14162	+2431	+196
a_3	+23.7	+16.7	+368.1	+672.1	−133	−29.2
a_4	−0.084	−0.065	−4.2	−8.7	+1.37	+0.29

The following dependence is proposed to describe a distribution of axial and circumferential residual stresses in the weld in the section A–A for vessels without surfacing (WWER-440/230):

$$\sigma^{res}(x) = \sigma_{max}^{res}(a_0 + a_1x + a_2x^2 + a_3x^3 + a_4x^4) \quad \text{at } 0 \le x \le 0.25S. \tag{10}$$

Coefficients a_i in (10) are also given in the Table.

Analysis of the effect of γ-Fe → α-Fe transformation on residual stresses. γ-Fe → α-Fe transformation proceeds at the thermal cycle from $T_{max} > T_4$ and is accompanied by an increase of the volume at the low temperatures, therefore the residual stresses remain low ($\cong 0.2\sigma_y$).

As it is followed from Figure 1, the postweld residual stresses in the weld metal (in the zone of the last runs) approach the yield point of the material in the tempered state. This indicates that the γ-Fe → α-Fe transformation has an inconsiderable effect on the residual stresses, which may be explained by the following. Every point of the weld is exposed in multi-run welding to a repeated action of the thermal cycles. With the next run moving away from the point considered a maximal temperature of the next thermal cycle in this point decreases. Hence, after thermal cycle from $T_{max} > T_4$ (see Figure 1) the thermal cycle, where $T_{max} \le T_3$, is found. In the thermal cycle from $T_{max} \le T_3$ the γ-Fe → α-Fe transformation is absent while maximal temperature is sufficiently high to create large plastic compression strains at the heating stage, therefore residual tensile stresses approaching the yield point are formed during cooling.

In other words, in the process of performing the weld the area, where α-Fe → γ-Fe transformation shows its effect, is practically limited by the last runs.

In the vessels with deposit near the inner surface the residual stresses will be actually created anew in the process of surfacing, so α-Fe → γ-Fe transformation in welding of the vessels will not have a considerable effect on the level and character of distribution of residual stresses in the weld. However, a different situation can develop with small number of runs, particularly when performing surfacing. Let us consider three cases as examples.

Case 1. When applying a second layer of deposition, T_{max} in HAZ is sufficiently high but lower than T_3. Such situation occurs in practice with design thickness of the first layer and with performing of the second layer in the design conditions. Residual stresses for this case are shown in Figures 6 and 7.

Case 2. When applying the second layer in those HAZ areas where $T_{max} > T_4$, the residual stresses will be low. Such situation may take place when the second layer is deposited with increased heat input or in the sites with a decreased thickness of the first layer. Residual stresses for this case are shown in Figures 9 and 10. Simulation of these cases is carried out by assigning an increased heat input in the second run.

Case 3. When applying the second layer, low temperatures of the HAZ (T_{max} < 300 °C) take place. Such situation may develop if the second layer is deposited at decreased heat input or in the sites with increased thickness of the first layer. In this case at

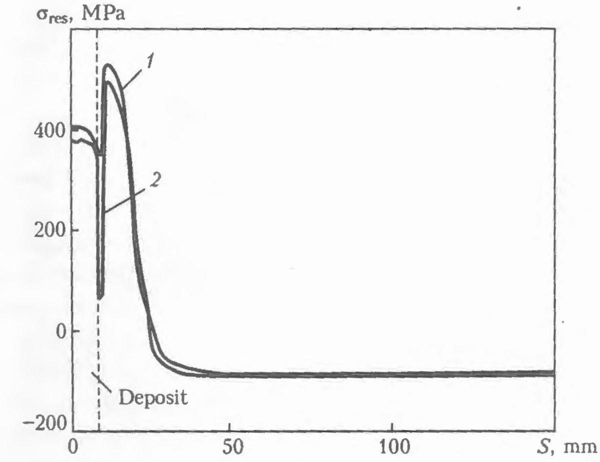

Figure 9. Distribution of residual circumferential (*1*) and axial (*2*) stresses after surfacing in section *B*–*B* (see Figure 2) outside the zone of weld No.4 for WWER-440/213

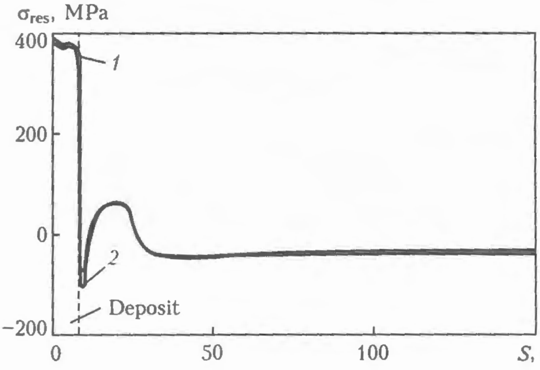

Figure 10. Distribution of residual circumferential (*1*) and axial (*2*) stresses outside the zone of weld No.4 in *B*–*B* section (see Figure 2) after surfacing and tempering (10 h) for WWER-440/213

the stage of heating plastic strains of shortening do not appear in HAZ and the residual stresses remain the same as after the first run and approach the stresses for case 2.

For obtaining a conservative estimation of the vessel resistance to the brittle failure it is necessary to use residual stresses corresponding to the case 1.

CONCLUSIONS

1. A procedure for calculation of residual stresses and strains, which considers α-Fe ↔ γ-Fe transformation and formation of stresses and strains after welding and surfacing, as well as the processes of stress relaxation during postweld tempering is proposed.

2. The proposed procedure is used to make calculations that allow analysing the residual stresses after welding, surfacing and tempering for vessels of the WWER-type reactor.

3. It is shown that in multi-run welding the effect of α-Fe ↔ γ-Fe transformation on residual stresses in the weld are inconsiderable, but with small number of runs, for example when making surfacing, the α-Fe ↔ γ-Fe transformation may have a considerable effect on the distribution of residual stresses. So, if in HAZ $T_{\max} > T_4$ in every run, then the α-Fe ↔ γ-Fe transformation has an effect on residual stresses, while if in the last run $T_{\max} < T_3$, then there is almost no effect on the residual stresses.

4. The results of the numerical calculations are presented in the analytical form. The obtained dependences may be used for conservative estimation of the strength of the reactor vessels since they give the upper limit of residual welding stresses.

1. Karzov, G.P., Timofeev, B.T., Leonov, V.P. (1982) *Welded pressure vessels: strength and life*. Leningrad: Mashinostroenie.
2. Sauter, A. (1983) Influence of cladding on linear elastic RPV-analysis during loss of coolant accident. *Nucl. Eng. Des.*, **78**, 347–358.
3. Smith, E. (1984) The restraining effect of austenitic cladding on the extension of a three-dimensional crack into the wall of a water-cooled nuclear reactor pressure vessels during a hypothetical overcoming accident. *Ibid.*, **78**, 79–84.
4. Baumjohann, F. (1986) Calculation thermoplastic stresses of a reactor pressure vessel with cladding from stress-relief annealing up to a thermal shock. *Ibid.*, **96**, 323–335.
5. Faure, F., Leggatt, R. (1996) Residual stresses in austenitic stainless steel primary coolant pipes and welds of pressurized water reactor. *Int. J. Pres. Ves. Piping*, **65**, 265–275.
6. Ferril, D.A. et al. (1966) Measurements of residual stresses in a heavy weldment. *Welding Res.*, 504–514.
7. Keim, E., Schopper, A., Hertlein, R. (2002) Application of a deterministic procedure for life management of reactor pressure vessels of Western and Eastern type of reactors under pressurized thermal shock loading. In: *Proc. of 7th Int. Conf. on Material Issues in Design, Manufacturing and Operation of Nuclear Power Plants Equipment* (St.-Petersburg, June 17–21, 2002). Vol. 1.
8. (1996) *Guidance on the reactor pressure vessel PTS assessment for WWER nuclear power plants: WWER-SC-157*. Int. Atomic Energy Agency.
9. Karzov, G.P., Margolin, B.Z., Shvetsova, V.A. (1993) *Physical-mechanical modeling of fracture processes*. St.-Petersburg: Politekhnika.
10. Kostylev, V.I., Margolin, B.Z. (2000) Determination of residual stress and strain fields caused by cladding and tempering of reactor pressure vessels. *Int. J. Pres. Ves. Piping*, **77**, 723–735.
11. Makhnenko, V.I. (1976) *Computational methods of investigation of welding stress and strain kinetics*. Kiev: Naukova Dumka.
12. Rovinsky, B.M., Lyutsau, V.G. (1957) Relaxation of microstresses. *Zhurnal Tekhn. Fiziki*, 27(**2**), 345–350.
13. Bordzyka, A.M., Getsov, L.B. (1972) *Stress relaxation in metals and alloys*. Moscow: Metallurgiya.
14. Vinokurov, V.A. (1968) *Welded stresses and strains*. Moscow: Mashinostroenie.
15. (1989) *PNAE G-7-002–86*: Design code on strength of equipment and pipings of nuclear power plants. Moscow: Energoatomizdat.

COMPUTER SYSTEM TO DESIGN TECHNOLOGIES FOR WELDING LIGHT ALLOYS

Selection of type of welded joint and shape of weld groove

Purpose. The computer system is intended for design of technologies for electric arc welding of light alloys with different alloying systems. It allows selection of shape of the weld groove, welding consumables, welding method and parameters depending upon the geometric features of a welded joint, base metal grade and other welding conditions. To make an optimal decision, a user is given an information support in the form of comparative characteristics of welding methods by 10 indicators, as well as information on welding-technological characteristics of non-consumable electrodes. Result of operation of the system has the form of a flow sheet.

Application. The system can be applied at machine building enterprises, technology and design bureaus, as well as at higher education institutions for training welding engineers.

EFFECT OF REDUCING RESIDUAL STRESSES IN WELDED JOINTS OF ALUMINIUM ALLOY D16 BY MAGNETIC FIELD TREATMENT

A.V. BRODOVOJ[1], **V.A. BRODOVOJ**[2], **O.I. GUSHCHA**[2] and **S.G. BUNCHUK**[3]
[1]I.N. Frantsevich Institute for Materials Science Problems, NASU, Kiev, Ukraine
[2]E.O. Paton Electric Welding Institute, NASU, Kiev, Ukraine
[3]Institute for Physics of Semiconductors, NASU, Kiev, Ukraine

The effect of exposure to non-uniform magnetic field on residual welding stresses in specimens of aluminium alloy D16 has been studied. It is shown that a long exposure of specimens containing a weld leads to a substantial decrease in the value of residual stresses. Suggested is an explanation to the observed effect.

Keywords: *metal structures, welded joints, residual stresses, non-uniform magnetic field, acoustic testing*

Initiation and propagation of cracks in real structures are associated with welded joints present in them. Tensile residual stresses formed in welding have a negative effect on the load-carrying capacity of welded joints and structures as a whole. Measures on decreasing tensile residual stresses include annealing of structural members, local annealing of welded joint zones using a gas torch or electric current, high-frequency peening, etc. This study suggests an ingenious method for reducing residual stresses in welded joints.

Reportedly [1–3], the dislocation structure of deformed materials changes to a substantial degree under the effect of electric and magnetic fields. Apparently, this should result in changes of residual stresses in specimens. The observed effect was studied on specimens measuring 140 × 60 × 3 mm, made of aluminium alloy D16 widely applied in aircraft engineering (σ_y = = 240 MPa), by testing them in magnetic field. Residual stresses were induced by performing spot argon-arc bead-on-plate welding (8 mm spot diameter). The fields of residual stresses were investigated using the acoustic non-destructive testing method [4].

Figure 1, *a*, shows the circumferential component of residual stresses within the welding zone at a maximal tension value of 160 MPa. The component gradually decreases with distance from the welding zone and transfers to the compression zone with a maximal value of –90 MPa. The radial component (Figure 1, *b*, curve *1*) in the welding zone is in tension with a maximal value of 190 MPa. With distance to the specimen edge, the values of the components gradually vanish.

The specimens after spot argon-arc bead-on-plate welding were exposed to the effect of uniform and non-uniform magnetic fields. No changes in the distribution of stresses were revealed in the specimens exposed to the effect of the uniform magnetic field with an intensity of 0.3 T for 6 months, compared with an initial specimen. Specimens of the other series were placed in the non-uniform magnetic field for 30 and 60 days. Non-uniformity of the external magnetic field with a value of $dH/dy = 0.1$ T/mm was achieved due to a relative position of the magnetic poles as shown in Figure 2. As seen from Figure 1, *a* and *b*, curves *2*, residual stresses within the argon-arc welding zone decrease to 90 MPa for the circumferential component and 140 MPa for the radial component after exposure of an aluminium alloy specimen containing the weld to the magnetic field for 30 days. With distance from the welding zone, the circumferential component of residual stresses first comes to the compression zone with a maximal value of –80 MPa, and then, with distance to the specimen edge, it decreases to –20 MPa. The value of the radial component of residual stresses decreases to zero. With further exposure of a specimen, the field of residual stresses continued changing. Thus, in exposure of specimens to the non-uniform magnetic field for 60 days the value of the circumferential component of residual stresses within the welding zone was 50 MPa (Figure 1, *a*, curve *3*) and radial component — 100 MPa. Some unbalance of the curves in Figure 1 is attributable to the fact that residual welding stresses were studied at a distance of 5 mm from the fusion line between the base and deposited metals.

Consider an element of volume of a specimen in the magnetic field, the potential energy of which can be written down as $W = -\overline{MH}$. Tensile and compressive residual stresses are present in an aluminium alloy specimen containing the weld, this leading to inhomogeneous magnetisation of the specimen, $\overline{M} = \chi(x, y, z)\overline{H}$, where χ is the magnetic susceptibility. Force F effects between the non-uniformly magnetised regions. The value of this force is determined by the derivative of potential energy depending upon the coordinate:

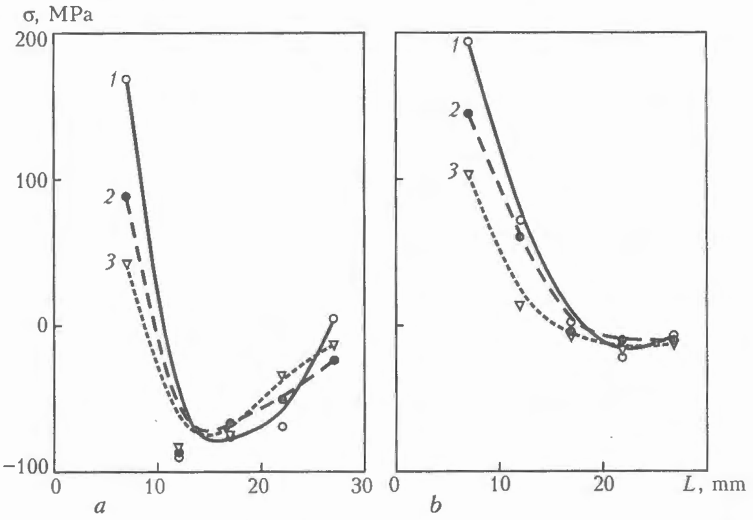

Figure 1. Distribution of circumferential (*a*) and radial (*b*) components of residual stresses in an aluminium alloy D16 specimen containing the weld in non-uniform magnetic field: *1* — in initial specimen; *2, 3* — after exposure for 30 and 60 days, respectively

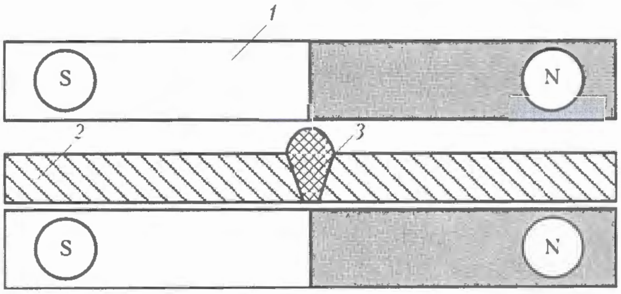

Figure 2. Schematic of exposure of an aluminium alloy specimen containing the weld to the effect of non-uniform magnetic field: *1* — magnets; *2* — specimen; *3* — welding zone

$$\bar{F} = F_1 + F_2 =$$

$$= -\left[M\left(\frac{\partial \bar{H}}{\partial x} + \frac{\partial \bar{H}}{\partial y} + \frac{\partial \bar{H}}{\partial z}\right) + H\left(\frac{\partial \bar{M}}{\partial x} + \frac{\partial \bar{M}}{\partial y} + \frac{\partial \bar{M}}{\partial z}\right)\right].$$

For a case of the uniform magnetic field, the force affecting a volume element is equal to

$$F_1 = -H\left(\frac{\partial \bar{M}}{\partial x} + \frac{\partial \bar{M}}{\partial y} + \frac{\partial \bar{M}}{\partial z}\right) = -H^2\left(\frac{\partial \chi}{\partial x} + \frac{\partial \chi}{\partial y} + \frac{\partial \chi}{\partial z}\right).$$

If the magnetic field is non-uniform $\left(\frac{\partial H}{\partial x} = \frac{\partial H}{\partial z} = 0;\ \frac{\partial H}{\partial y} \neq 0\right)$, this causes formation of an extra force effecting in crystal volume V:

$$F_2 = -\frac{1}{2}\,\mathrm{grad}\int_v \overline{MH}\,dV,$$

where dV is the volume element.

Therefore, the presence of two factors, i.e. dependence upon co-ordinates $\chi(x, y, z)$ and non-uniform magnetic field between individual elements of crystal volume, induces forces $\bar{F} = \bar{F}_1 + \bar{F}$, which are capable of causing additional deformation of a specimen.

Consider a simplified model of one-dimensional chain of atoms located at the same distance α from each other. A minimal length of the oscillation wave of such a chain is $\lambda_{\min} = 2\alpha$, corresponding to maximal frequency $\omega_{\max}$ related to wavelength $\lambda_{\min}$ through relationship $\omega_{\max} = \pi v/\alpha$, where v is the velocity of waves in crystal. Quantum of thermal oscillations for $\omega_{\max}$ is $\varepsilon_{\varphi_1} = h\omega_{\max} = \pi h v/\alpha$. If an increase in constant $b > \alpha$ (tension) occurs in some region of the chain during deformation, this will result in $\varepsilon_{\varphi_2} = h\omega_{\max} = \pi h v/b$ for this region and positive energy difference $\varepsilon_{\varphi_1} - \varepsilon_{\varphi_2}$. Otherwise, $b < \alpha$ (compression) and difference $\varepsilon_{\varphi_1} - \varepsilon_{\varphi_2}$ will be negative. In other words, loading is a source of phonons delivered from the compression to tension region. The probability of such a situation was first mentioned in study [5], which also noted that all elementary events of excitation of energy with increase in bonds (including its discharge in compression) were initiated by relatively low energy additions. It is likely that a small addition of magnetic energy is enough for the material to transfer to a more stable energy state. An external manifestation of these processes is an observed decrease in residual stresses in aluminium alloy D16 containing the weld after exposure of specimens to the effect of the non-uniform magnetic field.

1. Brodovoj, A.V., Kolesnichenko, V.G., Skorokhod, V.V. et al. (2001) Effect of electric field on magnetic susceptibility and healing of microcracks of deformed zinc crystals. *Metallofizika i Nov. Tekhnologii*, 23(**2**), 167.
2. Brodovoj, A.V., Brodovoj, V.A., Kolesnichenko, V.G. et al. (2001) Variations in magnetic and optical properties of nonferromagnetic crystals after exposure to electric and magnetic fields. *Uspekhi Fiziki Metallov*, **2**, 265.
3. Brodovoj, A.V., Brodovoj, V.A., Bunchuk, S.G. et al. (2003) Magnetic-plastic effect of semiconductor crystals GaAs and Si. In: *Proc. of Int. Sci.-Pract. Conf. on Structure Relaxation in Solids* (Vinnytsya, May 13–15, 2003).
4. Guz, A.N., Makhort, F.G., Gushcha, O.I. et al. (1974) *Principles of ultrasonic non-destructive method for determination of stresses in solids*. Kiev: Naukova Dumka.
5. Zhurkov, S.N. (1986) *Physics of strength and plasticity*. Leningrad: Nauka.

METHOD OF DETERMINATION OF WIRE TEMPERATURE AT NOZZLE OUTLET IN GAS-SHIELDED MECHANIZED WELDING

I.V. PENTEGOV and **O.I. PETRIENKO**
E.O. Paton Electric Welding Institute, NASU, Kiev, Ukraine

The paper presents the method for calculation of wire temperature, when it goes out of the nozzle, allowing for voltage drop in the point of electrode wire contact with the welding torch nozzle. Theoretical-calculation analysis results are in good agreement with experimental data.

Keywords: *mechanized welding, carbon dioxide gas, method for calculation, wire temperature, voltage drop*

Analysis of the existing theoretical and practical research into the thermal processes in the electrode extension in gas-shielded arc welding showed that the processes of temperature distribution are insufficiently well studied.

Stady [1] presents the method of calculation of temperature distribution along the electrode extension in CO_2 consumable-electrode arc welding, allowing for non-linearity of thermophysical coefficients and influence of heat coming from the drop. It permits calculation of temperature and its gradient in any point of electrode extension (from the nozzle to the drop) at the set temperature of electrode wire, going out of the nozzle.

Most of the studies of the processes of electrode wire heating in gas-shielded welding ignore electrode wire heating in the nozzle [2], although it is assumed that increase of wire temperature T_0 at nozzle outlet markedly influences its melting and may disturb the welding process [3]. Therefore, initial temperature T_0 of the wire going out of the nozzle, is one of the main parameters, influencing the voltage drop across electrode extension, and its determination is an important factor in construction of a mathematical model of consumable electrode gas-shielded arc welding in the power source–welding arc system.

Mathematical model of thermal and electric processes in the power source–welding arc system at consumable-electrode gas-shielded arc welding described in [1, 4] uses voltage drop in the region of electrode wire contact with the welding torch nozzle, which is assumed to the known. It follows from studies [2, 5–7] that wire temperature T_0 at nozzle outlet can be equal to 150 to 450 °C (lower boundary corresponds to unworn copper nozzle, upper boundary to nozzles from various grades of bronze and cermet at pronounced wear).

To construct a mathematical model and calculate T_0, it is necessary to know the actual value of voltage drop in the nozzle–wire contact and have its analytical description.

A lot of studies are devoted to determination of voltage drop in the region of contact of electrode wire with the welding torch nozzle, U_c, [3, 5–11]. Most of them, however, have deficiencies, not allowing the obtained data to be used in the developed mathematical model. Numerical values of voltage drop in the contact ($U_c = 0.6–0.9$ V) are given only in some studies, for instance [3]. However, such a small U_c value can hardly be obtained on a used nozzle. For instance, in welding with 2 mm austenitic wire with a bronze current-conducting tip, the voltage drop is equal to 2–4 V [11].

A special procedure was developed [12] to obtain more valid information on U_c values, allowing determination of U_c values in the point of electrode wire contact with the welding torch nozzle experimentally, using computer methods for experimental data processing. Also given is the exponential form of approximation of the dependence of U_c value mathematical expectation on current, wire feed rate and its diameter with an unworn copper nozzle, expressed as follows:

$$U_c(d,\ v_f,\ I) = \left[2.55\left(\frac{Id_b}{I_b d}\right)^{0.2} - 1.78\right]\left(\frac{v_f}{v_b}\right)^{0.2}\ [\mathrm{V}], \qquad (1)$$

where d is the electrode wire diameter, mm; v_f is the electrode wire feed rate, m/s; I is the welding current, A; I_b, d_b, v_b are the base values of welding current, electrode diameter and feed rate, respectively ($I_b = 180$ A; $d_b = 1$ mm; $v_b = 0.035$ m/s).

The objective of this study is determination of wire T_0 at nozzle outlet, which requires finding out what fraction of power, evolved in the contact, is applied to the electrode wire.

In studies [2, 5, 9, 13] it is shown that the wire may have several electric contacts in the guide of the current-conducting tip with 440–850 °C temperature [2]. However, their actual number practically does not affect the calculation results, therefore, it is enough to limit our consideration to one contact.

According to Holm theory [10], voltage drop in the contact in our case is focused in the area of elec-

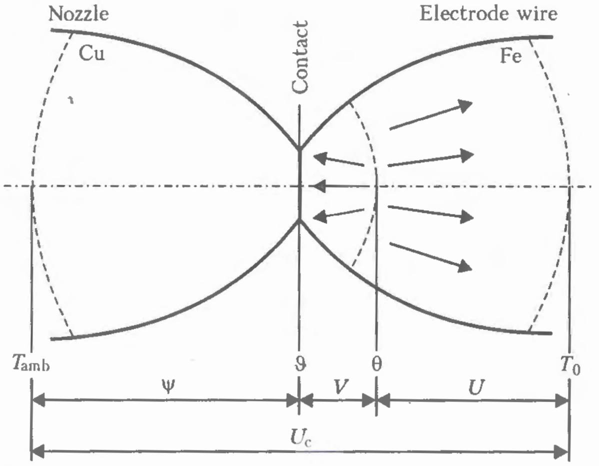

Schematic of temperature distribution and voltage drop in the contraction region of electric contact of two dissimilar metals (according to Holm theory)

trode wire contact with the welding torch nozzle (Figure) and has the following form:

$$U_c = \psi + V + U, \tag{2}$$

where ψ is the voltage drop in the nozzle, V; V is the voltage drop in steel (in electrode wire) from the point of contact to the interface boundary, where the maximum temperature is recorded, V; U is the fraction of contact voltage drop in steel (electrode wire) beyond the boundary of the surface with the maximum temperature, V.

As is seen from the Figure, temperature has a decisive effect on the contact zone resistance [2]. Maximum overheating θ of current contraction zone was recorded not in the point of wire contact with the nozzle, but at a certain distance from it in the steel wire. Heat propagates to both sides from the maximum overheating zone θ, namely into the nozzle and into the electrode wire. However, temperature distribution in them is different, because of different heat conductivity.

Maximum overheating in the wire section near the point of its contact with the nozzle can be expressed as

$$\theta = T_{max} - T_{amb}, \tag{3}$$

where T_{max} is the maximum temperature in the contact zone, K; T_{amb} is the ambient temperature, K. Directly on the wire–nozzle contact boundary the overheating is equal to

$$\vartheta = T_c - N_{amb}, \tag{4}$$

where T_c is the temperature on the boundary of the two metals, K.

For the case of contact of dissimilar metals (copper–steel) with specific electric resistance of metals ρ_{Cu}, ρ_{Fe} and heat conductivity λ_{Cu}, λ_{Fe}, it is exactly the wire that is heated up to maximum temperature.

From similarity of current fields in the contraction region (see the Figure) it follows [10] that

$$\psi \approx (V + U)\,\frac{\rho_{Cu}}{\rho_{Fe}}, \tag{5}$$

hence, expression (2) becomes

$$U_c = (V + U)\left(1 + \frac{\rho_{Cu}}{\rho_{Fe}}\right). \tag{6}$$

Total power evolves in the point of contact of the electrode wire and welding torch nozzle:

$$P_c = U_c\, I = P_n + P_w.$$

A fraction of this total power P_n evolved in the contact of electrode wire with the nozzle, is released from it and dissipated into the environment, while wire heating is performed by only a fraction of total power P_w found from the expression, which allows for (2) and (6):

$$P_w = UI = U_c\, I\,\frac{U}{U + V + \psi} = P_c \times \\ \times \frac{1}{(1 + V/U)\,(1 + \rho_{Cu}/\rho_{Fe})}. \tag{7}$$

According to Holm theory, if a quasi-stationary contact is in place, voltage drop in the electrode wire in the section from the contact to the boundary of the surface with maximum temperature is given by the following expression:

$$V = \sqrt{2\rho_{Fe}\lambda_{Fe}(\theta - \vartheta)}\,, \tag{8}$$

where ρ_{Fe} is the specific electric resistance of the wire, Ohm·m, which is the function of temperature. ρ_{Fe} approximation is given in [4], and approximation of temperature dependence of steel heat conductivity λ_{Fe}, W/(m·K) – in [1].

According to Holm, voltage drop in the electrode wire after the boundary with maximum temperature is equal to

$$U = \sqrt{2\rho_{Fe}\lambda_{Fe}\theta}\,. \tag{9}$$

Solving (8) and (9) we find

$$\frac{V}{U} = \sqrt{1 - \frac{\vartheta}{\theta}}. \tag{10}$$

Voltage drop in the nozzle (by Holm theory) is related to other parameters by a more complex dependence:

$$\psi^2 + 2\psi V = 2\rho_{Cu}\lambda_{Cu}\vartheta. \tag{11}$$

As the electric conductivity of the nozzle metal is much higher than that of electrode wire, then $\psi \ll V$, and expression (11) is simplified:

$$\psi \approx \frac{\rho_{Cu}\lambda_{Cu}\vartheta}{V}. \tag{12}$$

Equating (5) and (12), we have

$$\frac{\rho_{Cu}\lambda_{Cu}\vartheta}{V} = V\left(1 + \frac{U}{V}\right)\frac{\rho_{Cu}}{\rho_{Fe}},$$

whence

$$\rho_{Fe}\lambda_{Cu}\vartheta = V^2\left(1 + \frac{U}{V}\right).$$

Substituting the square of expression (8) instead of V^2 and using (10), after transformations we obtain

$$\frac{\lambda_{Cu}}{2\lambda_{Cu}} = \frac{\theta}{\vartheta}\left[1 - \frac{\vartheta}{\theta} + \sqrt{1 - \frac{\vartheta}{\theta}}\right].$$

Solving this equation for $\sqrt{1 - \vartheta/\theta}$, we get

$$\sqrt{1 - \frac{\vartheta}{\theta}} = \left(1 + \frac{2\lambda_{Fe}}{\lambda_{Cu}}\right)^{-1}. \qquad (13)$$

Allowing for expression (9), let us find

$$\frac{V}{U} = \left(1 + \frac{2\lambda_{Fe}}{\lambda_{Cu}}\right)^{-1}. \qquad (14)$$

Using (7) and (14), the power evolved in the point of contact with the wire can be expressed as

$$P_w = UI = \frac{P_c}{2\left(1 + \frac{\rho_{Cu}}{\rho_{Fe}}\right)}\frac{\left(1 + \frac{2\lambda_{Fe}}{\lambda_{Cu}}\right)}{\left(1 + \frac{2\lambda_{Fe}}{\lambda_{Cu}}\right)},$$

while voltage drop in the electrode wire after the boundary of the surface with the maximum temperature is given by

$$U = \frac{U_c}{2\left(1 + \frac{\rho_{Cu}}{\rho_{Fe}}\right)}\frac{\left(1 + \frac{2\lambda_{Fe}}{\lambda_{Cu}}\right)}{\left(1 + \frac{2\lambda_{Fe}}{\lambda_{Cu}}\right)}. \qquad (15)$$

At $\rho_{Cu}/\rho_{Fe} = 0.093$ and $\lambda_{Fe}/\lambda_{Cu} = 0.1$ (these relations are practically constant in a broad temperature range) value $U = 0.51U_c$.

After U value has been determined, voltage drop in the electrode wire from the contact up to the boundary with the maximum temperature is given by expression (6)

$$V = \frac{U_c}{(1 + \rho_{Cu}/\rho_{Fe})} - U = \frac{U_c}{2(1 + \rho_{Cu}/\rho_{Fe})(1 + \lambda_{Fe}/\lambda_{Cu})}.$$

Using (5) to determine the voltage drop in the nozzle, let us write the following expression:

$$\psi = (V + U)\frac{\rho_{Cu}}{\rho_{Fe}} = \frac{U_c}{1 + \rho_{Fe}/\rho_{Cu}}.$$

Performed calculations allow establishing the fraction of power P_n, applied to the nozzle:

$$P_n = I(V + \psi) = I\frac{U_c}{1 + \rho_{Cu}/\rho_{Fe}}\left(\left(2 + \frac{2\lambda_{Fe}}{\lambda_{Cu}}\right)^{-1} + \frac{\rho_{Cu}}{\rho_{Fe}}\right).$$

Knowing the values of voltage drop in the electrode wire before (V) and after (U) the boundary with maximum temperature, T_{max} can be calculated by (3) and (9):

$$T_{max} = \frac{U^2}{2\rho_{Fe}\lambda_{Fe}} + T_{amb}$$

and temperature on the contact boundary by (4), (9) and (13):

$$T_c = \frac{U^2}{2\rho_{Fe}\lambda_{Fe}}\left[1 - \left(1 + \frac{2\lambda_{Fe}}{\lambda_{Cu}}\right)^{-2}\right] + T_{amb}. \qquad (16)$$

Note that at $U > 0.36$ V and $U_c > 0.706$ V, if $T_{amb} = 20$ °C (293 K), then T_{max} becomes equal to the steel melting temperature, i.e. $T_{max} = T_{st.m} = 1535$ °C (1808 K), and with further increase of U, T_{max} does not rise any more, as part of the heat is consumed in steel melting. In this case, T_c calculations, according to Holm theory, become inaccurate. However, this value can be determined by (16). It is undesirable for the level of T_c values to exceed those of copper melting temperature of $T_{Cu\,m} = 1083$ °C (1356 K), as this imposes a limitation on maximum admissible values of U and U_c.

There exist admissible values of the fraction of total voltage drop U_{ad} and voltage drop in the contact $U_{c.ad}$. Calculation of U_{ad} by (16) at $T_c = 1083$ °C (1356 K), $\lambda_{Cu} = 380$ W/(m·K), $\lambda_{Fe} = 32$ W/(m·K), $\rho_{Fe} = 1.3\cdot10^{-6}$ Ohm·m and $T_{amb} = 20$ °C allows evaluation of the level of voltage drop in the area of contact:

$$U_{ad} = 0.6 \text{ V}; \quad U_{c.ad} = 1.2 \text{ V}.$$

In practice this requirement is often not met [12]. If U_c is greater than the above value, nozzle wear is markedly increased due to its melting. Such welding modes are undesirable, because of shortening of nozzle operating life. To avoid nozzle melting, it is necessary, as follows from formula (1), to impose restrictions on selection of the values of welding current I and electrode wire feed rate v_f.

As follows from (15), the fraction of contact voltage drop in the electrode wire after the boundary with maximum temperature is proportional to thermal power applied to the wire. Therefore, in simplified calculations it may be calculated using the following expressions: for the copper nozzle $U = 0.51U_c$; for bronze $U = 0.60U_c$.

These relationships are calculated at the following thermophysical parameters: $\rho_{Cu} = 1.75\cdot10^{-8}$ Ohm·m; $\rho_{Br} = 19\cdot10^{-8}$ Ohm·m; $\rho_{Fe} = 1.3\cdot10^{-6}$ Ohm·m; $\lambda_{Cu} = 380$ W/(m·K); $\lambda_{Br} = 80$ W/(m·K); $\lambda_{Fe} = 32$ W/(m·K).

Calculations showed that the derived relationships practically do not change at variation of welding parameters and modes.

Parameter	d, mm			
	0.8		1.2	
I, A	100	150	150	200
v_f, m/s	0.083	0.133	0.063	0.137
U_c, V	0.702	1.033	0.664	0.960
U, V	0.358	0.527	0.339	0.490
T_0, K	597.4	574.55	664.4	549.2
T_c, K	830.5	1457	774.4	1299

U values from expression (15) can be used to determine of T_0. U fraction of contact voltage drop in the electrode wire after boundary with temperature T_{max} is connected to T_0 of the wire at the nozzle outlet by a dependence derived in [4]:

$$U = \frac{\gamma v_f}{j}\int\limits_{T_{amb}}^{T_0} C_p(T)dT, \qquad (17)$$

where $\gamma = 7860$ kg/m^3 is the steel density; $j = 4I/\pi d^2$ A/m is the current density in the electrode wire; $C_p(T)$ is the current value of specific isobaric heat capacity of the wire metal, J/(kg·K), which may be determined using an approximation from [4].

Proceeding from [1], allowing for (17), we have

$$T_0 = \mathrm{root}\left[v_f\gamma\int\limits_{T_{amb}}^{x} C_p(\theta)d\theta - jU,\ x\right]. \qquad (18)$$

Here U is calculated from (15). The above-mentioned error of calculation by Holm theory, arising at $U > 0.36$ V and $U_c > 0.706$ V, practically does not affect the accuracy of T_0 determination, as all the heat consumed in the temporary local melting of the metal in T_{max} zone is spent for increasing the average temperature of the wire at nozzle outlet. Expression (18) is used for determination of wire temperature T_0 at nozzle outlet, which is the necessary parameter in construction of a mathematical model of the processes of mechanized gas-shielded welding of steels in the power source–welding arc system.

Calculation results are given in the Table.

CONCLUSIONS

1. The fraction of the total contact voltage drop in the electrode wire after the boundary with the maximum temperature in the nozzle–wire contact was determined, allowing for the Holm theory. This fraction is responsible for electrode wire heating in the nozzle in consumable electrode arc welding. Formulas for its determination were derived.

2. The proposed procedure of establishing the initial temperature of electrode wire T_0 at nozzle outlet can be used to construct a mathematical model of the system of power source–welding arc in mechanized gas-shielded welding of steels.

3. Expressions were obtained for determination of total power evolved in the point of contact of electrode wire and welding head nozzle, as well as expressions, allowing determination of the fraction of this power released into the nozzle and dissipating into the environment, and the fraction removed into the wire as the heat of contact. Values of contact zone overheating were found.

1. Pentegov, I.V., Petrienko, O.I. (2003) Calculation of temperature distribution along the electrode extension, taking into account the heat contributed by the drop. *The Paton Welding J.*, **7**, 19–24.
2. Marishkin, A.K., Popkov, A.M., Postaushkin, V.F. (1970) Melting of electrode wire in automatic welding with systematic short circuits of arc gap. *Avtomatich. Svarka*, **4**, 9–11.
3. Koshkarev, B.T., Mikhajlov, A.N., Budnik, N.M. (1971) Influence of extension on electrode melting process in CO_2 welding. *Svarochn. Proizvodstvo*, **11**, 30–32.
4. Pentegov, I.V., Petrienko, O.I. (2002) Method of calculation of voltage drop along the electrode extension length with allowance for non-linearity of thermophysical parameters. *The Paton Welding J.*, **4**, 27–30.
5. Brigidin, V.Ya. (1979) On operation of current-carrying tips in arc welding. *Svarochn. Proizvodstvo*, **8**, 20–21.
6. Varukha, E.N. (1997) Taking into account the wire preheating in mathematical model of electrode melting in mechanized welding. In: *Proc. of Russian Sci.-Techn. Conf. on Current Problems of Welding Science and Engineering* (Voronezh, 1997). Voronezh: VGASA.
7. (2002) The contact-tube distance in gas-shielded metal-arc welding. How does it work? *Welding and Cutting*, **2**, 80–83.
8. Eichhorn, F., Engel, A. (1971) Verzweigungen des Schweissstromes im Kontaktrohr und der stromfuerenden Schlacke beim Unterpulverschweissen. *Schweissen und Schneiden*, **3**, 27–30.
9. Chubukov, A.A. (1980) Resistance in tip–welding wire contact in CO_2-welding. *Svarochn. Proizvodstvo*, **12**, 31–32.
10. Holm, R. (1961) *Electric contacts*. Ed. by D.E. Bruskin, A.A. Rudnitsky. Moscow: Inostr. Literatura.
11. Brigidin, V.Ya., Konotop, D.A. (1977) Current distribution in contact pair of electrode wire–tip of automatic or semi-automatic welding machine. *Avtomatich. Svarka*, **6**, 21–24.
12. Pentegov, I.V., Petrienko, O.I., Pustovojt, S.V. et al. (2005) Determination of voltage drop in the zone of contact of electrode wire with the welding torch nozzle in mechanized processes of arc welding. *The Paton Welding J.*, **6**, 10–15.
13. Zwickert, H. (1987) Untersuchung der Kontaktverhaeltnisse bei der Stromuebertragung auf den Schweissdraht. *Wissenschaftliche Zeitschrift der Technischen Universitaet «Otto von Guericke»*, **4**, 96–102.

TYPICAL DAMAGES OF WELDED METAL STRUCTURES OF BRIDGES

V.A. KOVTUNENKO, A.G. SINEOK, A.M. GERASIMENKO and **V.A. ZADOROZHNY**
E.O. Paton Electric Welding Institute, NASU, Kiev, Ukraine

Analysis results are presented on characteristic damages of weldments and welded joints in metal structures of active bridge spans in Kiev. Main factors affecting formation and propagation of the above damages are given. The top priority measures aimed at improvement of operational safety of bridges are recommended.

Keywords: welded metal structures, weldments and welded joints, bridge framework, metal structures life, corrosive damage, stress-strained state

More than 20,000 motor-road bridges and viaducts as well as 8050 railway bridges of the total extent 210.4 km are currently in service in Ukraine. Under the action of numerous factors a term of the reliable operation of bridges reduces, various types of damages appear (cracks, deformations, corrosion), which endanger the safe operation of the object and often lead to its emergency condition. To prolong the life of the bridge means to provide a continuous movement of transport on it and to considerably save financial resources.

The results of the analysis of the real condition of bridge metal structures and conditions of their operation [1–4] suggest the revision of the requirements to designing, selection of materials, design solutions, technologies for production and assembling of new constructions as well as research and development of effective solutions for repair of bridges under operation and to increase their service life.

The number of morally and physically obsolete transport structures is continuously growing. The designed service life of many of them is established in the range of 50–100 years. A lack of financial resources allocated for maintenance of the transport objects in the operational condition specifies an importance of effective measures on restoration and prolongation of service life for support structures of bridge frameworks. In this case in condition of scientific and technical progress of the industrial production the requirements to evaluation of engineering bridge structures have correspondingly changed.

In accordance with the effective technical regulations [5] the bridge objects (structures) being in the long-term operation are classified by the following categories of their incompliance with the criteria of the normal operation:

- operational without restriction of the operational period irrespective of separate deviations from the norms of the state standards and specifications;
- with restricted serviceability because of the change of state standards regulating the specified values of the mobile loads towards their increase;
- with restricted serviceability revealed by the evaluation of the technical condition and with a possibility to restore the normal operation by taking special technological measures, for example, repair of a small number of bearing members by welding;
- unserviceable where examination or verification calculation detected inadmissible defects, weakening of the most of support structures; their current condition in accordance with the accepted classification is final and their cannot be put into operation without removal or replacement of damaged structures.

As a result of studies of technical condition of steel and steel reinforced concrete framework carried out by the authors of the project with participation of the specialists of the Laboratory of Welding in Engineering of the E.O. Paton Electric Welding Institute some bridges in Kiev fall under the category of incompliance with the requirements of the normal operation:

- the E.O. Paton bridge is a construction with restricted serviceability; it is required to replace transversal beams, stays, functional welds, steel reinforced concrete plate of the bridge floor;
- the Gavan bridge to the Rybalsky island is the unserviceable construction subject to dissembling due to uncover of the bunch of the bearing bars, corrosive damage of stays of wire ropes with slackening of the section achieving 50–70 %;
- the Park pedestrian bridge to the Trukhanov island is the unserviceable construction where the support components of suspenders should be replaced (repaired); jack beams, knife edges, stays are considerably corroded; control welds should be replaced etc.

Works in the area of determination and study of the actual condition of the metal structures of the operating bridge framework were conducted in compliance with the domestic and foreign technical regulations.

The following typical damages affecting the serviceability and operational usability of metal structures: failure of protection coatings and the subsequent metal corrosion; ruptures and cracks in the parent metal and in welds; imperfections, local flexures, curling; slackening of bolt and rivet joints; cutting of components or their complete dissembling due to laying of communication lines; deformation caused by overloads or heterogeneous settlements and lurches of the ground work; abrasive wear.

Defects and damages of the components in structures depending on the importance of the component for serviceability of the construction on the whole, as well as on a degree of danger of the defect or damage are divided into three categories [6]:

A — defects and damages of critical components and joints dangerous because of a possibility of immediate failure, for example, cracks in the transverse joints of the lower extended booms of the main framework beams;

B — defects and damages with no immediate danger at the moment of their detection but with a possibility to cause eventually the damages in other components (weldments and welded joints) and in the event of their development to turn into the category A, for example, a crack in the longitudinal butt weld of the ribbed plate of the lower boom of the main beam in the immediate vicinity to the cross joint of the lower boom;

C — defects and damages that are not related to the danger of failure, for example, the fatigue crack near the boundary of the cavetto (deconcentrator) in the wall of the transversal beam of the orthotropic plate in the bridge floor in the area of longitudinal rib pass.

As it was mentioned above the defects and damages in the bridge framework may be detected and determined both by visual examination (visual-optical method) and by the methods of modern technical diagnosis.

The visual examination allowed detecting the metal corrosion centers and defects of the outer formation of the weld, namely cracks, raptures, dents, local weakening, leakiness, slackening of the rivet, non-drawn-up bolts and others.

Technical diagnosis allowed detecting internal defects of the welds, a degree of decreasing of the section of bearing members as a result of corrosion, geometrical characteristics of the framework (camber, deviation of the axles etc.). The results of the study of the steel structures showed that corrosion whose development is conditioned by their design and technological imperfections is the main type of their damage.

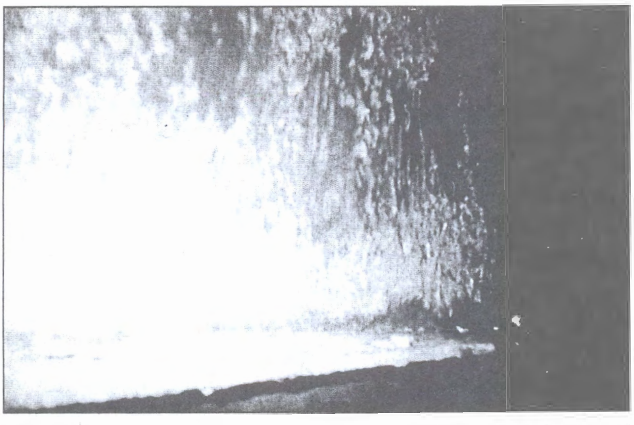

Figure 1. Appearance of corrosion damage on the sites of walls of main beams in the E.O. Paton bridge

Design imperfections include the created pockets and the so-called sacks with poor airing of the surface of the supports (especially in the main hollow beams) as well as the sites with insufficient water drain and breaks where the components are cracked because of corrosion. More often such phenomena take place in the sites where the fillet welds of the lap-welded components are not closed by contour.

The following technological factors contribute to the intensive corrosion:

- poor preparation of the metal surface for precoating and painting (only newly constructed metallic bridges are exposed in the recent time to the blasting treatment of structures at the producing plants);
- unsatisfactory quality of domestic primers and paints used for the bridges constructed 10 years back and earlier;
- the absence of painting and drying chambers on the metalwork plants;
- exclusion of such technological operations as application of protection coatings, degreasing etc.

Combination of design and technological imperfections together with the practice of using conventional constructional steel in the bridges built in the later periods aggravated and enhanced the corrosion processes in the structure.

Thus, a low-carbon steel of M16S grade corresponding to steel 16D (GOST 6713–91) in terms of weldability and other physicomechanical characteristics was used for producing metal structures for frameworks of the E.O. Paton bridge, the Park pedestrian bridge to the Trukhanov island and other bridges in Kiev. However, the lack of copper in composition of this steel specifies its lower corrosion resistance as compared to steel 16D.

As a result of a detailed study of the E.O. Paton bridge performed by the V.N. Shimanovsky UkrNIIPSK together with the E.O. Paton Electric Welding Institute in July–September 2001 the objective data about the condition of the metal structures are received. A degree of the corrosion damage of metallic supports and secondary structures (including main and transversal beams, stays) as well as the condition of the reinforced concrete plate of the bridge floor and the functional welds were estimated in the process of study.

The study was carried out visually using the measurement instruments: magnifier with 8-fold zooming and ultrasonic caliper. Ultrasonic and magnetic-powder methods of non-destructive testing were used for sampling of the welds. These methods allowed detecting the following changes in thickness of the bearing members of the main beams: lower booms of the main beams — from 1.5 to 2.0 %; walls of the main beams in the above-pier sites — up to 3 % (Figure 1); sites of the pier ribs — up to 9 % accompanied by the stratum rust (Figure 2); cross ribs of the lower row by the walls of the main beams — up to 9 %. No damages in the upper boom were detected.

Figure 2. Appearance of corrosion damage of booms, ribs of main beams, joint members in over-supporting members of framework in the E.O. Paton bridge

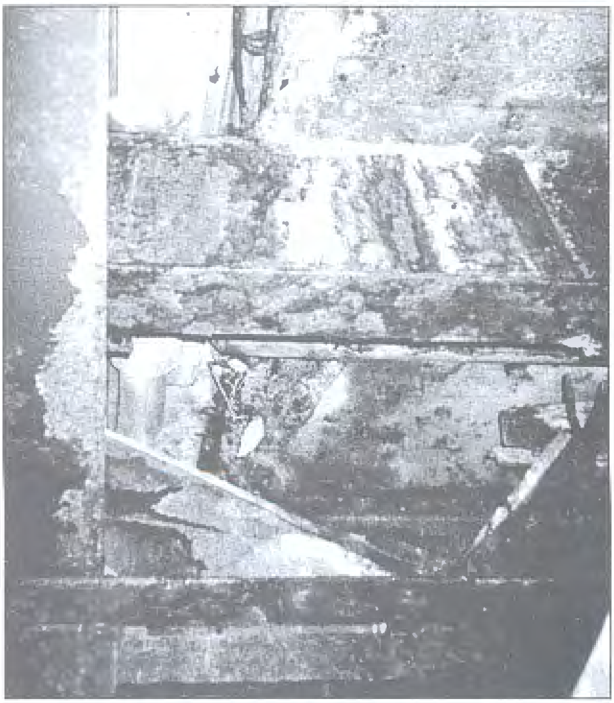

Figure 3. Appearance of corrosion failure of transversal beams in the E.O. Paton bridge

It should be noted that these changes are most of all expressed in the upper and lower lines, i.e. in the sites where the surface of the components is the least air-flown and where the moisture in the form of precipitations and salt used in the cold weather to fight the ice and snow on the bridge floor is accumulated. Moisture and precipitations penetrate without hindrance to the bearing members of the main beams through slots in the steel reinforced concrete plate formed by installing the supporting pillars of bumper beam profile and through completely failed (as a result of 100 % corrosion damage) spouting chutes on the functional welds (Figure 3).

The condition of varnish-and-paint coating on the surface of the bearing members of the main beams is in most cases unsatisfactory. A layer of the old paint more than 1 mm thick was built up due to the repeated painting, which resulted in the peeling off the pain and rolling scale. The air interlayer promotes condensate formation on these sites due to the temperature differential.

The specialists drew attention to the inadmissibility of welding of bearing and secondary members with fillet lap welds without linking up the weld by the bearing contour, which agrees with the results obtained during examination of the object.

Thus, the steel lugs from 12 to 20 mm long are left on the upper longitudinal ribs on the walls of the main beam after assembling. They are most likely the fragments of the components of temporary trestlework removed by the gas-oxygen cutting. These bars are welded by the double angle welds across the section of the longitudinal ribs. Moisture that found its way into the crevice between the planes of the ribs and bars led to the initiation of the active crevice corrosion. As a result one and in some cases two fillet welds ruptured due to thawing (Figure 4). Failures of the fillet welds used to fasten the corners to the vertical corner plates on the walls of the main beam were detected in the sites of the lap welding of the twinned corners. The failures were caused by the crevice corrosion in the sites of the absence of the contour linking-up of the fillet welds of fastening the corners to the corner plates.

Main beams of the E.O. Paton bridge framework can be operational without restrictions of the temporary loads after a set of repair works.

The problems of reinforcing and repair of separate joints and weldments, as well as the issues related to deviation from the current specifications for design and production of the bridge structures employed for a long period of time, will be resolved in development of the bridge renovation project.

Figure 4. Welding with fillet side welds of temporary assembling facilities to cross ribs of main beams in the E.O. Paton bridge

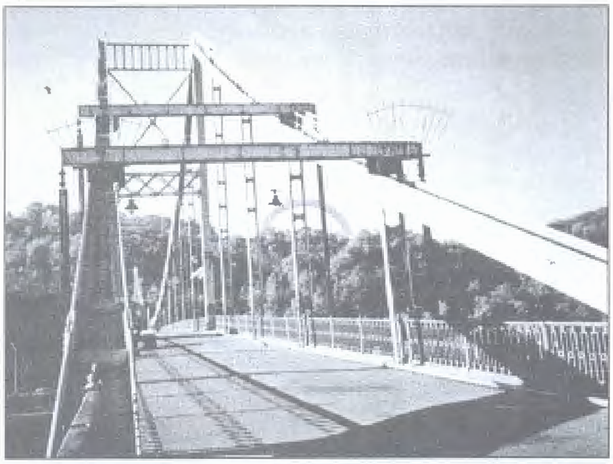

Figure 5. The Park pedestrian bridge to Trukhanov island with devices for unloading of suspension rods

In most cases transversal beams in the E.O. Paton bridge have considerable corrosion failures. As it was mentioned above they are caused by a major failure of the steel reinforced concrete plate of the bridge floor as a result of poor waterproofing and white scouring of concrete, occurrence of moisture and salt in the holes of the plate and the furctional weld chutes. Besides, the sites of installation and location of the transversal beams are poorly ventilated by air. In this case it is also necessary to take into account the heat pipelines under the plate of the bridge floor. Insufficient heat insulation and in some cases even its absence is the reason for temperature differential and thus formation of the condensate.

In the course of the last examination carried out by the specialists of the V.N. Shimanovsky UkrNIIPSK together with the E.O. Paton Electric Welding Institute it was discovered that the service life of the majority of the transversal beams has been already exhausted because of considerable corrosion damage (up to 70 % decrease of the section of the booms and walls). Bridge repair team of the Mostobud company reinforced certain components of the beams, which mostly required restoration of the sections according to the reinforcement scheme proposed by the E.O. Paton Electric Welding Institute. However, during a small period of time the condition of the non-reinforced beams could be characterized as critical while the reinforced transversal beams also suffered considerable corrosion damages — up to 21 % of the section of the walls and up to 19.5 % of the section of lower booms (see Figure 4).

It is not advisable to repair the transversal beams of the mentioned framework due to a corrosion damage of a large area of their surface. The transversal beams in most cases require restoration, which can be implemented by replacing the plate of the bridge floor. Successive replacement of the beams by jacking up separate parts of the steel reinforced concrete plate is unrealistic from the engineering point of view since the plate in this case will be completely destroyed.

Corrosion proved to be the most widely spread damage. It was also detected during examination of the Park pedestrian bridge to the Trukhanov island (Figures 5–7). There are several reasons for such failures.

Little attention was paid to the quality of insulation (protection) of the sites of suspension rods hidden in the concrete during construction of the bridge. At that time there was not reliable technology for the waterproofing in place. No regular inspections of this bridge as well as other bridges to detect defects were carried out, so this facilitated the development of corrosion sites.

Oscillations of the branches of suspension rods caused by the wind are the reason of initiation and development of cracks in the metal of the corners (suspension rods). Taking into account large rigidity of the unit for fastening the suspension rod to the vertical ribs on the wall of the main beams it is easy to imagine that the accumulated cycles of the suspension rod with section of the components changed as a result of corrosion initiated the fatigue crack nucleation in the site of the corner suspension rod fixing into the reinforced cover plate. According to the data of preliminary study such cracks are identified in the sites where the suspension rods were repaired without their preliminary unloading by means of battening plates. Such engineering solution cannot be recognized as a correct one since these joints have inconsiderable endurance because of a sharp change of the shape and

Figure 6. Appearance of fatigue crack in unit of suspension rod fastening in the Park pedestrian bridge to Trukhanov island where a distance between side and end fillet welds is not observed

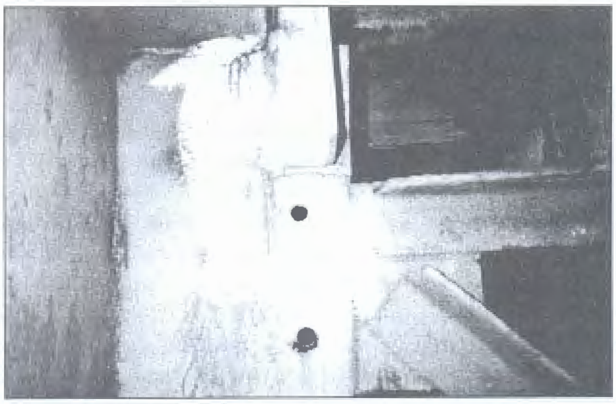

Figure 7. Appearance of longitudinal crack in side fillet weld of fastening of suspension rod to vertical rib on the main beam wall of the Park pedestrian bridge to Trukhanov island

high concentration of stresses. At present the works on restoration of the service life of the suspension rods of this bridge are being completed. Damaged corners are replaced with new ones in all suspension rods.

In addition to corrosion the cracks are another spread type of damages in the operating metallic welded frameworks. In examining the bridge structures a special attention was paid to cracks. In case the cracks were detected the reason of their appearance was determined and a level of their danger to the bearing ability of the bridge was evaluated.

Concentration of stresses, residual welding stresses, fatigue phenomena and increased cold brittleness of metal may be the reasons for crack nucleation.

As a rule, the cracks are initiated under the action of several factors. Most frequently the cracks are formed in the sites of stress concentration where the section of the components considerably changes (breaks of plates, non-smooth change of thickness and width, places of fastening of cover plates, ribs, diaphragms and others). Stress concentration takes place on the non-treated faces of the butt weld joints, in different defects of the welds, such as lacks of fusion by the edges, undercuts of the edges, overlaps, slag inclusions, pores, burn-through, non-filled craters, holes with weak rivets and non-tightened high-strength bolts.

Residual stresses after welding have a significant effect on crack formation. Therefore, the places with clusters of welds were most thoroughly examined.

Little attention was paid to the sequence of producing particular welds at the plants producing the bridge structures when developing the welding-assembling technology. As a result the most critical weldments where the sequence of welding operations determines a level of residual stresses are welded incorrectly, thus the cold cracks are often initiated during turn over of the parts in the shop of the plant.

Various flexures, dents, raptures caused by mechanical actions on the bearing members are a separate group of damages of motor-road and partially pedestrian bridges with a limited passage of transport (Figures 8 and 9). In most cases it is specified by a non-standard size of the bridge floor formed in the times when the design standards did not consider the intensity of transport flows and loads, as well as dimensions of transport facilities.

Technical condition of metal structures of the bridge framework and its belonging to one of the groups were estimated by the results of the visual inspection and test calculation.

Reinforcing and reconstruction of metal structures employing the new repair technology for the first time introduced into production should be carried out with the author's supervision. The design documents specify the necessity of the author's supervision of the introduction of both design and technological developments.

Technology of works on reinforcing the loaded structures should provide a minimally possible weakening (resulted from heating in welding) of the sections of the components to be reinforced. In reinforcing the components of the structures by enlarging the sections with welding the following sequence of works is recommended:

- joining of the reinforcing components by the whole length of the structure using cramps, wedges etc.;
- welding of end sites including the reinforcing components into functioning;
- welding of reinforcing components on tacks with a step 300–500 mm and length 30–50 mm;
- application of initially joining seams, which provide a joint work of the component to be reinforced and the reinforcing component;

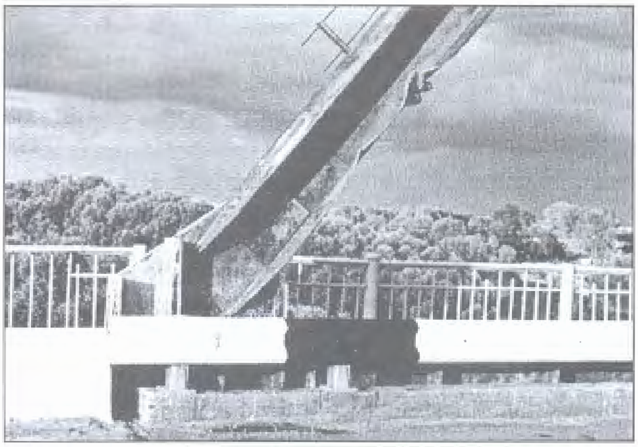

Figure 8. Deformation of support strut of the bridge over Desna river in Chernigov city

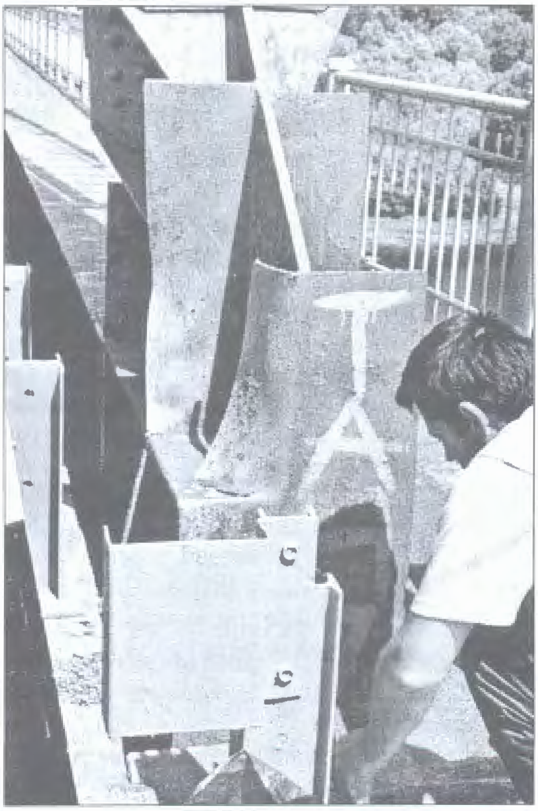

Figure 9. Mechanical damage of support strut of the bridge over Desna river in Chernigov city

- works on reinforcing (welding and cutting operations) when the load from transport is removed (its movement is terminated).

For reinforcing by enlargement of the sections of two or more spans of statically non-determined main beams, it is necessary in the first place to join the reinforcing components in all components to be reinforced on tacks and then to weld the end sites and connecting seams. It is necessary to weld seams of the components to be reinforced beginning from the less loaded span of the structure.

Under two-sided schemes of enlarging the sections it is necessary to weld in the first place the reinforcing components located by the sides of the stretched fibers and then by the sides of the compressed ones. Under two-sided schemes of the reinforcing of beams first the lower stretched reinforcing component is welded and then the upper one.

It is important to avoid application of welds across the acting stresses especially the tensile ones in the components to be reinforced, which are under the load of own weight. If it is impossible to observe this condition it is necessary to develop special technological measures providing safe welding of the structures.

When developing the technology for reinforcing of welded joints in bridges in addition to the mentioned ones it is necessary to observe the following conditions:

- during deposition of supplementary layers heat input into the loaded components should be as less as possible;
- start deposition of the layer in the sites of the defects of the weld to be reinforced (undercuts, overlaps, non-fused craters etc.).

For decreasing a danger of brittle failure in welded joints at lower temperatures the new welds should be located in the structures to be reinforced possibly in the less stressed sections and as far as possible from the places of the section decrease, cuts and ribs. It is necessary to avoid clustering of welds, their intersection at the acute angle as well as closely located parallel butt and filet welds.

As a result of the performed studies the main factors affecting the strength of the bridge framework are determined, analysis of the obtained results is carried out and preliminary recommendations for measures to be taken to increase the safety of the bridge structure operation are developed.

The experts of the E.O. Paton Electric Welding Institute together with the authors of the V.N. Shimanovsky UkrNIIPSK performed a preliminary examination of the E.O. Paton bridge, the Park pedestrian bridge to the Trukhanov island, the bridge to the Rybalsky island and others. In the course of this work a number of damages in the welded joints and weldments are identified, their classification by typical features is carried out and the main factors affecting the formation of these damages are determined. Conclusion on operational strength of the span joints in this bridges and appropriateness of their repair, reinforcing etc. was made for each bridge separately.

Technological cracks related to imperfections of weldment design appear in motor-road bridges and steel reinforced concrete bridges constructed in the 1950s. Often these cracks develop in contour-open welds of the around-welded rib as well as in the sites of deconcentrators and coves. A considerable number of dangers in motor-road bridges (cracks, loss of stability of the form of bearing members, essential decrease of the sections of walls and booms of the main beams resulted from corrosion) appear because of unsatisfactory condition of the leveling devices and functional welds, chutes on the bank risers and the risers that cut the bridge into separate spans. It is necessary to develop the repair technology for every particular case of the detected damages. A decrease of the section of booms and walls of the beams as a result of corrosion is the main damages in the motor road bridges with steel reinforced concrete bridge floor and steel main and transversal beams (for example, the E.O. Paton bridge, the Park pedestrian bridge to the Trukhanov island).

A necessity of the repair of the components exposed to corrosion should be determined depending on their load and a level of damage. As a rule, such components and weldments require reinforcing by introduction of additional sections. On the whole the problem can be solved by application of steel with increased corrosion resistance, design of weldments and joints that exclude formation of non-aired cavities or creation of completely air-tight closed sections, increase of the quality of surface preparation for prime coating and painting as well as the use of the high-quality materials.

1. *SNiP 3.06.07–86*: Bridges and pipes. Rules of inspections and tests. Gosstroj SSSR. Introd. 01.07.87.
2. *VSN 4–81*: Instruction on conducting of inspection of bridges and pipes on highways. Minavtodor RSFSR. Introd. 01.01.82.
3. (1989) *Guidelines on inspection and reinforcement of operated welded span structures*. MPS of Russia, NIIM, LIIZhT. Introd. 01.01.90.
4. (1989) *Manual on design of steel structure reinforcement (to SNiP II-23–81)*. Ukrniiproektstalkonstruktsiya. Moscow: Strojizdat.
5. *DBNV 3-6–2002*: Structures of transportation. Bridges and pipes. Inspections and tests. Derzhbud of Ukraine. Introd. 01.10.2002.
6. *DBN 362–92*: Evaluation of technical state of steel structures, maintained production premises and buildings. Ukrarkhstrojinform. Introd. 01.07.92.

AMORPHOUS FILLER ALLOYS — PROMISING MATERIAL FOR ADVANCED BRAZING PROCESSES (REVIEW)

V.F. KHORUNOV and **S.V. MAKSYMOVA**
E.O. Paton Electric Welding Institute, NASU, Kiev, Ukraine

Different methods for production of alloys in the amorphous and nanocrystalline states are considered. It is shown that the main advantage of amorphous brazing filler alloys is that they are produced in the form of thin ductile foils, which can be used as inserted elements of any shape to fabricate unique structures, primarily for aerospace and nuclear power engineering. High chemical homogeneity of amorphous brazing alloys and their narrow melting point ranges provide good wetting of the surface treated, and reduction of the probability of formation of lacks of penetration and brittle phases, thus ensuring high strength of the brazed joints.

Keywords: *brazing, brazing filler alloys, amorphous and nanostructural alloys, foil, structure, intermetallic compound, strength, ductility*

Nanostructural materials include such metals and alloys, in which one or several structural parameters (e.g. size of crystalline grains or individual phases, thickness of layers in multi-layer coatings) range from fractions to 100 nm in size. Conventional dispersion-strengthened or precipitation-hardening alloys containing very fine particles in their structure, the content of which is no more than 5–10 vol.%, do not belong to nanomaterials [1–3].

Many studies are dedicated to theory and practice of producing alloys in the amorphous state [4–22]. As established, brazing filler alloys in this form can be produced by the following methods: solidification from the liquid or gaseous phase, chemical or electrochemical deposition, or subjecting structure of a crystalline solid to different external effects (e.g. intensive plastic deformation). The above methods allow producing amorphous metallic materials in the form of foils, strips, films, coatings, powders or fibres. The method of super rapid quenching by deposition on a substrate from the gaseous phase makes it possible to form a non-crystalline state even for compositions that resist amorphisation in melt quenching. It should be noted that coatings and films thus produced have lower density than materials subjected to melt quenching. In addition, this method requires very complicated and expensive equipment [7].

The noted peculiarities impose certain limitations on practical application. Amorphous materials produced by physical and chemical deposition differ in structure from materials of the same composition but produced by super rapid quenching from the liquid state. Brazing filler alloys made by super rapid melt quenching can be in the amorphous or fine-crystalline (including nanocrystalline) state. The most common method for production of brazing filler alloys in the amorphous state is rapid (10^4–10^6 K/s) solidification of melt on the external surface of a disk cooler rotating at a high speed [23, 24]. Subjected to the effect of the inert gas pressure, the liquid metal flows through a nozzle and gets on the external surface of a rotating disk, where it solidifies in the form of a thin strip. The strip is then removed from the disk under the effect of centrifugal forces.

In spinning, the initial material can be heated by the high-frequency, resistance, electric arc, plasma or other heating methods. High-frequency heating is used most often. It allow the heating process to be made much quicker, provides increase in productivity, and improves mixing of the melt and chemical homogeneity of the resulting foils. At the same time, with this method it is more difficult to adjust temperature of the melt within the set narrow ranges.

Special requirements are imposed on the material of the disk cooler, its surface finish and beating. The disk material determines the rate of heat removal, adhesion of the melt and heat transfer from it to the cooler. As a rule, the disks are made from copper or bronze. Beating of the disk should not exceed 0.01 mm, its working surface should have no tool marks or scratches, and should be machined to class 7 of the surface finish. Sometimes, a thin coating, e.g. of molybdenum sulphide, can be deposited on the working surface of the disk [25].

Fused quartz, oxide (based on Al_2O_3, ZrO_2, BeO, etc.) or oxygen-free (BN, AlN, BCN, Si_3N_4, etc.) ceramic materials are employed to manufacture crucibles. Quartz crucibles are convenient in operation, but they are resistant to a temperature of no more than about 1500 °C, and may interact with many melts at lower temperatures than their thermal stability limit [7]. Aluminium oxide-based crucibles can operate at higher temperatures (> 1700 °C) and are compatible with the majority of commercial alloys, but they are very sensitive to sudden temperature differences. To increase their heat resistance, ceramic crucibles are coated with organic-silicon compounds or fused SiO_2.

Quality of the amorphous foils depends not only upon the above factors, but also upon other technological parameters of the spinning process. They include liquid metal temperature, nozzle section, disk rotation speed, distance between the disk and nozzle, composition and pressure of gas atmosphere, time of contact of the cooled melt with the disk surface, and angle of collision of a capillary on the disk rim. Necessary overheating of liquid metal prior to its pouring out decreases the cooling rate and, at the same time, reduces viscosity and surface tension of the liquid metal, thus resulting in a thinner amorphous foil [7]. Determination of an optimal value of overheating (above the melting point of an alloy) plays an important role in production of amorphous materials. Overheating by about 75–100 °C is used to produce Ni-base alloys, 30–200 °C – to produce Fe-, Co- and Ni-base alloys, and 100–450 °C – to produce alloys of the Fe–B system.

The method of spinning of a melt on the external surface of the disk is applied at the Institute of Metal Physics and Institute for Materials Science Problems of the National Academy of Sciences of Ukraine to produce rapidly quenched strips in the amorphous and microcrystalline states [7]. The authors of study [23] use this method for production of amorphous and microcrystalline brazing filler alloys in the form of flexible ductile strips 20–100 μm thick and up to 50 mm wide from hard-to-deform brittle alloys.

The main advantage of amorphous brazing filler alloys is that they are ductile, i.e. they can be shaped as required, in spite of the fact that they are made from brittle materials. In addition, these alloys are easy to measure out, as they have the form of thin foils, which makes it possible to place a small amount of an alloy on a large surface. These filler alloys are characterised by the absence of segregation of elements, which usually results from cooling of an ingot. Utilisation of brittle fillers in the form of powders, as was the case before the development of amorphous filler alloys, involves difficulties associated with their uniform distribution over a large surface, removal of a binder during heating in vacuum, formation of high concentrations of a coarse-grained filler at certain points, and substantial increase in oxide contents in the case of fine-grained fillers. The above-noted does not rule out application of the powdered filler alloys in general, e.g. in the form of pastes.

The development of amorphous brazing filler alloys is an outstanding success of materials scientists, which affected advancement of many industries. Amorphous filler alloys led to a breakthrough in brazing by providing the possibility of fabrication of unique structures, and first of all in aerospace and nuclear power engineering, as well as in manufacture of hard-alloy tools. This can be illustrated by an example of such structures as honeycomb panels and compact plate-ribbed heat exchangers of different materials (stainless steels, titanium alloys, refractory metals, etc.). It can be concluded a priori that availability of the technology for production of amorphous alloys is one of the indicators of the technical level of a country as a whole.

As such structures are made primarily from stainless steels and titanium alloys, the focus in most research has been on production of amorphous alloys for brazing these materials [11–24, 26–34]. Domestic and American scientists investigated most comprehensively alloys of the Ni–Cr–Si–B system [11–21]. Such standard filler alloys as BNi-1, BNi-2 and BPr-11 can be readily amorphised to produce foils 0.025–0.050 mm thick. Their boron content is not less than 2.5 %.

In the USA, the B- and Si-containing brazing filler alloys (BNi-1, BNi-2, BNi-3, BNi-4) emerged as early as during the Second World War, in a period of rapid development of aviation. At that time nobody even thought about amorphisation of filler alloys or producing them in the nanocrystalline state. They were brittle and widely applied as powdered filler alloys.

Brazed joints produced with filler alloys BNi-2, BNi-3 and BNi-4 consist of three phases [18]: Ni-based γ-solid solution adjoining the base metal, as well as nickel borides and eutectic consisting of nickel silicides and borides located at the seam centre. Brittle phases in the seam centre determine brittleness of a joint as a whole, and cracks propagate particularly in these phases. The γ-Ni layer that effectively arrests the cracks grows with increase in brazing temperature and holding time at the expense of other phases, as a result of diffusion of boron into the base metal. At a sufficiently high temperature and long holding time the seam is composed only of γ-Ni. The smaller the seam thickness, the faster the transformations. The use of filler alloys in the form of thin amorphous strips allows a substantial decrease in the seam thickness [20, 35, 36]. Thus, decrease in thickness of the 81.2Ni–7.7Cr–4.1B–3.5Si–6.5Fe filler alloy foil from 0.125 to 0.025 mm allows strength of the joint to be raised from 100 to 230 MPa. The fact that the foil is located directly in the gap, and the filler alloy does not need to fill the gap under the effect of capillary forces, as is the case where it is located near the gap, is not less important than small thickness of the alloy.

In 1981, Allied Corporation (USA) received a patent for the homogeneous ductile foil 0.025–0.060 mm thick to be used as a brazing filler alloy. The patent covered all possible modifications of filler alloys containing boron, silicon and phosphorus depressants, wt.%: 0–19 B, 0–12 Si, 0–22 P, 0–4 Fe, 0–21 Cr, and Ni – base. It should be emphasised that any of the above elements may be absent in a specific alloy. Under this patent, Allied Corporation offered a number of alloys to be produced in the amorphous state [14–17]. They include alloys with a high content of boron, silicon, chromium and iron (MBF 10/10A, MBF 15/15A, Table 1), chromium-free alloy (MBF 30/30A), and alloy with a high content of boron and chromium, containing no iron and silicon (MBF 80/80A).

Table 1. Chemical composition and melting range of amorphous nickel-base filler alloys

Filler alloy grade	Content of elements, wt.%							Melting point T_{melt}, brazing temperature T_b (°C), form of filler alloy
	Cr	Si	B	P	Fe	C	Other elements	
MBF 10/10A	13–15	4–5	2.75–3.50	–	4–5	< 0.06	–	970–1040, foil
MBF 15/15A	12–14	4–5	2.5–3.2	–	3.5–5.0	< 0.03	–	Foil
MBF 30/30A	–	4–5	2.75–3.50	–	≤ 0.5	0.06	–	980–1040, foil
MBF 80/80A	14.5–16.0	–	3.17–4.20	–	–	< 0.06	–	T_b = 1175, strip
STEMET 1301	7	4.6	3.1	–	3		–	T_{melt} = 980, T_b = 1010–1177, strip
STEMET 1311	0.4	4	4	–	5		16Co	T_{melt} = 985, T_b = 1020–1050
MBF-50	19	7.3	1.5	–	–		–	
MBF-51	15	7.25	1.4	–	–		–	1030–1126
VPr 11	14–16	4–5	1.8–3.2	–	3–5	0.3–1.0	(0.1–1.0)Al	980–1050
VPr 24	6–7	2.5–3.0	0.2–0.3	–	–		1Ti; (10–12)Nb; (8.5–9.5)W; (1.6–2.0)Mo; (4–5)Al	T_{melt} = 1150–1190, T_b = 1200–1220, powder
VPr 27 (Ni–Cr–Al–B)	–	–	–	–	–	–	–	T_{melt} = 1030–1080, T_b = 1150–1200, amorphous strip
VPr 42 (Ni–Cr–Si–B)	–	–	–	–	–	–	–	1050–1070, powder, paste, amorphous strip

Study [21] focuses on thermal stability of amorphous filler alloy BNi-2, examined by the methods of internal friction, transmission electron microscopy, X-ray diffraction and differential thermal analysis. It is shown that crystallisation begins from a homogeneous nucleation of Ni-based solid solution crystals having a large amount of imperfections, on which the intermetallic phases and borides precipitate afterwards. The crystallisation process ends with removal of imperfections, disappearance of metastable phases and formation of grain boundaries with a low degree of distortion. Results of many-year investigations in this field are presented in study [11]. It is highlighted that boron actively diffuses into stainless steel adjoining the seam during brazing at a high temperature to form boride phases along the grain boundaries. Presence of a large amount of phases leads to decrease in fatigue strength and corrosion resistance of steel. Moreover, a large amount of boron leads to high erosion of thin elements in honeycomb panels and plate-ribbed heat exchangers.

Considering the above-said, the authors of study [11] offer an alloy based on brazing filler alloy BNi-5 (MBF-50, see Table 1), where the boron content is decreased to 1.5 %. The alloy of the Ni–15Cr–7.25Si–1.4B system (MBF-51, see Table 1) offered by the authors permitted production of the amorphous foil 0.05–0.06 mm thick and up to 200 mm wide, which was a major achievement. The authors of study [11] comprehensively investigated properties of the joints subjected to complicated heat treatments, and provided satisfactory properties of the brazed joints. However, borides are detected along the grain boundaries in the base metal adjoining the seam even after optimal heat treatment.

Nevertheless, amorphous filler alloys provide higher properties of the brazed joints than powdered ones, and can replace scarce Au–Ni alloys. Study [37] examined properties of the stainless steel AISI 410 joints produced by using filler alloys of the Ni–82Au and Ni–Cr–Si–B systems (BNi-1, BNi-2 and BNi-3 types). The latter were used in the form of foil 0.036 mm thick. Specimens were brazed in vacuum furnace and subjected after brazing to heat treatment by austenising at a temperature of 982 °C with subsequent quenching in nitrogen and tempering at 565 °C. Results of mechanical tests (shear resistance at 538 °C) and ductility were compared, and corrosion properties in vapours of solution of 10 % NaCl in H_2O at a temperature of 538 °C for 336 h were investigated. All the specimens fractured in base metal during strength tests. It is shown that deformation of the specimens at a twist angle of 90° does not lead to cracking when using the Au-containing filler alloy and BNi-1. The joints brazed using the BNi filler alloy are characterised by a less intensive pitting corrosion of the base metal, compared with the joints brazed using filler alloys of the Ni–82Au system. The joints brazed using filler alloys with a chromium content below 6 % or with no chromium are characterised by the lowest corrosion resistance.

Many different brazing filler alloys, e.g. silver, aluminium or titanium, are used for brazing titanium and its alloys. At the same time, it should be noted

	–14Cu–14	
	20Zr–20Cu–20Ni	
	Ti–15Cu–15Ni	
	Ti–15Cu–25Ni	
Ag	Ag–27Cu–(4–5)Ti	
STEMET 1201	Ti–12Ni–12Zr–24Cu	
STEMET 1202	Ti–12Ni–12Zr–22Cu–1.5Be–0.8V	
STEMET 1203	Ti–50Cu	
STEMET 1204	Cu–28Ti	
STEMET 1406	Zr–11Ti–14Ni–13Cu	
STEMET 1409	Zr–11Ti–14Ni–12Cu–2Nb–1.5Be	750
VPr16	Ti–(22–24)Cu–(8.5–9.5)Ni–(12.0–13.5)Zr	920–97
VPr28	Ti–16.5Cu–15.5Ni–23Zr	850–870

the Ti-base filler alloys have been dominant in
years in the world market. In the USA, it is
e Ti–Cu–Ni system in different forms (rap-
ed, rolled or powdered), and in the CIS
he Ti–Zr–Cu–Ni system, also in different
alloys (Table 2) are close in compo-
tic ones, and provide good mechani-
rrosion resistance of brazed joints.
Cu–Ni system are most suitable
d structures, as they have low
ct to the base metal.
1970s, the A.A. Bajkov
ed research and devel-
rinciples for making
non-ferrous and
on-metallic ele-
) Equipment
alloys in
rphous
eac-

Laves phase, as well as
presence of non-variant t
formation of the above bina
volume-amorphising alloys in
tems of Ti–Cu–Ni, Ti–Zr–Cu–N
Ti, etc. For example, strips more
and rods up to 4 mm in diameter wi
structure were made from alloy 10
High susceptibility of these alloys to
phisation is caused by interaction of binar
allic compounds TiCu, Zr_2Cu, $ZrCu_{3.6}$ and Z
the ternary Laves phase $TiZrCu_4$ [22].

Further efforts on investigation of alloys of
series has been reported in the last years. For examp
brazing filler alloys of the Zr–Ti–Cu–Ni–Mg system
were developed [33, 38]. The alloys have a low critical
cooling rate (10^3–10^4 K/min), which makes it possi-
ble to produce by casting a strip 2–20 mm wide, and
a flat wire 0.8–2.0 mm wide and 0.15–0.30 mm thick
with the amorphous structure. A comparatively low
melting point (805–825 °C) and a thermal expansion
coefficient similar to that of titanium and zircon
vide formation of a brazed joint free from re
es and chemical heterogeneity, having
vacuum tightness and corrosio
he base metal. The strip w
rovides high properti
330 MPa an
s reporte

Table 2. Filler alloys for brazing titanium-base alloys and their properties

Filler alloy grade	Composition, wt.%	T_b, °C	T_{melt}, °C	
			Solidus	Liquidus
TiBraze 375	Ti–37.5Zr–15Cu–10Ni	850–880	825	835
TiBraze 240	Ti–24Zr–16Cu–16Ni–0.5Mo	890–920	835	850
TiBraze 260	Ti–26Zr–14Cu–14Ni–0.5Mo	880–920	840	860
TiBraze 200	Ti–20Zr–20Cu–20Ni	870–900	848	856
TiBraze 15-15	Ti–15Cu–15Ni	980–1050	902	950
TiBraze 15-25	Ti–15Cu–25Ni	930–950	901	915
TiBraze70Ag	Ag–27Cu–(4–5)Ti	850–900	780	800
STEMET 1201	Ti–12Ni–12Zr–24Cu	900–1000	830	955
STEMET 1202	Ti–12Ni–12Zr–22Cu–1.5Be–0.8V	850–950	748	857
STEMET 1203	Ti–50Cu	1000–1050	950	990
STEMET 1204	Cu–28Ti	1000–1100	–	875
STEMET 1406	Zr–11Ti–14Ni–13Cu	900	770	833
STEMET 1409	Zr–11Ti–14Ni–12Cu–2Nb–1.5Be	750–859	685	767
VPr16	Ti–(22–24)Cu–(8.5–9.5)Ni–(12.0–13.5)Zr	920–970	880	890
VPr28	Ti–16.5Cu–15.5Ni–23Zr	850–870	830	840

that the Ti-base filler alloys have been dominant in the last years in the world market. In the USA, it is mostly the Ti–Cu–Ni system in different forms (rapidly quenched, rolled or powdered), and in the CIS countries – the Ti–Zr–Cu–Ni system, also in different forms. All these alloys (Table 2) are close in composition to the eutectic ones, and provide good mechanical properties and corrosion resistance of brazed joints. Alloys of the Ti–Zr–Cu–Ni system are most suitable for brazing of thin-walled structures, as they have low erosion activity with respect to the base metal.

In the second half of the 1970s, the A.A. Bajkov Institute of Metallurgy initiated research and development to elaborate scientific principles for making amorphous alloys based on ferrous, non-ferrous and rare metals, free from amorphising non-metallic elements (boron, phosphorus, silicon, etc.). Equipment was built to produce amorphous metallic alloys in vacuum and inert atmosphere, and new amorphous alloys based on light and refractory, including reactive, metals were developed. Investigation of susceptibility of alloys to amorphisation was conducted with allowance for a certain set of physical-chemical parameters characterising individual properties of the initial components of an alloy (aspect ratio of atomic radii and position in the periodic table), character of their interaction in a given system and calculation of thermodynamic parameters and glass-transition temperature [22, 32]. A relationship was established between susceptibility of alloys to volume amorphisation, their chemical properties and constitutional diagrams. It was found that the volume-amorphising alloys could be produced in eutectic systems, where the high probability exists of formation of two, three or more intermetallic phases with a complex crystalline structure of the Frank–Casper type, e.g. σ- or μ-phase, Laves phase, as well as ternary intermetallics (at the presence of non-variant transformations), along with formation of the above binary intermetallics. Metallic volume-amorphising alloys include alloys of the systems of Ti–Cu–Ni, Ti–Zr–Cu–Ni, Zr–Ti–Ni, Cu–Zr–Ti, etc. For example, strips more than 1.5 mm wide and rods up to 4 mm in diameter with the amorphous structure were made from alloy 10Ti–40Zr–50Cu. High susceptibility of these alloys to volume amorphisation is caused by interaction of binary intermetallic compounds TiCu, Zr_2Cu, $ZrCu_{3.6}$ and ZrCu with the ternary Laves phase $TiZrCu_4$ [22].

Further efforts on investigation of alloys of this series has been reported in the last years. For example, brazing filler alloys of the Zr–Ti–Cu–Ni–Mg system were developed [33, 38]. The alloys have a low critical cooling rate (10^3–10^4 K/min), which makes it possible to produce by casting a strip 2–20 mm wide, and a flat wire 0.8–2.0 mm wide and 0.15–0.30 mm thick with the amorphous structure. A comparatively low melting point (805–825 °C) and a thermal expansion coefficient similar to that of titanium and zirconium provide formation of a brazed joint free from residual stresses and chemical heterogeneity, having strength, ductility, vacuum tightness and corrosion resistance similar to the base metal. The strip withstands up to 10 bends and provides high properties of brazed joints: shear strength 330 MPa and impact toughness 60 J/cm^2 [38]. It is reported [39, 40] that amorphous filler alloys based on titanium and zirconium allow brazing at a temperature below the α–β transformation temperature (880 °C), when the seam metal fully retains the fine structure of the base metal. Some additional decrease in the brazing temperature when using filler alloys based on the Ti–Zr–Cu–Ni was achieved

26] note that the state o
on with a corresponding con-
a melt is fixed in quenching
10^4–10^6 m / s. The amorphous
cture with alloying elements
uted in its volume is formed in
ng to rapid cooling of the homo-

eterogeneity of the filler alloy pro-
ting range and uniform melting of
lk, good wetting of the surface and
tivity of the alloy, as well as high
y of components. This leads to a uni-
on of components within the brazing
the probability of formation of both
ration and brittle phases, and, finally,
mal strength of the joints and their high
sistance. In this case, the brazing zone in
l sense is absent, but there is a narrow zone
alloy components, which is a homogeneous
transition composition [26].
ies dedicated to development of amorphous
alloys are much fewer in number than those
ted to Ni- and Ti-base alloys, but progress in
rea is substantial.
1981, Allied Corporation [41] suggested a ho-
eneous ductile metal-glass foil, containing (at.%)
Ni, 15–20 P, Cu — base, to be used as a filler
y for brazing parts of copper and its alloys. The
t practicable composition of the foil is as follows
.%): 9–11 Ni, 17–19 P, Cu — base. The foil is
25–0.625 mm thick. Solidus temperature of the
loy is about 630 °C, and liquidus temperature is
30–814 °C, depending upon the composition. In 1985,
llied Corporation offered a Cu-base composition [42]
ontaining (at.%) 10–52 Ni, 2–10 Sn, 10–15 P and
Cu — balance, by satisfying a condition of 85–90 %
(Cu + Ni + Sn). Liquidus temperature of the alloys
is 645–863 °C and solidus temperature is 610–825 °C.
The amorphous structure results from a super rapid
quenching at a rate of more than 10^5 °C/s on the
surface of a cooled drum rotating at a high speed.

Study [43] considers physical, technological and
mechanical characteristics of alloys MBF 2002P
(78Cu–10Ni–4Sn–8P) (wt.%) and MBF 2005P
(77Cu–6Ni–10Sn–7P) (wt.%) in the form of foil strips
0.025 mm thick and 25–50 mm wide, produced by
solidification of the melt jet on a rotating copper roll
to achieve a cooling rate of 10^6 °C/s and provide the
amorphous structure of a filler alloy. Melting point
ranges of the alloys are 610–645 and 585–647 °C,
ctively. These alloys can be used to advantage
lver ones. They are less expensive and do
dmium. Their main application
heat exchangers, electric
spreading of

the BAg-1 a
and scandium conta
strength properties of the jo
erosion activity of the alloys. The o
nickel in the alloys is 6 %.

Study [44] is dedicated to measurement of el
cal resistance of Cu–Cu brazed joints produced
traditional silver alloys BAg-1 (45Ag–15Cu–
24Cd), BAg-4 (40Ag–30Cu–25Zn–5Ni) and B
(15Ag–80Cu–5P), as well as amorphous Cu-b
loys METGLASS of the 2002 series (78Cu–10N
8P) and 2005 (77Cu–6Ni–10Sn–7P). Brazing
formed in nitrogen atmosphere at a temperatu
higher than the liquidus temperature of an a
the brazing time was 16 min. The joints bra
amorphous alloys and alloys with a high silv
had close values of electrical conductivity.

As evidenced by the above data, amor
nanocrystalline brazing filler alloys are pr
application in many industries. Therefore
dient to continue investigations in this a

1. Andrievsky, R.A., Glezer, A.M. (1999) Dim
in nanocrystalline materials. Part 1: Peculiar
re. Thermodynamics. Phase equilibria. Kin
Fizika Metallov i Metallovedenie, **1**, 50–73
2. Andrievsky, R.A. (2003) Trends of curren
field of nanoparticles. *Poroshk. Metallurg*
101.
3. Noskova, N.I. (1998) Structure, strength a
nocrystalline and amorphous materials.
Metallovedenie, **2**, 101–116.
4. Kovneristy, Yu.K. (1992) *Amorphous gl*
als. Moscow: Nauka.
5. Lyuborsky, F.E., Devis, H.A., Liberm
(1987) *Amorphous metallic alloys*. Mosc
6. (1984) *Amorphous metallic materials*
khin. Moscow: Nauka.
7. Nemoshkalenko, V.V., Romanov, A.V
(1987) *Amorphous metallic alloys*. K
8. Shpak, A.P., Kunitsky, Yu.A., Lys
and nanostructural materials. Vol.
ka.
9. Kunitsky, Yu.A., Korzhik, V.N
Non-crystalline metallic materia
ring. Kiev: Tekhnika.
10. Kovneristy, Yu.K., Osipov, E
Physical-chemical principles
metallic alloys. Moscow: Nau
11. Rabinkin, A., Wenski, E., F
inless steel using a new MB
us brazing foils. *Welding J*
12. Wittke, K. (1986) Loeten
technik, 36(**3**), 97, 100–1
13. Szewieczek, D., Tyrlik-H
phous ductile tapes of n
ses. *Zvaranie-Svarovan*
14. (1981) METGLASS
alloy). *Alloy Digest*,
15. (1983) METGLASS
alloy). *Ibid*., **7**.
16. (1981) METGLAS
alloy). *Ibid*., **11**/
17. (1983) METGLA
alloy). *Ibid*., **5**/
18. Johnson, R. (19
perature brazin
Amorphous foi

through alloying them with beryllium (STEMET 1202 and 1409) [34].

The authors of study [26] note that the state of oversaturated solid solution with a corresponding concentration of elements in a melt is fixed in quenching of metal melts at rates of 10^4–10^6 m/s. The amorphous or nanocrystalline structure with alloying elements homogeneously distributed in its volume is formed in a solidified alloy owing to rapid cooling of the homogeneous melt.

High chemical heterogeneity of the filler alloy provides a narrow melting range and uniform melting of the alloy in the bulk, good wetting of the surface and high capillary activity of the alloy, as well as high diffusion activity of components. This leads to a uniform distribution of components within the brazing zone, reduces the probability of formation of both lacks of penetration and brittle phases, and, finally, provides optimal strength of the joints and their high corrosion resistance. In this case, the brazing zone in the classical sense is absent, but there is a narrow zone rich in the alloy components, which is a homogeneous alloy of a transition composition [26].

Studies dedicated to development of amorphous Cu-base alloys are much fewer in number than those dedicated to Ni- and Ti-base alloys, but progress in this area is substantial.

In 1981, Allied Corporation [41] suggested a homogeneous ductile metal-glass foil, containing (at.%) 5–10 Ni, 15–20 P, Cu — base, to be used as a filler alloy for brazing parts of copper and its alloys. The most practicable composition of the foil is as follows (wt.%): 9–11 Ni, 17–19 P, Cu — base. The foil is 0.025 – 0.625 mm thick. Solidus temperature of the alloy is about 630 °C, and liquidus temperature is 680–814 °C, depending upon the composition. In 1985, Allied Corporation offered a Cu-base composition [42] containing (at.%) 10–52 Ni, 2–10 Sn, 10–15 P and Cu — balance, by satisfying a condition of 85–90 % (Cu + Ni + Sn). Liquidus temperature of the alloys is 645–863 °C and solidus temperature is 610–825 °C. The amorphous structure results from a super rapid quenching at a rate of more than 10^5 °C/s on the surface of a cooled drum rotating at a high speed.

Study [43] considers physical, technological and mechanical characteristics of alloys MBF 2002P (78Cu–10Ni–4Sn–8P) (wt.%) and MBF 2005P (77Cu–6Ni–10Sn–7P) (wt.%) in the form of foil strips 0.025 mm thick and 25–50 mm wide, produced by solidification of the melt jet on a rotating copper roll to achieve a cooling rate of 10^6 °C/s and provide the amorphous structure of a filler alloy. Melting point ranges of the alloys are 610–645 and 585–647 °C, respectively. These alloys can be used to advantage instead of silver ones. They are less expensive and do not contain toxic cadmium. Their main application fields include manufacture of heat exchangers, electric contacts and copper parts. Wetting and spreading of these alloys are better compared with alloys BAg-1 (~ 40 % Ag) and BCuP-5. Strength properties of the copper joints brazed using these alloys (tensile strength, shear strength, impact toughness) are the same or better than those of the joints brazed using the BAg-1 and BCuP-5 alloys. The amount of nickel and scandium contained in them does not deteriorate strength properties of the joints, and does not increase erosion activity of the alloys. The optimal content of nickel in the alloys is 6 %.

Study [44] is dedicated to measurement of electrical resistance of Cu–Cu brazed joints produced using traditional silver alloys BAg-1 (45Ag–15Cu–16Zn–24Cd), BAg-4 (40Ag–30Cu–25Zn–5Ni) and BCuP-5 (15Ag–80Cu–5P), as well as amorphous Cu-base alloys METGLASS of the 2002 series (78Cu–10Ni–4Sn–8P) and 2005 (77Cu–6Ni–10Sn–7P). Brazing was performed in nitrogen atmosphere at a temperature 100 °C higher than the liquidus temperature of an alloy, and the brazing time was 16 min. The joints brazed using amorphous alloys and alloys with a high silver content had close values of electrical conductivity.

As evidenced by the above data, amorphous and nanocrystalline brazing filler alloys are promising for application in many industries. Therefore, it is expedient to continue investigations in this area.

1. Andrievsky, R.A., Glezer, A.M. (1999) Dimensional effects in nanocrystalline materials. Part 1: Peculiarities of structure. Thermodynamics. Phase equilibria. Kinetic phenomena. *Fizika Metallov i Metallovedenie*, **1**, 50–73.
2. Andrievsky, R.A. (2003) Trends of current research in the field of nanoparticles. *Poroshk. Metallurgiya*, **11/12**, 96–101.
3. Noskova, N.I. (1998) Structure, strength and ductility of nanocrystalline and amorphous materials. *Fizika Metallov i Metallovedenie*, **2**, 101–116.
4. Kovneristy, Yu.K. (1992) *Amorphous glass-metallic materials*. Moscow: Nauka.
5. Lyuborsky, F.E., Devis, H.A., Liberman, Kh.Kh. et al. (1987) *Amorphous metallic alloys*. Moscow: Metallurgiya.
6. (1984) *Amorphous metallic materials*. Ed. by A.I. Manokhin. Moscow: Nauka.
7. Nemoshkalenko, V.V., Romanov, A.V., Iliinsky, A.G. et al. (1987) *Amorphous metallic alloys*. Kiev: Naukova Dumka.
8. Shpak, A.P., Kunitsky, Yu.A., Lysov, V.I. (2002) *Cluster and nanostructural materials*. Vol. 2. Kiev: Akademperiodika.
9. Kunitsky, Yu.A., Korzhik, V.N., Borisov, Yu.S. (1988) *Non-crystalline metallic materials and coatings in engineering*. Kiev: Tekhnika.
10. Kovneristy, Yu.K., Osipov, E.K., Trofimova, U.A. (1983) *Physical-chemical principles of development of amorphous metallic alloys*. Moscow: Nauka.
11. Rabinkin, A., Wenski, E., Ribaudo, A. (1998) Brazing stainless steel using a new MBF-series of Ni–Cr–B–Si amorphous brazing foils. *Welding J.*, **2**, 66–75.
12. Wittke, K. (1986) Loeten mit Amorphen Loeten. *Schweisstechnik*, 36(**3**), 97, 100–102.
13. Szewieczek, D., Tyrlik-Held, J. (1999) Application of amorphous ductile tapes of nickel based alloys in brazing processes. *Zvaranie-Svarovani*, 48(**1**), 3–5.
14. (1981) METGLASS MBF 10/10A (metallic-glass brazing alloy). *Alloy Digest*, **7–9**.
15. (1983) METGLASS MBF 15/15A (metallic-glass brazing alloy). *Ibid.*, **7**.
16. (1981) METGLASS MBF 30/30A (metallic-glass brazing alloy). *Ibid.*, **11/12**.
17. (1983) METGLASS MBF 80/80A (metallic-glass brazing alloy). *Ibid.*, **5/6**.
18. Johnson, R. (1981) The use of TETIG diagrams in high temperature brazing. *Welding J.*, 60(**10**), 185–193.
19. Amorphous foils — a natural for jet tailpipe brazing. *Ibid.*, 62(**10**), 57–58.

20. De Cristofaro, N.J., Sexton, P. *Homogeneous ductile brazing foils*. Pat. 4314661 USA. Publ. 09.02.82.
21. Cieslàk, L., Poloczek, T., Griner, S. (1986) Thermal stability of amorphous BNi-2 alloy. *Archiv Huett.*, 31(**3**), 439–455.
22. Kovneristy, Yu.K. (1999) *Volume-amorphising metallic alloys*. Moscow: Nauka.
23. Kalin, B.A., Fedotov, V.T., Sevryukov, O.N. et al. (1996) Amorphous strip brazing filler alloys. Experience of development of the production and application technology. *Svarochn. Proizvodstvo*, **1**, 15–19.
24. Kalin, B.A., Plyushchev, A.N., Fedotov, V.T. et al. (2001) Influence of structural state of filler alloy on physical-mechanical properties of brazed joints. *Ibid.*, **8**, 38–41.
25. Mulbach, H., Illgen, L., Pfannkuchen, H. et al. *Verfahren zur Herstellung von Halbzeug, insbesondere von Metallbaendern durch Schnellerstarrung*. Pat. 296862 DDR. Int. Cl. B 21 B 1/00, B 22 D 11/06. Publ. 19.12.91.
26. Kalin, B.A., Fedotov, V.T., Sevryukov, O.N. et al. (2001) Experience of application of rapidly quenched brazing filler alloys for joining structural materials. *Perspekt. Materialy*, **6**, 82–87.
27. Plyushchev, A.N., Mamedova, T.T., Fedotov, V.T. et al. (2000) Development of amorphous strip filler alloy for brazing of spacer grid. In: *Proc. of Sci.-Pract. Conf. of Russian Materials Science Societies on New Structural Materials*. Moscow: MIFI.
28. Yurchenko, A.D., Sokolov, V.F., Kutuzov, S.M. et al. (2000) Application of amorphous brazing alloys of the STEMET series in production of dissimilar-metal small-sized parts for nuclear engineering. *Ibid*.
29. Kalin, B.A., Fedotov, V.T., Sevryukov, O.N. (2000) Experience of application of rapidly quenched brazing filler alloys for joining structural materials. *Ibid*.
30. Sevryukov, O.N., Fedotov, V.T. (2000) New amorphous filler alloys for brazing of titanium and its alloys. *Ibid*.
31. Kalin, B.A., Sevryukov, O.N., Fedotov, V.T. et al. (2004) Application of rapidly quenched filler alloys for brazing structural components of fusion reactors. *Svarochn. Proizvodstvo*, **12**, 45–50.
32. Landa, I.A., Kovneristy, Yu.K., Yuriev, A.A. (1991) Calculation of thermodynamic and kinetic characteristics of transition metal melts by the method of non-local model pseudopotential. *Rasplavy*, **2**, 20–38.
33. Korolev, J., Sukhachyov, A., Molokanov, V. et al. (1992) Amorphous solders for brazing products made of titanium and zirconium. *DVS-Berichte*, **148**, 116.
34. Kalin, B.A., Fedotov, V.T., Sevryukov, O.N. et al. (2004) Amorphous brazing filler alloys STEMET. In: *Proc. of Int. Conf. on State-of-the-Art and Prospects of Development of Brazing* (Moscow, Nov. 24–25, 2004). Moscow: TsRDZ.
35. Chekunov, I.P., Orlov, S.V., Arapov, V.S. et al. *Filler alloy for brazing corrosion-resistant steel*. USSR author's cert. 1673352. Int. Cl. B 23 K 35/32. Publ. 30.08.91.
36. (1991) Biegsame Folie zum Hartloeten hat eine Breite von 152 mm. *Maschinenmarkt*, 97(**46**), 172.
37. Bose, D., Datta, A., De Cristofaro, N.J. (1981) Comparison of gold–nickel with nickel base metallic glass brazing foils. *Welding J.*, 60(**10**), 29–34.
38. Chebotnikov, V.N., Sukhachev, A.P., Molokanov, V.V. et al. *Filler alloy for brazing of titanium and its alloys*. USSR author's cert. 1580722. Int. Cl. B 23 K 35/32. Publ. 15.05.91.
39. Ko, M.W., Suzumura, A., Onzama, T. (1990) Brazing of titanium using low melting point Ti-base filler metals. In: *Proc. of Int. Conf. on Titanium Prod. and Appl.* (Dayton, Ohio, 1990). Vol. 2.
40. Watanabe, T., Hoshino, M. (1991) Brazing of titanium using Zr-base filler metals. *Quart. J. JWS*, 9(**3**), 372–379.
41. De Cristofaro, N.J. *Homogeneous brazing foils of copper based metallic glasses*. Pat. 4209570 USA. Int. Cl. C 22 C 9/10, C 25 D 7/06. Publ. 24.06.80.
42. Bose, D., Datta, A., De Cristofaro, N.J. *Homogeneous low melting point copper based alloys*. Pat. 4460658 USA. Int. Cl. C 22 C 9/06, B 22 D 15/02. Publ. 17.07.84.
43. Datta, A., Rabinkin, A., Bose, D. (1984) Rapidly solidified copper-phosphorus base brazing foils. *Welding J.*, 63(**10**), 14–21.
44. Rabinkin, A. (1984) Resistance of copper/copper joints brazed with silver-base and amorphous METGLASS alloys. *Mater. Lett.*, 2(**6A/6B**), 487–491.

TECHNOLOGY FOR REPAIR AND RECONDITIONING OF WORN OUT PISTONS AND OTHER MACHINE AND MECHANISM PARTS

Modern technologies for repair and reconditioning of worn out machine parts and imparting them the initial or even high properties and technical characteristics become increasingly topical under the present conditions of growing shortage of raw materials and energy crisis.

For example, two versions of repair of worn out pistons are available for the ZIL-130 car and «Ikarus» bus pistons: in the first case it is cladding of the worn out cavity under the first compressor impeller using filler wire, and in the second — turning of the worn out piston head with subsequent welding of a band and its machining.

In both cases the repaired piston has higher characteristics of the deposited layer or welded band than base metal of a new piston. Therefore, this guarantees its renewed life not shorter than that of a new part.

Normally, the cost of repair and reconditioning is not in excess of 30–50 % of the initial cost of a new part. Cost effectiveness of the offered technology grows with growth of weight and cost of parts to be repaired.

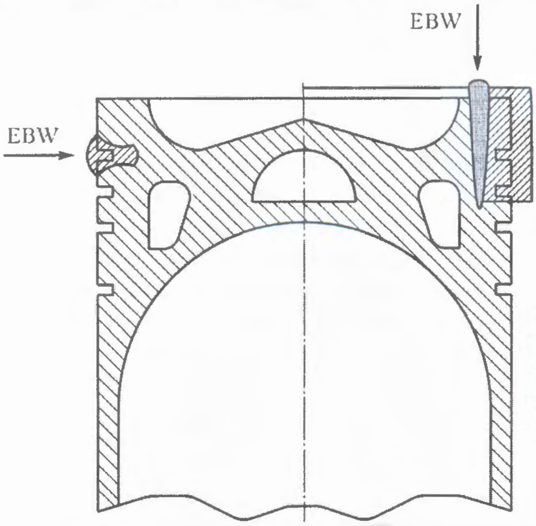

Proposals for co-operation. Development of technical documents, transfer of know-how for the technology, technical consultations and engineering services in commercial application of the technology.

TO THE PROBLEM OF SELECTION OF THE TECHNOLOGY FOR WELDING ELEMENTS OF MCP Dn 850 IN REPLACEMENT OF STEAM GENERATORS PGV-1000M AT NPP

A.K. TSARYUK[1], **V.Yu. SKULSKY**[1], **V.V. VOLKOV**[1], **A.I. BYVALKEVICH**[2], **V.V. PODIACHEV**[2], **N.A. IVANOV**[2], **N.V. NEMLEJ**[3], **A.P. MIROSHNICHENKO**[3] and **A.V. BAZHUKOV**[3]
[1]E.O. Paton Electric Welding Institute, NASU, Kiev, Ukraine
[2]Pilot Enterprise «Atomremontservis», National Atomic Power Generation Company «Energoatom», Slavutich, Ukraine
[3]Pilot Enterprise «Yuzhno-Ukrainskaya» NPP, National Atomic Power Generation Company «Energoatom»,
Yuzhnoukrainsk, Ukraine

It is recommended to use the tested and certified method of automatic argon-arc welding with 0.8–0.9 mm filler wire, instead of manual welding, to produce sound joints between elements of the main circulation piping and steam generator branch pipes. The suggested process allows reduction in labour consumption and welding operation cycle, provides high and consistent quality of welded joints, and makes it possible to decrease dose of the radiation effect on personnel performing welding operations.

Keywords: *arc welding, piping, steam generator, welding technology, non-consumable electrode, welding wire, shielding gas, chemical composition, mechanical properties*

Nuclear power generation makes a substantial contribution to the current economy of Ukraine, i.e. about 50 % of the total power is generated now by 4 nuclear power plants having 15 active power units, which are equipped with reactors of the WWER-1000 and WWER-440 types.

However, nuclear power plants (NPP) are the facilities of a potential technogenic hazard, the accidents at which may lead to irremediable consequences. Therefore, monitoring of the technical state of process equipment and timely repair of damages are the major prerequisites of reliable operation of NPP. As requirements to safety of nuclear power plants are extremely high and are becoming increasingly more stringent, the problem of repair the NPP equipment and piping components to extend their service life takes on special significance.

Steam generators (SG) of the PGV-1000M type operating in the WWER-1000 reactors experience the most severe service conditions [1, 2]. Defects in SG are most often formed in heat exchanger tubes. As no efficient methods are available so far to repair them, after the permissible quantity of defects is exceeded, it is necessary to replace SG that failed, while this involves a package of technological operations to be performed [3]. The most complicated and expensive of them are alignment, welding, heat treatment and inspection of the quality of welded joints between the main circulation piping (MCP) Dn 850 and SG collectors under field conditions. The operation cycle lasts about 20 days. The MCP piping Dn 850 and SG collector are made from alloyed pearlitic steel of the 10GN2MFA grade (TU 108.1197–83), clad from the inside with austenitic steel of the EI-898 grade (04Kh20N10G2B). Thickness of the base pearlitic metal is 60 mm, and that of cladding is 5–7 mm.

At present the main methods used for joining elements of MCP Dn 850 with ST branch pipes are manual arc welding (MAW) using covered electrodes and manual argon-arc welding (MAAW) using tungsten electrodes and a filler [3, 4]. Root welds are made by MAAW with 2–3 mm filler wire Sv-08G2S, and the groove is filled using 4 mm electrodes PT-30. Assembly and welding are performed with preliminary and concurrent heating to a temperature of 120–250 °C. The intermediate cladding layer is deposited with electrodes ZIO-8, and the second layer – with electrodes EA-898/21B. Also, both layers through the entire thickness may be deposited with electrodes of the TsL-25/1 grade.

However, application of MAW and MAAW for joining elements of MCP Dn 850 with SG collectors, where welded joints in equipment and piping of group A belong to category 1 [5–7], involves not only high labour consumption and long welding cycle, but also the necessity to achieve the required quality of welded joints [4]. In this connection, it would be more appropriate to apply mechanised welding for making the above joints.

Traditional MAAW, compared with other welding methods, is a low-efficiency process. However, this welding method has some peculiar advantages, such as high quality of the welds and absence of slag and oxidation on the weld surface. Moreover, in such indicators as density of the weld metal and insignificant quantity of defects this welding method is superior to the majority of traditional methods, having a high deposition efficiency. Owing to stability and possibility of safe operation under different conditions, MAAW can be easily automated and mechanised. In the cases where it is necessary to ensure a high level of mechanical properties, the use is made of automatic argon-arc welding (AAAW) [8, 9].

AAAW is the most reliable welding method in terms of achieving crack-resistant welded joints. Also, AAAW provides the weld root of an optimal geometry [10], requiring no postweld machining, grinding, cleaning, etc.

Analysis of available mechanised welding methods shows that AAAW is most efficient for welding elements of MCP Dn 850. The AAAW technology provides decrease in labour consumed for welding operations, reduction in time needed to perform them, high and consistent quality of welded joints, and decrease in dose of the radiation impact on welding personnel. The experience of application of AAAW for making steel 08Kh18N10T piping Dn 850 in construction of NPP with reactors WWER-440 confirms the high quality of welded joints and efficiency of the said technology [11].

Development of the procedure for performing experimental-technological operations was based on the following premises:

- all efforts associated with development of the technology should be made in full compliance with the regulations and standards in force in nuclear power generation [5–7];
- the AAAW technology should be developed for a design groove preparation (Figure 1) according to [7], as no specialised portable equipment for field machining of branch pipes of the SG collectors with a narrow groove is available now (manufacturer supplies SG with standard grooves in branch pipes);
- AAAW should be used to perform horizontal welds on a vertical plane;
- appropriate welding consumables, temperature of preliminary and concurrent heating, optimal thermal parameters of welding, and postweld heat treatment conditions should be thoroughly selected; the chosen technology should be optimised; physical-chemical properties of welded joints should be studied; the results should be generalised; and technological recommendations should be worked out.

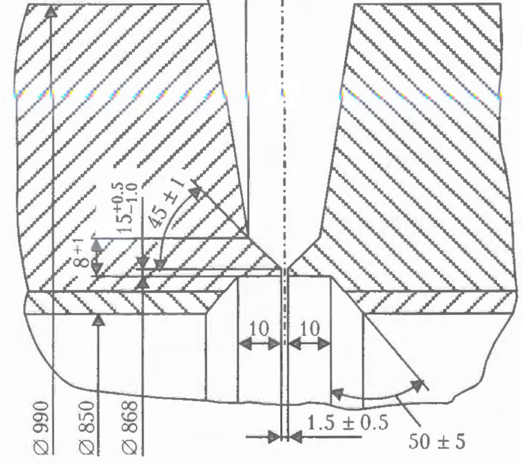

Figure 1. Schematic of standard groove in welded joints made by the AAAW method using non-consumable electrode and welding wire

According to [7], it is recommended to use welding wire of the Sv-10GNMA grade with a silicon content of not less than 0.22 wt.% for argon-arc welding of steel 10GN2MFA. Specifications TU 14-1-2869–79 for the said wire limit its silicon content to no more than 0.30 wt.%. The probability of formation of pores in the argon-arc welds can be eliminated only with the welding wire containing 0.26–0.30 wt.% silicon [4]. As this welding wire is meant primarily for submerged-arc welding, the above content of silicon in it is very uncommon. Besides, such wire is produced only in Russia.

In view of the above-said, to ensure quality and required properties of welded joints in MCP Dn 850 made from clad steel 10GN2MFA by the AAAW method, it is necessary to use standard welding wire with a similar alloying system and silicon content of not less than 0.26–0.30 wt.%. The marketing search for such a welding wire was conducted by comparing similar welding wires produced by different companies, their chemical composition and mechanical properties of deposited metal. The results showed that the domestic welding wire Sv-08G1NMA produced by the «Krodeks» Company (Ukraine) could be a good choice. This wire differs from the baseline grade Sv-10GNMA [7] in an optimal (up to 0.45 wt.%) content of silicon, increased (to 1.5 wt.%) content of manganese, and decreased (to 0.7 wt.%) content of nickel.

While estimating chemical composition of wire Sv-08G1NMA (TU 14-15-373–95), it should be noted that the welding process leads to formation of preconditions for reducing the probability of porosity of the deposited metal, increasing its crack resistance and providing the required level of mechanical properties (exceeding the level of properties of the baseline wire).

Preliminary investigations were conducted to study the possibility of using welding wire Sv-08G1NMA for AAAW of piping elements made from steel 10GN2MFA. The above investigations included selection of optimal gas shielding for non-consumable electrode welding using welding wire Sv-08G1NMA, study of mechanical properties of the weld metal in welded joints of steel 10GN2MFA, and evaluation of quality and structure of the weld and HAZ metal in steel 10GN2MFA allowing for the required postweld heat treatment.

Argon, helium and their mixtures are most extensively used for TIG welding. Several variants of gas shielding were tried out to find the most optimal one for AAAW of steel 10GN2MFA using welding wire Sv-08G1NMA: pure argon, 70 % Ar + 30 % He, 50 % Ar + 50 % He, and 30 % Ar + 70 % He. All these variants of gas shielding provided arc stability and

Table 1. Chemical composition (wt.%) of base and deposited metals

Test object	C	Si	Mn	Cr	Ni	Mo	V	S	P
Steel 10GN2MFA	0.13	0.24	1.29	0.24	1.09	0.48	0.07	0.011	0.019
Welding wire Sv-08G1NMA	0.09	0.66	1.70	0.10	0.68	0.95	0.02	–	–
Weld metal	0.05	0.38	1.31	0.06	0.68	0.60	0.02	0.011	0.019

high quality of the welds. However, shielding of the arc and weld pool from air is more reliable in welding with a standard groove if pure argon is used as a shielding atmosphere, compared with a mixture of helium and argon. The high helium content of a mixture leads to growth of arc voltage and, therefore, temperature of the weld pool. As a result, penetration of the base metal and fluidity of the weld pool increase, this requiring an increased (up to 1800 l/h) consumption of a gas mixture and leading to burnout of alloying elements.

Analysis of different variants of gas shielding shows that AAAW in pure argon is most suitable for welding with the standard groove. This choice is associated, first of all, with the reliability of shielding in pure argon and increased fluidity in the case of welding in a helium and argon mixture. When welding is performed in a narrow groove, a mixture of 30 % Ar + 70 % He and 50 % Ar + 50 % He is indicated to provide a guaranteed fusion of the deposited metal with the groove edges.

10GH2MFA steel plates 350 × 80 mm in size and 40 mm thick were butt joined by AAAW with the standard groove (Figure 1). Welding wire Sv-08G1NMA 0.9 mm in diameter was used as a filler. AAAW of butt joints was performed in flat position.

Quantitative and qualitative estimation methods were employed to study sensitivity of welded joints to cold cracking and determine the temperature of preheating. Quantitative estimation of crack resistance of welded joints in steel 10GN2MFA was made on simulation samples by the implant method, which is based on determination of strength and deformation characteristics of delayed fracture. Qualitative estimation was performed by welding a restraint test sample of the Tekken type. The investigation results show that preliminary and concurrent heating to a temperature of 150 °C is required to provide crack-resistant welded joints made by the AAAW method using filler wire Sv-08G1NMA. This leads to a dramatic growth of the ability of the weld and HAZ metal to withstand a high loading level. In addition, this heating results in decreasing the concentration of diffusible hydrogen in the deposited metal to 1.5 $cm^3/100$ g.

Conditions for making the root weld were selected on the basis of the requirements for providing full penetration and convexity of the weld root [6]: welding current $I_w = 140$ A, arc voltage $U_a = 9.5$ V, welding speed $v_w = 4.5$ m/h, welding wire feed speed $v_f = 400$ m/h (wire is fed to the tailing portion of the weld pool), and argon flow rate – 800 l/h.

Welding conditions for filling the groove were selected on the basis of the results on formation and ensuring of a reliable fusion of the weld with groove walls and between passes: $I_w = 250$ A, $U_a = 11.5$ V, $v_w = 5.5$ m/h, $v_f = 900$ m/h (wire is fed to the leading portion of the weld pool, 3 mm dia. non-consumable electrode – tungsten of the EVT-15 grade) and argon flow rate – 850 l/h.

100 % layer-by-layer visual and measurement inspection was performed during the butt welding process.

After welding, the joints were subjected to heat treatment under the final high tempering conditions [7]: heating to 650 °C, holding at this temperature for 6 h, furnace cooling to 200 °C and air cooling.

Results of ultrasonic (100 %) and X-ray (100 %) inspection showed that welded joints subjected to heat treatment were free from defects. Results of chemical analysis and mechanical tests are given in Tables 1 and 2, respectively. As seen from the obtained data, mechanical properties of the deposited metal meet in full the imposed requirements. Strength characteristics σ_y and σ_t, as well as ductile properties δ_5 and ψ, are higher than the requirements. A critical brittle temperature determined from impact toughness (59 J/cm^2) and toughness of fibres in fracture of destroyed specimens (more than 50 %) corresponds to a temperature of −7 °C, which also correlates with the standards in force [4].

Examinations of macro- and microstructure of welded joints showed that the weld and HAZ metals were free from pores, cracks, lacks of fusion, slag inclusions and other defects. The weld and HAZ metals in the as-welded condition and after heat treatment are characterised by mostly the bainitic structure, as a well as an insignificant amount of the ferrite-pearlite component. This provides good mechanical properties of welded joints and their crack resistance.

Therefore, results of preliminary tests conducted with wire Sv-08G1NMA are indicative of a high quality and required mechanical properties of welded joints in steel 10GN2MFA made by the AAAW method.

Qualification tests of welding wire Sv-08G1NMA were conducted at the «Yuzhno-Ukrainskaya» NPP on a circumferential joint of clad steel 10GN2MFA with an outside diameter of 990 mm and wall thickness of 70 mm.

The groove shape corresponded to the standard one (see Figure 1). Specialised welding equipment AutoTIG 600PC manufactured by the French Company «Polysoude» (Figure 2) was used for welding.

Table 2. Mechanical properties of weld metal in steel 10GN2MFA welded joints made by the AAAW method using welding wire Sv-08G1NMA

Test object	Test temperature, °C	σ_y, MPa	σ_t, MPa	δ_5, %	ψ, %
Weld metal	+20	447.6–495.7 471.7	628.4–648.1 638.3	19.7–26.0 22.9	75.1–76.5 75.8
	+350	437.6–454.1 445.9	587.0–591.6 589.3	25.8–29.3 27.55	73.0–73.2 63.1
Steel 10GN2MFA	+20	594.1 595.2	694.7 689.2	16.0 17.7	45.9 53.0
Requirements acc. to [6] (Appendix 5, Table P5.4)	+20	343	539	16.0	55.0
	+350	294	490	14.0	50.0

Table 2 (cont.)

Test object	*KCV*, J/cm^2, at temperature, °C				Critical brittle temperature, °C
	+20	0	–10	–20	
Weld metal	206.2–215.3 210.9	43.4–146.1 90.4	36.3–73.8 59.1	30.7–41.6 36.2	–7
Steel 10GN2MFA	–	–	–	–	–
Requirements acc. to [6] (Appendix 5, Table P5.4)	–	–	–	–	–10 – +15

Prior to welding, the joints were preheated to 150–200 °C at a rate of not more than 150 °C/h using the Standard Europe 82/6 unit (Company «Weldotherm»). The root weld was made by the AAAW method using 3 mm dia. tungsten electrode of the EVT-15 grade with a pointing angle of 30°. Welding wire was fed to the tailing portion of the weld pool, thus providing the required penetration and back bead formation in the weld root.

Welding parameters in making the root weld and deposition of subsequent layers for filling the groove are given in Table 3. When filling the groove, the welding wire was fed to the leading portion of the weld pool. Arrangement of the beads in welding a joint is shown in Figure 3. Overlap at the start and end of a pass was 20–25 mm. During the groove filling process the weld metal surface was cleaned with a metal brush, and each pass was visually examined. Upon completion of welding, the joint was subjected to thermal «holding» at a temperature of 150 °C for 8 h (according to [7]).

Inspection (100 %) of welded joints was carried out by the ultrasonic, X-ray and capillary methods.

After non-destructive testing, a welded joint was subjected to heat treatment under conditions of final high tempering at a temperature of 650 °C for 6 h.

In accordance with the Program of Qualification Tests of Welding Wire Sv-08G1NMA for Automatic Argon-Arc Welding of Elements of MCP Dn 850 Made from Steel 10GN2MFA, samples were taken and specimens were cut from a welded joint to study physical-

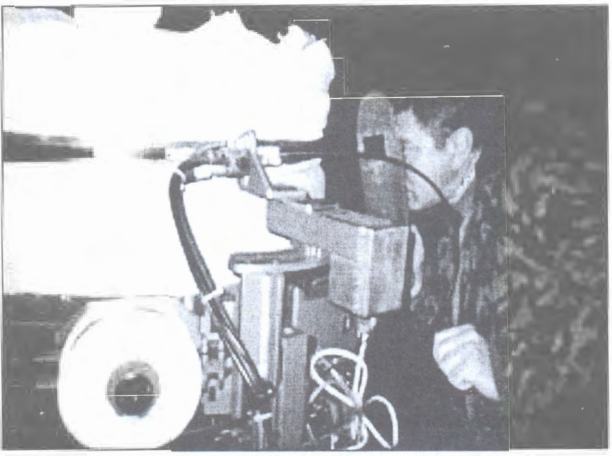

Figure 2. General view of the AutoTIG 600PC device produced by the French Company «Polysoude» for welding of control circumferential joints

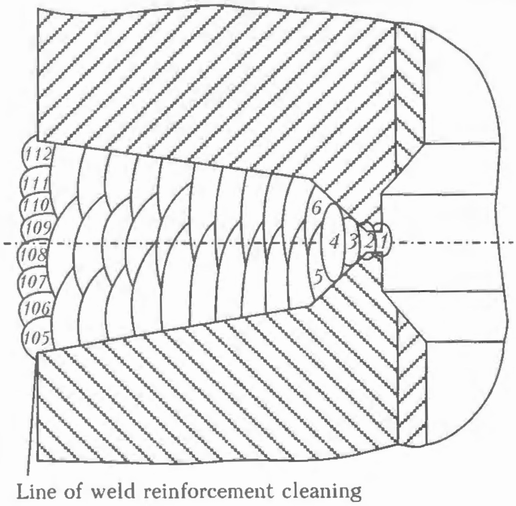

Figure 3. Schematic of arrangement of beads in groove of the full-scale model horizontal butt welded joint on MCP Dn 850: *1* – root pass bead; *2* – smoothing layer; *3, 4* – root weld; *5–8* – intermediate filling layer; *9–104* – main filling layer; *105–112* – weld reinforcement layer

Table 3. Parameters of AAAW in filling the standard groove using 0.9 mm wire

Sequence of filling the standard groove acc. to Figure 3	Welding parameters				
	I_w, A	U_a, V	v_w, mm/min	v_f, mm/min	Time, μs
First root pass (*1*)	150/120	9.5	80	880/360 (to tailing portion of pool)	100/100
Smoothing layer (*2*)	160/90	10.0	86	–	100/100
Third root pass (*3*)*	220/130	11.5	91	2000/1000 (to leading portion of pool)	225/275
Fourth root pass (*4*)	250/150	11.5	89	2600/1300	225/275
Fourth filling layer (*5–8*)	300/180	11.5	89	3400/1620	225/275
Main filling layer (*9–104*)	340/200	12.0	110	3200/1620	225/275
Weld reinforcement layer (*105–112*)	260/110	11.15	80.3	1520/1000	175/325

Notes. 1. Data obtained in a current pulse are given in the numerator, and those obtained in a current pause are given in the denominator. 2. Argon flow rate – 20–25 l/min. 3. Asterisk marks cases when wire is fed to the leading portion of the weld pool in passes 3 to 112.

mechanical properties of the weld metal and welded joints, and determine the critical brittle temperature of the weld metal, as well as sections were prepared for metallographic examinations.

Investigations of distribution of alloying elements through thickness of the weld metal on a steel 10GN2MFA welded joint made by the AAAW method using welding wire Sv-08G1NMA showed that the deposited metal had a uniform chemical composition over the entire cross section area of the weld.

As seen from Figure 4, mechanical properties of the weld metal at room and working temperatures meet all the requirements for the weld metal made by the AAAW method [6]. Results of mechanical tests of welded joints in steel 10GH2MFA indicate that strength properties and ductile characteristics of the welded joints are superior to those of the base metal. Fracture in all the specimens of the welded joints occurred in the base metal at a distance of not less than 8 mm from the fusion line.

Bend angle of test specimens of the welded joints (with a cross section of 35 × 45 mm) is not less that 120°, which is higher than the required value (according to [6], it should be not less than 40°). It should be noted that the test specimens did not only remain intact, but also contained no cracks.

The critical brittle temperature of the weld metal was determined according to [12] by subjecting the weld metal to impact tests on the Charpy specimens with a sharp V-notch (type IX according to GOST 6996–66). Results of these tests shown in Figures 5 and 6 are used as a source information for determination the critical brittle temperature T_{cr}. It is assumed that T_{cr} is a temperature for which the following conditions are met:

- at T_{cr} the arithmetic mean of impact toughness should be not lower than 59 J/cm^2, and minimal value – not lower than 70 % of the above, i.e. not lower than 41.3 J/cm^2;
- at T_{cr} = 30 °C, the arithmetic mean of impact toughness should be not lower than 89 J/cm^2, and minimal value – not lower than 70 % of the above, i.e. not lower than 62.3 J/cm^2; the minimal value of a tough component in fracture should be not lower

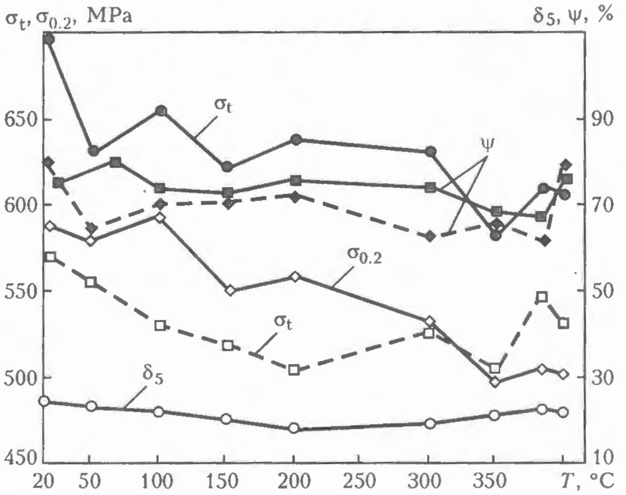

Figure 4. Mechanical properties of the weld metal (*solid curves*) and welded joints in steel 10GN2MFA (*dashed curves*) made by the AAAW method using welding wire Sv-08G1NMA at different test temperatures

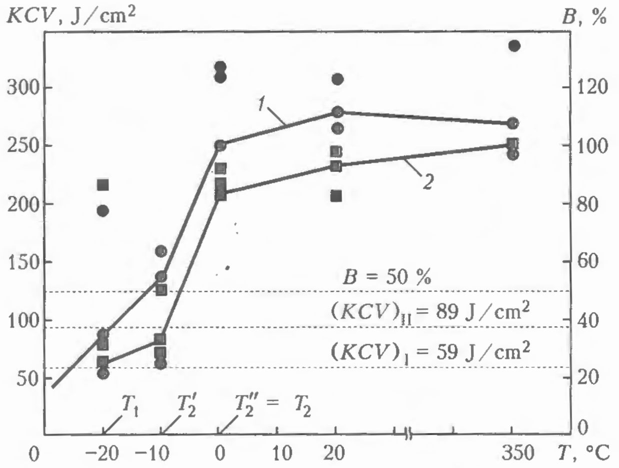

Figure 5. Effect of test temperature of the weld metal on its impact toughness *KCV* (*1*) and quantity of tough fibres *B* (*2*): ●, ■ – experimental points (the rest of the designations are given in [12])

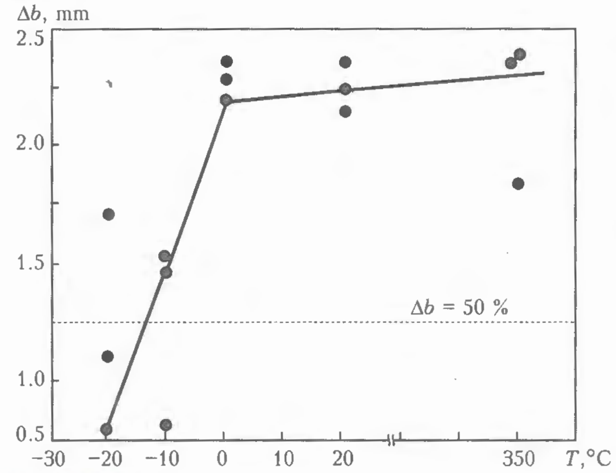

Figure 6. Effect of test temperature on cross section Δb of impact test specimens

than 50 %. Then, on the basis of the calculation recommended in [12], temperature $T_1 = -20$ °C (see Figure 5) is taken as T_{cr}.

Therefore, T_{cr} and mechanical properties of the weld metal and welded joints in steel 10GN2MFA made by the AAAW method using welding wire Sv-08G1NMA meet requirements stipulated in [6].

Examinations of microstructure were conducted as described in study [6], for which templates cut across a welded joint were used. A layered structure of the weld metal was studied to reveal inter-layer and inter-bead defects, and crystalline structure of the weld metal was examined to evaluate integrity and homogeneity of the welds. Analysis of macrostructure of metal of a welded joint shown in Figure 7 indicated that beads had a uniform structure and approximately identical section in the weld metal, and constant width through the entire weld thickness in the HAZ. This suggests that welding conditions were stable during the entire process of making of a joint. No defects were revealed between the beads and between the layers in the weld metal, as well as in the fusion zone. The weld metal was dense. And no defects in the form of cracks, pores, inadmissible clusters of slag inclusions or lack of penetration were detected.

Therefore, the examination results prove that the weld and HAZ metals meet requirements for the quality of the welded joints.

Of notice is a high purity of metal of a welded joint as to non-metallic inclusions, which was shown by microstructural examinations. Detected non-metallic inclusions of the type of complex manganese oxysulphides are fine (less than 0.01 mm in size) and rare. Structure of the weld metal consists of tempered bainite and a ferritic component characterised by small grains (grains have size # 8–9).

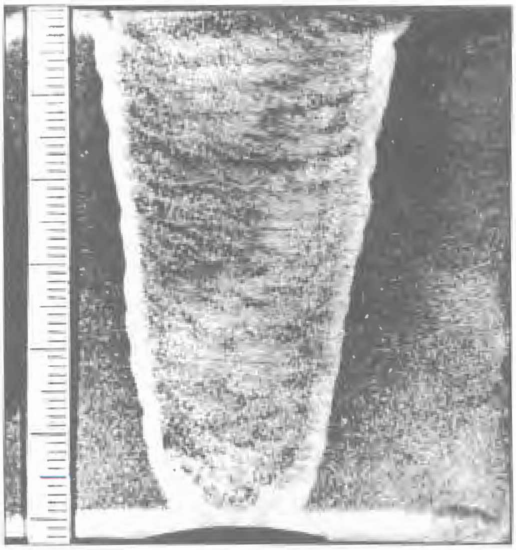

Figure 7. Macrostructure of control welded joint in MCP Dn 850 made by the AAAW method using welding wire Sv-08G1NMA (×2.2)

No coarse-grained region is detected in microstructure of the HAZ metal near the fusion line of a welded joint. This is attributable to the fact that in multi-pass welding the HAZ metal near the fusion line is subjected to heat effect (normalising) and tempering due to making each next pass. As a rule, a fine-grained bainitic-ferritic structure is formed in these regions. Grain size decreases to some extent with distance from the fusion line, and metal structure consists of fine bainite. Then the HAZ gradually transfers to the base metal, the structure of which consists of bainite and a ferrite-carbide component.

As seen from Figure 8, the weld metal has hardness HV 225–230, which is characteristic of the tempered bainite structure. Hardness of the HAZ metal near the fusion line increases to some extent (to HV 240–245) and decreases to the base metal level of HV 185 with distance from the fusion line.

It can be seen from the above data that the character of structure of the weld and HAZ metals of welded joints in steel 10GN2MFA is in good agree-

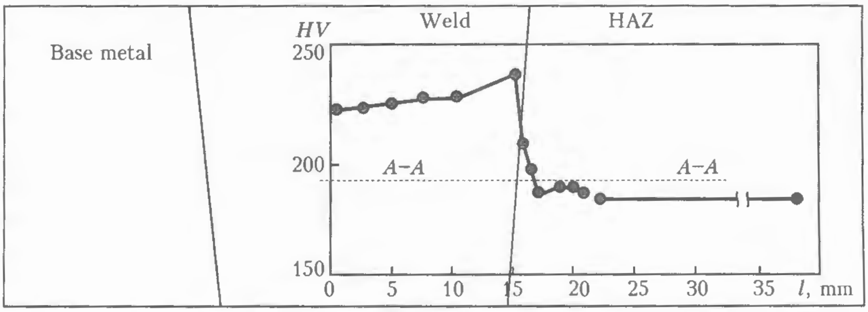

Figure 8. Distribution of hardness in control welded joint in steel 10GN2MFA made by the AAAW method using welding wire Sv-08G1NMA depending upon distance l from the weld centre (dotted line is the line of hardness measurement)

ment with values of distribution of hardness and mechanical properties of the deposited metal and welded joints.

Therefore, the investigation results showed that welded joints in steel 10GN2MFA made by the AAAW method using welding wire Sv-08G1NMA had physical-mechanical properties that meet in full the imposed requirements. The results obtained allow a conclusion (TR-M.1.2.3.4.03.030–02) that welding wire Sv-08G1NMA can be used for AAAW of elements of MCP Dn 850 made from clad steel 10GN2MFA.

For practical application of AAAW using welding wire Sv-08G1NMA, to join elements of MCP Dn 850 in replacement of SG it is required that industrial qualification of the suggested technology should be conducted in accordance with the established procedure.

CONCLUSIONS

1. Multi-pass AAAW using welding wire 0.8–0.9 mm in diameter is recommended for joining elements of MCP Dn 850 of steel 10GN2MFA to SG branch pipes with horizontal welds on a vertical plane.

2. Welding wire Sv-08G1NMA produced by the «Krodeks» Company (Ukraine) was offered, tested and qualified for performing multi-pass AAAW of steel 10GN2MFA.

3. Weld metal in AAAW using wire Sv-08G1NMA has required physical-mechanical properties and necessary level of critical brittle temperature.

4. Industrial qualification tests of the offered technology should be performed to allow practical application of standard-groove AAAW of elements of MCP Dn 850.

1. Kharchenko, V.V., Stepanov, G.V., Romanov, S.V. et al. (2004) Some actual problems of evaluation of strength and life of critical equipment components of NPP in heat-force loading. *Problemy Prochnosti*, **1**, 140–146.
2. Melekhov, R.K., Pokhmursky, V.I. (2003) *Structural materials of power generation equipment*. Kyiv: Naukova Dumka.
3. Kuran, R.I., Tsyba, V.I., Tsaryuk, A.K. (2004) Heat treatment of welded joints of main circulation piping Dn 850 in replacement of steam generators PGV-1000M at the Yuzhno-Ukrainskaya NPP. *Svarshchik*, **1**, 32–34.
4. Belkin, S.A., Ivanova, I.V., Borisenko, M.M. et al. (1992) Properties of welded joints in NPP main circulation loop piping Dn 850 made by automatic argon-arc welding. *Energet. Stroitelstvo*, **5**, 50–55.
5. (1990) *PNAE G-7-008–89*: Rules of arrangement and safe operation of equipment and piping at nuclear power plants. Moscow: Energoatomizdat.
6. (1990) *PNAE G-7-010–89*: Equipment and piping of nuclear power plants. Welded joints and deposited beads. Monitoring rules. Moscow: Energoatomizdat.
7. (1990) *PNAE G-7-009–89*: Equipment and piping of nuclear power plants. Welding and surfacing. Main provisions. Moscow: Energoatomizdat.
8. Poloskov, S.I., Bukarov, V.A., Ishchenko, Yu.S. (2003) Peculiarities of groove filling (deposition) in automatic orbital position butt welding. *Svarochn. Proizvodstvo*, **8**, 3–11.
9. Poloskov, S.I., Ishchenko, Yu.S., Bukarov, V.A. (2003) Minimisation of the probability of formation of exterior defect in welds during automatic orbital welding. *Ibid.*, **10**, 6–13.
10. Poloskov, S.I., Bukarov, V.A., Ishchenko, Yu.S. (2003) Peculiarities of control of the weld root formation in orbital position butt welding. *Ibid.*, **4**, 3–10.
11. Loskutov, M.I., Belkin, S.A., Shefel, V.V. et al. (1976) Automatic welding of the main circulation loop piping at NPP with apparatuses WWER-440. *Energet. Stroitelstvo*, **7**, 7–10.
12. (1989) *PNAE G-7-002–86*: Rates of strength design for NPP equipment and piping. Moscow: Energoatomizdat.

ELECTRON BEAM HARDWARE «UNIVERSAL»

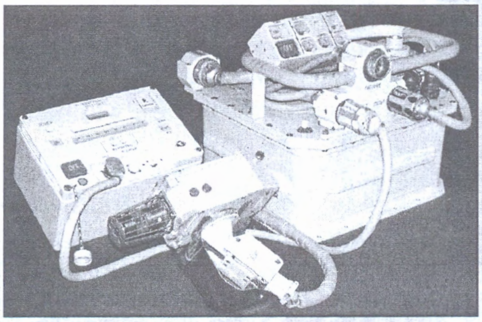

The E.O. Paton Electric Welding Institute developed the electron beam hardware «Universal» to perform assembly and repair welding operations on the external surface of space objects.

The hardware is powered from the DC 28 V mains and comprises a secondary power supply, control panel, test set to check its functioning and a set of electron beam tools for welding (including by feeding a filler wire), cutting, heating and coating by the thermal evaporation method.

Operating voltage of the electron beam gun used with the «Universal» hardware is not in excess of 10 kV, which excludes the need to apply additional X-ray radiation protection means. The electron beam power of up to 1000 W allows welding of stainless steels, titanium and aluminium alloys up to 3 mm thick and their cutting at thickness of up to 1 mm.

Purpose. The hardware can be applied to perform both mechanised (welding manipulators or robots) and manual welding operations (welding operator dressed in spacesuit) under the outer space conditions, as well as for education and training of welding cosmonauts in ground pressure chambers.

MULTI-PASS WELDING OF HEAVY STEEL SECTIONS USING LASER RADIATION

V.D. SHELYAGIN[1], **V.Yu. KHASKIN**[1], **L.G. SHITOVA**[1], **T.N. NABOK**[1], **A.V. SIORA**[1], **A.V. BERNATSKY**[1]
and **T.G. CHIZHSKAYA**[2]
[1]E.O. Paton Electric Welding Institute, NASU, Kiev, Ukraine
[2]National Technical University of Ukraine «Kiev Polytechnic Institute», Kiev, Ukraine

Technology of automated multi-pass laser and laser-arc welding of structural steels with thickness of up to 20 mm is described. Productivity of the hybrid welding method is several times higher compared with laser welding.

Keywords: *laser welding, filler wire, consumable electrode, hybrid process, thick carbon steels, number of passes, conditions, heat input, metallography, structure, hardness, impact toughness*

The industrial demand for improving quality of the welds and productivity of the welding process stimulates upgrading of the existing welding technologies and development of the new ones. Arc welding in active gases, submerged-arc and electroslag welding received wide acceptance for the fabrication of steel structures from carbon steel plates 10–50 mm thick to manufacture sea ships, large-size vessels and oil and gas pipelines [1]. However, besides certain technological advantages, these welding methods also have a number of drawbacks, such as large size of the weld pool and HAZ, susceptibility to hot cracking, high consumption of filler wire, necessity for postweld heat treatment (tempering), presence of high residual thermal strains, requirement for preliminary edge beveling at an angle of 30° or more, and low process productivity.

The E.O. Paton Electric Welding Institute developed a technology for automated multi-pass consumable-electrode narrow-gap arc welding of steels up to 100 mm thick [2]. The distinctive feature of the technology is that the weld edges beveled at an angle of 1.0–1.5° are made with a gap of 10–18 mm on a backing, the welding torch is introduced into the gap, and then the gap is filled with a molten filler wire 1.6 or 2–3 mm in diameter at reciprocating movement of the torch. The process is carried out in the Ar + 20 % CO_2 shielding gas mixture at a speed of 16–22 m/h. To prevent formation of longitudinal hot cracks at the weld centre, welding is performed at a forward angle (the angle is about 30–35°). Electrode extension is adjusted automatically during the welding process.

As proved [2], multi-pass narrow-gap welding provides high mechanical properties of welded joints in thick steel plates without postweld high-temperature heat treatment (normalising), and not only high strength, but also ductility of the weld and HAZ metal. The reason is that in multi-pass welding the subsequent metal layers provide heat treatment of the previously deposited ones, and optimal conditions are created for cooling of the weld bead. The welding process is characterised by a relatively low heat input. The most common drawbacks of narrow-gap arc welding are lacks of fusion between the weld edges, as well as pores, cracks and slag inclusions present in the weld metal [2]. It is rather difficult to remove lacks of fusion and prevent pores and slag inclusions. In addition, cold cracks formed in welding of hardening steels without preheating also present a problem. In this case, the authors recommend to use two- and multi-pass arc welding. To achieve reliability of multi-pass narrow-gap arc welding and quality of the resulting welds, it is necessary to make special measures to ensure a stable position of the arc relative to the weld edges. Various designs of welding heads, guiding contact tubes, torch tips, flat nozzles and process tabs were developed for this purpose.

One of the alternative technologies allowing elimination of the above drawbacks and preservation of the advantages is multi-pass laser welding using filler wire [3]. According to the method offered in this study, steel plates 50 mm thick were butt welded with a serrated groove preparation, width of the groove in the upper part being 6 mm. Welding was performed in five passes using filler wire with a diameter of 1.6–2.0 mm at a speed of 21 m/h and 10 kW power of the CO_2-laser. Argon or helium was used as a shielding gas. A special feature of the process was that laser radiation was focused on the tip of a filler wire, which was fed to the welding zone at an angle of 45°. Melting of the wire resulted in drop-like metal transfer. Temperature of the drops was measured with a pyrometer. This technology allowed avoidance of a limitation of the penetration depth caused by screening of the laser beam by the plasma plume emitted from the keyhole. This screening increases proportionally to the radiation power [4]. The drawbacks of multi-pass laser welding by the method described in study [3] include a comparatively low process productivity, complexity of groove preparation for welding, necessity to use high power (10–15 kW) lasers, and probability of lack of fusion between the filler and base metal.

The purpose of this study consisted in technological validation of multi-pass laser and hybrid laser-arc welding of steels 10–20 mm thick to avoid drawbacks

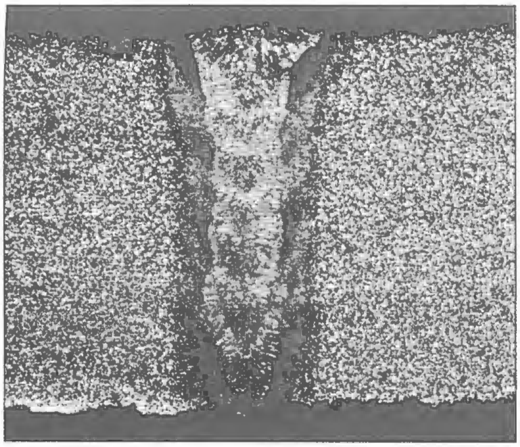

Figure 1. Macrostructure of the butt joint between steel St3ps plates 20 mm thick, made by laser welding in eight passes using filler wire Sv-08G2S 0.8 mm in diameter ($P = 2.8$ kW, $v_w = 12$ m/h, $v_f = 120$ m/h) (×3)

of the multi-pass technologies [2, 3]. Experiments were conducted using equipment, the design and description of which are given in study [5]. Test specimens were made from steels St3ps (semi-killed) and X70 (analogue of steel 10G2FBYu). Filler wire Sv-08G2S with a diameter of 0.8 and 1.2 mm was used for welding. The edges prepared for welding were either square-grooved or with a V- (up to 10°) or Y-groove. In the last case the root face height was 5 mm. Welding was performed in carbon dioxide gas used as a shielding atmosphere. Power P of the laser beam focused on a specimen was 2–3 kW. The electric arc power supply was of the VDU-601 and PSG-500 types. Welding current was $I_w = 120$–230 A, arc voltage was $U_a = 20$–32 V, welding speed v_w was varied from 12 to 56 m/h, and filler wire feed speed v_f was varied from 100 to 400 m/h.

Figure 1 shows macrostructure of the butt joint between the steel plates made by multi-pass laser welding using filler wire. A variant of laser welding of the root weld up to 5 mm high followed by hybrid laser-arc welding to fill the groove (Figure 2) was tried out to raise the process productivity. Variants of one- and two-sided butt welding were studied. Narrow-gap (3 mm) two-pass square-groove laser-arc welding showed promise for the case of a free two-sided access to the joint. A variant of four-pass laser-arc welding was tried out for the case of one-sided access to the joint. This variant turned out to be optimal for conditions of the conducted experiments (Figure 3). In the first three passes the weld aspect ratio was close to 1.0, and in the fourth (last) pass it was close to 1.4.

Sufficiently high quality of the resulting joints was provided in the case of multi-pass laser welding using a filler (see Figure 1). Compared with laser-arc welding, this process is characterised by lower residual strains and a smaller HAZ size. Its drawbacks include the need to perform a large number of passes and a low welding speed. In the case of combining laser and hybrid welding methods, the weld metal was found to be sensitive to formation of pores at the transition point from one metal layer to the other (see Figure 2) under conditions of the conducted experiments. Therefore, the variant of laser welding of the root pass was recommended for making a technological weld, which was to be re-welded further on. It should be noted that in the described experiments the laser and arc power supplies had an insufficient capacity to provide a sound weld in the case of two-sided two-pass welding. The root weld zone contained lacks of fusion between the filler wire and base metals.

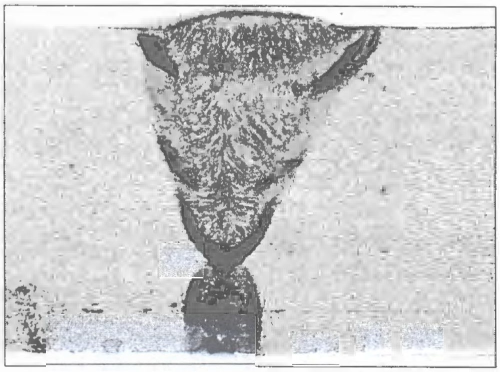

Figure 2. Macrostructure of the butt joint between steel X70 plates 18.7 mm thick, made by the hybrid welding method in three passes with preliminary laser welding of the root pass, using filler wire Sv-08G2S 1.2 mm in diameter ($P = 2.8$ kW, $I_w = 150$ A, $U_a = 26$ V, $v_w = 18$ m/h, $v_f = 240$ m/h) (×3)

It was found that in the case of hybrid welding the laser beam stabilised the welding arc and made it go down into a narrow (up to 10°) gap of the V-groove to a depth of 20 mm. This effect was used as a basis for the development of technologies for hybrid welding of heavy steel sections (see Figure 3). In this case the weld pool has a comparatively small (up to 20–30 mm) size. The rigid thermal cycle characteristic of one-pass laser welding is mitigated due to the arc component. Repeated passes decrease sensitivity of the weld and HAZ metal to the formation of quenching structures. In laser welding of a specimen the macrostructure of which is shown in Figure 1, the heat input per pass was equal to 0.84 MJ/m. In the case of hybrid welding of a specimen (see Figure 3), the heat input per pass was 1.125 MJ/m. Comparing parameters at which the above specimens were produced allows a conclusion that approximately a one-third increase in the heat input leads to a 4 times increase in the productivity of the multi-pass welding process in the case of transition from the laser to hybrid laser-arc welding process. It should be noted that mechanical properties of metal of the joints in pipe steel X80,

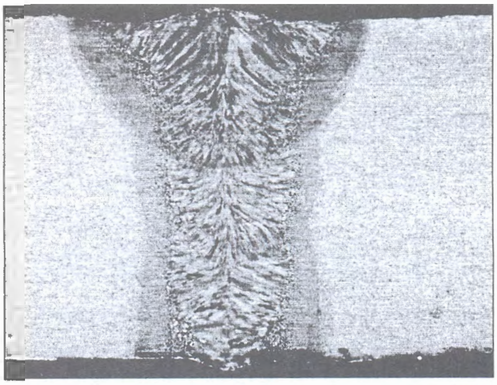

Figure 3. Macrostructure of the butt joint between steel X70 plates 18.7 mm thick, made by the hybrid welding method in four passes using filler wire Sv-08G2S 1.2 mm in diameter ($P = 2.5$ kW, $I_w = 200$ A, $U_a = 26$ V, $v_w = 24$ m/h, $v_f = 400$ m/h) (×3)

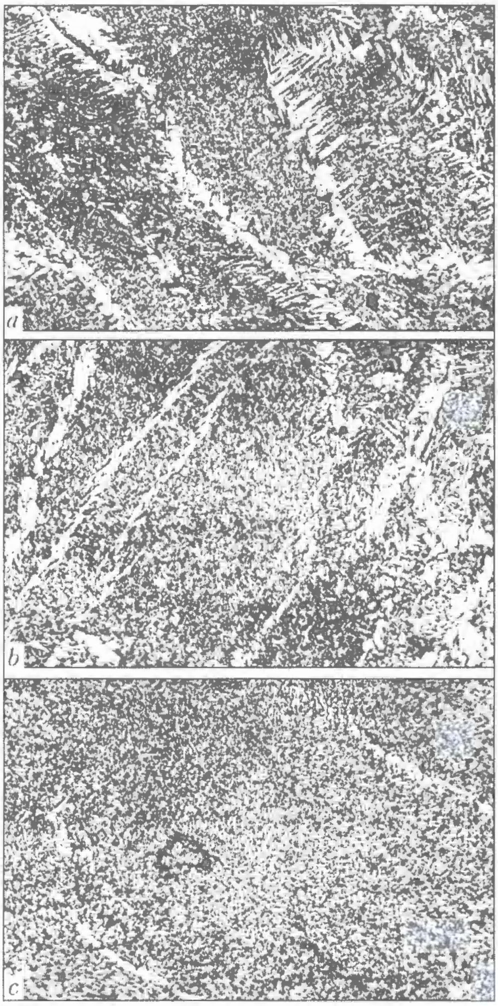

Figure 4. Microstructure of the weld metal (see Figure 3) in the fourth (*a*), second (*b*) and first (*c*) passes (×500)

close to those we obtained, were achieved by five-pass consumable-electrode arc welding at a heat input of about 2 MJ/m [6]. Therefore, hybrid welding is characterised by a heat input that is almost half as that in arc welding and, therefore, by much lower welding strains.

Structure of metal of a welded joint in controlled-rolling steel X70 (see Figure 3) was examined using optical microscope «Nephot-21» with a ×(50–600)-magnification, after etching a section in a solution of 4 % nitric acid in ethyl alcohol. Hardness of the welded joint metal was determined using the LECO hardness meter M-400 at a load of 4.9 N (500 g). It was revealed that structure of the base metal (steel X70) was sufficiently uniform through thickness of the rolled material and consisted of ferrite-pearlite grains with index 7–9 according to scale I (GOST 5639–80). Banded structure of the steel is classified as index 2–3 (GOST 5640–80). Hardness of steel X70 is *HV* 192–205.

Width of the multi-pass weld varies from 4.2 (in the lower part of the first pass) to 11.2 mm (in the upper part of the last fourth pass). Size of the HAZ limited by visible changes in steel structure varies from 1.5 to 3.0 mm, and amounts to 3.7 mm in the first pass. After four passes, the weld is dense, free from pores or cracks. Microstructure of the weld metal is non-uniform through thickness. A mixture of laminated ferrite and ferrite grains of an irregular shape with the MAC-phase of a different packing density degree is formed in the upper part of the weld (Figure 4, *a*), and interlayers of polygonal ferrite up to 0.06 mm thick with precipitates of the disoordered MAC-phase, as well as considerable regions of lateral laminated ferrite with elongated particles of the MAC-phase, are formed along the secondary boundaries. The total content of primary ferrite in the upper part of the weld after the last pass is 30 vol.%. The root part of the weld contains almost no laminated ferrite (Figure 4, *b*). Microstructure of metal of this part of the weld consists mostly of ferrite grains with the close-packed MAC-phase and a bainite component, as well as precipitates up to 0.02 μm thick in mostly lateral laminated ferrite with the ordered MAC-phase. Precipitates of the bainite component dominate in microstructure of the weld metal after the first pass (Figure 4, *c*). Hardness of metal of the welds studied depends upon the peculiarities of its microstructure. The weld metal produced after the fourth (last) pass has hardness ranging from *HV* 220 (in the upper part) to *HV* 245 (in the root part). Hardness of the weld metal in the third and second passes is not in excess of *HV* 250, while in the root part of the first pass it is a bit higher (*HV* 265–270).

Microstructure of metal of the coarse grain region, immediately adjoining the weld, is a mixture of upper and lower bainites with grain of index 4–6 (Figure 5, *a*). No ferrite interlayers along the grain boundaries were revealed. Size of the coarse grain zone varies from 0.7 to 1.3 mm. Maximal hardness of metal of this zone is *HV* 244–249. Structure of metal of the fine-grain zone is 0.8–1.3 mm in size (Figure 5, *b*). Structure of metal of the partial re-crystallisation zone 0.7–1.1 mm in size is composed of loose spheroidised pearlite grains and ferrite grains that underwent almost no changes (Figure 5, *c*).

One of the important parameters characterising mechanical properties of a welded joint is impact toughness a_n (J/cm^2). The latter was determined on standard specimens with U-shaped notch at a temperature of 20 °C. The specimens were cut from a middle part of the joints made by the laser and hybrid welding methods (three specimens of each type). To compare the obtained values of a_n with those of the base metal, two similar specimens were made from the latter and tested (Figure 6). Decrease in impact toughness of the weld metal in all cases was not in excess of 7–8 %, which is a satisfactory indicator of ductility [7]. As expected, when using laser welding with filler wire, impact toughness of the weld metal is higher than of the HAZ, whereas in the case of hybrid welding the situation is reverse.

As shown by the investigations, the weld width and HAZ size increase to a substantial degree in the case of application of the hybrid welding method. Microstructure of the weld and HAZ metal is close to that of the arc welded joints. As found earlier, the laser welded joints in low-alloyed or alloyed pipe steels, including controlled-rolling steels, are characterised by formation of unfavourable structures of in-

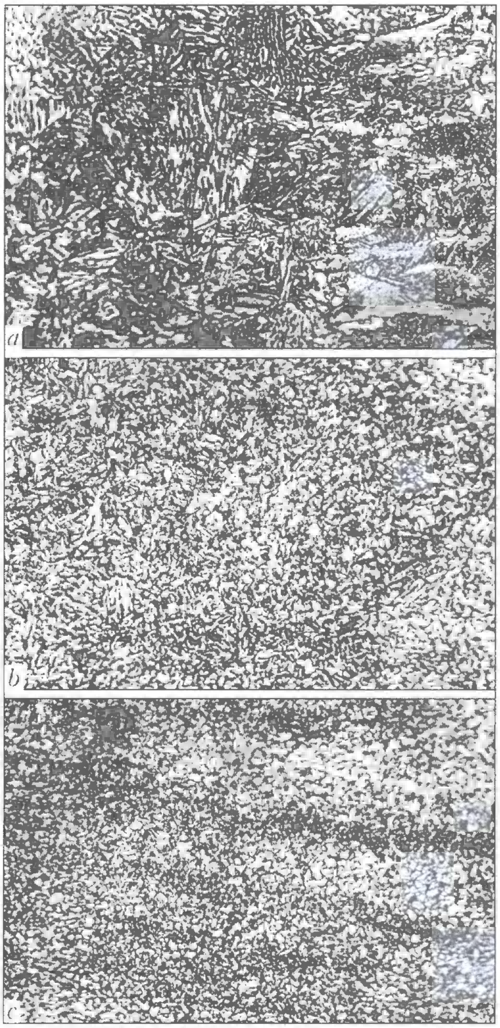

Figure 5. Microstructure of the metal in different weld and HAZ regions (see Figure 3): *a* — coarse grain region; *b* — fine grain region; *c* — partial re-crystallisation region (×500)

creased hardness in the weld and HAZ metal. This makes it necessary to subject workpieces to postweld high-temperature heat treatment. Decreasing the rate of metal cooling by using hybrid welding provides a substantial decrease in the risk of formation of quenching structures (including martensite). Such temperature conditions make it possible to ensure the level of metal hardness equal to *HV* 260, which is recommended by regulatory documents for the arc welding process. In this respect, the use of multi-pass hybrid welding is indicated, as it allows avoidance of heat treatment of welded joints, which is especially important for welding of critical-application pipes made from high-quality controlled-rolling steel.

CONCLUSIONS

1. In narrow-gap laser-arc welding of steels 10–20 mm thick, the arc column is located between the welding wire tip and point of entry of the laser beam into a workpiece. In this case, the arc column is immersed into a narrow (2–3 mm) gap to a depth of 20 mm, and the power supply features stable electrodynamic characteristics.

2. The multi-pass laser and laser-arc welding methods provide sound butt welded joints in steel plates of large thickness (10–20 mm). Metal hardness is *HV* 260–280, and impact toughness is close to that of the base metal at a temperature of 20 °C. Size of the weld pool and HAZ in this case decrease 5–10 times compared with arc welding of steels of a similar thickness.

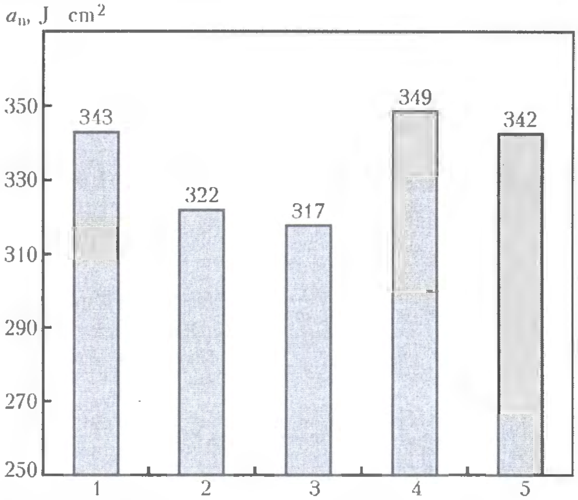

Figure 6. Impact toughness a_n at a temperature of 20 °C of the joints, made in steel X70 by the multi-pass laser and hybrid welding methods using filler wire Sv-08G2S: *1, 2* — metal of laser weld and HAZ, respectively; *3, 4* — metal of hybrid weld and HAZ, respectively; *5* — base metal

3. In the case of hybrid welding, the arc component allows the welding thermal cycle to be controlled and its rigidity to be decreased due to increasing flatness of a rear front and preservation of its steepness. This prevents the risk of formation of quenching structures in welding of low-alloyed steels and leads to increase in impact toughness of the welded joint metal.

4. In multi-pass laser and laser-arc welding, the subsequent pass provides heat treatment of the previous one, thus creating conditions for decreasing the rate of cooling of a metal welded. This makes it unnecessary to subject large-size welded structures to finishing heat treatment.

5. Comparison of multi-pass laser welding using filler wire and hybrid laser-arc welding shows that the presence of the arc component provides a one-third increase in heat input of the process. In this case the productivity of the hybrid welding process grows several times, compared with multi-pass laser welding.

1. (1974) *Technology of electric welding of metals and alloys.* Ed. by B.E. Paton. Moscow: Mashinostroenie.
2. Nazarchuk, A.T., Sterenbogen, Yu.A. (1984) Narrow-gap gas-shielded arc welding and some of its peculiarities. *Avtomatich. Svarka*, **5**, 57–62.
3. Arata, Y., Maruo, H., Miyamoto, I. et al. (1986) CO_2 laser welding of thick plate and multipass welding with filler wire. In: *Proc. of Int. Conf. on Electron and Laser Beam Welding* (Tokyo, July 14–15, 1986). Oxford.
4. Grigoriants, A.G., Shiganov, I.N. (1988) *Laser technique and technology.* Manual for higher-education institutions. Book 5: Laser welding of metals. Ed. by A.G. Grigoriants. Moscow: Vysshaya Shkola.
5. Shelyagin, V.D., Khaskin, V.Yu., Garashchuk, V.P. et al. (2002) Hybrid CO_2-laser and CO_2 consumable-arc welding. *The Paton Welding J.*, **10**, 35–37.
6. Motohashi, H., Hagiwara, N., Masuda, T. (2004) Tensile properties and microstructure of weld metal of X80 steel by MAG welding. *Quart. J. JWS*, 22(**1**), 69–77.
7. Semyonov, S.E., Mandelberg, S.L., Goncharenko, L.V. (1989) Optimal level of impact strength of weld metal of gas pipeline pipes. *Avtomatich. Svarka*, **11**, 55–57.

CALCULATION OF PRODUCTIVITY OF LOCAL EXHAUST VENTILATION FOR CONDITIONS OF THE FLUX-CORED STRIP SURFACING

O.G. LEVCHENKO[1] and **V.V. CHIGAREV**[2]
[1]E.O. Paton Electric Welding Institute, NASU, Kiev, Ukraine
[2]Priazovsky Technical University, Mariupol, Ukraine

Peculiarities of selection of optimal parameters for local exhaust ventilation, allowing for the air velocity within the arc zone and amount of the removed air, are considered in terms of improvement of the efficiency of entrapping harmful materials from the flux-cored strip surfacing zone.

Keywords: welding aerosols, harmful substances, concentration, filter-ventilation assemblies, arc surfacing, flux-cored strip, volume of removed air, calculations

Local exhaust systems together with filter-ventilation assemblies are the most effective means for protection of production and natural environment from harmful substances formed in the process of electric-arc welding (surfacing). They entrap welding aerosols (WA) directly in the welding zone, purify air from them and then return the purified air back to the premises, thus solving hygienic, ecological and economical problems [1]. The main task in calculation of the local exhaust systems for the working place of the welders is to determine the speed of the air removal from the source of the WA formation, which provides high efficiency (at least 75 vol.%) of the removal of harmful substances according to the effective standards [2]. The rest volume ratio of WA (25 %) should be diluted to the maximum allowable concentration (MAC) by means of the general ventilation. In this case the main requirement to the air of the working zone (according to GOST 12.1.005–88) is a decrease of the concentration of harmful substances in the air of the working zone down to MAC.

In order to provide efficiency of the WA removal it is necessary to take into account that the efficiency depends on the characteristics of the exhaust system (form, conditions of the air entrance into the suction hole), a source of release of the harmful substances (welding method, type of welding equipment, grade of welding consumables), conditions of the air inflow into the suction hole (a sized and a form of the limiting surfaces) and on a distance between the exhaust system and the source of the WA formation (welding arc). Besides, it is necessary to consider that the flow of the air removed by the local exhaust practically always correlates in the welding processes with the shielding atmosphere, which may lead (with certain consumption of the removed air) to the unfavorable consequences — changes in the chemical composition of the deposited metal. The speed of the air removal should be established so that to avoid disturbance of the gas shield of the molten metal. For effective WA trapping it is enough to provide in the surfacing zone (near the arc) the required speed of the movement of the air to be removed through the suction hole. Therefore, calculation of the parameters of the local exhaust is reduced to determination of the air speed in the suction zone, selection of a distance for effective WA trapping and achievement of the required movement speed of the air to be removed [3]. Efficiency of the WA trapping increases in direct proportion to the indicated speed. Power of the welding arc, the availability of the gas shield and a number of other factors affect the selection of the values of the speed in the zone of welding (surfacing). The speed varies within 0.2–0.5 m/s depending on the method of welding [2]. So, the intensity of the WA formation in automatic surfacing with flux-cored strips is several times higher than in manual arc welding with coated electrodes and surfacing with flux-cored wires [4]. Therefore, facilities of the local ventilation used for the indicated welding methods [1] do not provide an effective WA removal from the zone of flux-cored strip surfacing.

The aim of this work is to choose the optimal parameters of the local exhaust ventilation (speed and the volume of the removed air) for increasing efficiency of the trapping of harmful substances from the zone of flux-cored strip surfacing.

The air suction speed is studied for its effect on the variations of the chemical composition of the metal produced by the surfacing with flux-cored strip of PL-AN-101 type with the core of different composition. For one set of experiments the flux-cored strip with the core of a complex-alloyed alloy was used, for another set of experiment the core was made of mechanical mixture of the same components as in the alloy, which allows producing the metal of the sormite-1 type in the surfacing. A shell of the flux-cored strip consisted of two steel strips 0.4 × 24 and 0.4 × 22 mm in size connected with a help of the lock into a single strip with a section of the rectangular form 3 × 19 mm in size. Mechanical mixture of the components of the flux-cored strip core consisted of the powders of ferrochrome, graphite, ferromanganese, nickel, ferrosilicon, aluminium and manganese.

Effect of air suction speed on chemical composition of deposited metal

Composition of flux-cored strip core	Speed of air movement, m/s		Chemical composition, wt.%					HRC
	At the level of weld	At the level of suction	C	Mn	Si	Cr	Ni	
Mechanical mixture of components	0.8	9.0	2.80	1.80	2.40	23.1	2.92	52
	0.8	9.0	2.80	1.50	2.40	20.5	2.30	51
	0.8	9.0	2.65	1.33	2.54	21.0	2.46	50
	0.5	6.4	2.55	1.52	2.35	22.0	3.02	51
	0.5	6.4	3.15	1.40	2.30	19.7	2.76	49
	0.2	2.5	2.50	1.50	3.00	23.4	3.02	50
	Without suction	Without suction	2.55	1.44	2.99	20.6	2.82	50
Complex-alloyed alloy	0.8	9.0	2.75	2.12	3.06	24.2	3.80	52
	0.8	9.0	2.80	1.50	2.96	23.7	3.01	53
	0.8	9.0	2.90	1.50	2.54	23.5	3.02	50
	0.5	6.4	2.75	1.83	2.55	22.8	3.50	52
	0.5	6.4	2.80	1.50	2.58	20.5	2.79	53
	0.2	2.5	2.70	1.50	2.04	22.1	2.79	52
	Without suction	Without suction	2.71	1.40	2.15	20.4	2.66	52

The complex alloy included the same elements but preliminary fused. Al–Mg mixture of powders in correlation 1:1 was additionally introduced during preparation of the core of the flux-cored strip. The flux-cored strips were produced with observation of technological conditions that remained constant during the whole process of the drawing on the mill.

The experiments were carried out on the following conditions: direct welding current (reverse polarity) $I_w = 750–800$ A; arc voltage $U_a = 30–32$ V; surfacing speed $v_s = 36.5$ m/h.

Speed of the air suction depending on the position of the flue damper at the level of the air-intake device was 9.0, 6.4 and 2.5 m/s while at the level of welding arc (level of the weld) it was 0.8, 0.5 and 0.2 m/s. Small values of this speed was determined by means of the hot-wire anemometer. Reliability of the data on the necessary chemical composition and hardness of the deposited metal was achieved by an increase of the number of measurements [5]. The obtained data are presented in the Table.

It was established as a result of the study that the speed of the air movement at the level of arc within 0.2–0.6 m/s does not have an essential effect on the chemical composition and hardness of the deposited metal. Further increase of this speed leads to a noticeable change of these parameters. Therefore, to increase efficiency of the WA trapping by the local exhaust the permissible speed of the air removal may be increased from 0.5 (as accepted for arc welding [2]) to 0.8 m/s. Proceeding from the value of the air movement speed the volume of the air L removed by the local exhaust (m^3/h) is calculated:

$$L = 3600 F_0 v_0, \qquad (1)$$

where F_0 is the area of the suction hole, m^2; v_0 is the rated speed of the air movement in this hole, m/s. F_0 values are determined by the design peculiarities of the technological equipment and the chosen suction hole, v_0 is obtained taking into account the conditions required to achieve the preset speed of the air move-

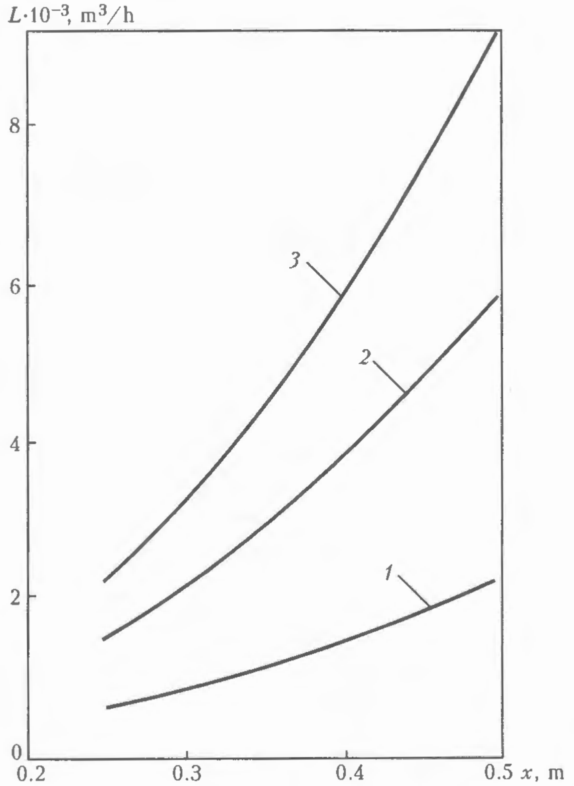

Dependence of required volume L of air removed by local exhaust system from the distance x of intake hole location to welding arc at different speed of air movement in surfacing zone $v_x = 0.2$ (*1*), 0.5 (*2*) and 0.8 (*3*) m/s ment v_x in the zone of welding (surfacing) at a distance of x from the center of the suction hole. For the suctions of the simplest forms with round and square holes without shield [6]

$$v_0 = 16(x/d)^2, \quad (2)$$

where d is the diameter of the round hole or hydraulic diameter for the square hole.

For selection of the optimal parameters of the local exhaust ventilation (speed and consumption of the air to be removed) with different values of x and d, v_0 was determined by (2) and L – by (1). Calculations performed at d = 0.16 and 0.20 m (as assumed in the modern exhaust systems) showed that the diameter of the local exhaust suction does not depend on the air consumption in it. Increase of the distance of the exhaust hole to the surfacing zone (an optimal range of 0.25–0.50 m [1] was selected for calculations) should be provided by the volume of the removed air with observance of the required speed of the air movement (0.8 m/s). Due to the obtained dependence (Figure) the volume of the air removed by the exhaust hole from the distance of its location to the welding arc it is possible to calculate the parameters of the local exhaust ventilation. The obtained dependence allowed determining that the developed new facilities of the local exhaust with production of 2000 and 4000 m^3/h [7] may be effectively employed for flux-cored strip surfacing by locating the intake devices at a distance of 0.25 and 0.35 m from the welding arc. In this case it is possible to provide the required efficiency of the WA trapping without changing the chemical composition and hardness of the deposited metal.

CONCLUSIONS

1. For protection of the production environment from harmful substances formed in surfacing with the flux-cored strips it is recommended to apply local exhaust systems with the productivity from 2000 to 4000 m^3/h, which provide an effective WA trapping at a distance of not more than 0.25–0.35 m from the welding arc.

2. Maximal speed of movement of the air removed from the surfacing zone should be 0.8 m/s.

3. With increase (if need be) of a distance between the intake exhaust device and a zone of surfacing with the flux-cored strip the volume of the removed air should be increased in compliance with the obtained dependence.

1. Levchenko, O.G. (2004) *Occupational hygiene and industrial sanitation in welding production*. Manual. Kyiv: Osnova.
2. (1973) *1009–73*: Sanitary rules in welding, surfacing and cutting of metals. Moscow: Minzdrav SSSR.
3. Grimitlin, M.I., Lifshitz, G.D., Pozin, G.M. (1990) Theoretical principles of calculation of local exhausts in welding production. In: *Proc. of Seminar on Actual Problems of Ventilation and Environmental Safety in Welding Production* (Leningrad, July 5–6, 1990). Leningrad: Znanie.
4. Demchenko, V.F., Levchenko, O.G., Metlitsky, V.A. et al. (2001) Information storage and retrieval system on hygienic characteristics of welding aerosols. *Svarochn. Proizvodstvo*, **8**, 41–45.
5. Himmelblau, D. (1973) *Analysis of processes by statistic methods*. Moscow: Mir.
6. Belov, S.V., Brinza, V.N., Vekshin, B.S. et al. (1985) *Safety of production processes*. Refer. Book. Ed. by S.V. Belov. Moscow: Mashinostroenie.
7. Levchenko, O.G., Agasian, N.Yu. (2004) Current means of local ventilation for welding production. *Svarshchik*, **5**, 40–42.

COMPUTER SYSTEM FOR EVALUATION OF STRENGTH AND LIFE OF PIPELINES WITH EROSION-CORROSION WEAR

The computer system allows evaluation of residual life and strength of pipeline systems on the basis of information about an object, its material, as well as results of examination of its technical condition.

The system can help to improve reliability of objects in operation, reduce equipment costs and extend the overhaul period.

Application. The computer system is intended for evaluation of strength and residual life of power engineering equipment components (pipeline systems for transportation of steam and hot water, heat exchangers, pressure vessels) with local thinning of walls formed as a result of erosion-corrosion wear. It can be applied for evaluation of performance of power engineering equipment operating at enterprises of power generation and other industries.

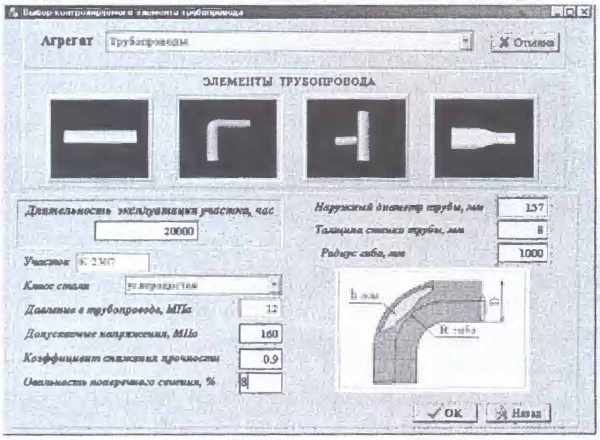

Выбор контролируемого элемента трубопровода

Агрегат: Трубопроводы

ЭЛЕМЕНТЫ ТРУБОПРОВОДА

Длительность эксплуатации участка, час: 20000

Участок: [illegible]

Класс стали: [illegible]

Давление в трубопроводе, МПа: 12

Допускаемые напряжения, МПа: 160

Коэффициент снижения прочности: 0.9

Овальность поперечного сечения, %: 8

Наружный диаметр трубы, мм: 137

Толщина стенки трубы, мм: 8

Радиус гиба, мм: 1000

MONITORING SYSTEM FOR A PIPE-WELDING MILL

F.N. KISILEVSKY, E.V. SHAPOVALOV and E.S. MELNIK
E.O. Paton Electric Welding Institute, NASU, Kiev, Ukraine

Welding process monitoring and control system for a pipe welding mill has been developed. The system consists of three subsystems, namely for control of penetration from the reverse side of the weld pool, control of the pipe weld formation and weld following. Design of these subsystems using a technical vision system, as well as hardware and algorithmic methods for minimizing the effect of optical (blinks and flashes due to the welding arc) and mechanical (scratches, rust, burrs) interferences, are considered. The system provides high real-time measurement accuracy.

Keywords: *arc welding, butt joint, welding process monitoring, technical vision system, automatic control of the welding process, penetration monitoring, following system, weld formation monitoring, reinforcement bead*

Application of a monitoring system in welding fabrication allows producing weldments of a stable quality and reducing the influence of the human factor on the welding process. The main objective of welding process monitoring is formation of a weld with the specified geometrical parameters. The monitoring system consists of the following subsystems: monitoring of the main welding parameters during welding, welding process control, forecasting the welding quality and weld geometry monitoring.

Monitoring the main parameters of the weld, such as current, voltage, welding speed, shielding gas flow rate, does not run into any particular problems, but in most of the cases availability of these parameters is insufficient for a sound performance of the monitoring system. Additional data on the groove depth, gap, edge misalignment, groove shape and position of the butt joint line relative to the torch are often required, a rational way of obtaining these data being the use of technical vision devices (TVD).

Sensory devices, which include the TVD, allow revealing the external disturbances of the welding process, which not only enables forecasting the welding process quality, but also controlling its mode.

Development of the weld following system is the greatest challenge in welding process control. Solution of this problem includes two stages, namely determination of butt joint line position and guiding the welding tool to the butt joint.

Forecasting of the welding process quality can be performed by mathematical simulation. The mathematical model uses as the initial data the same data as for the control subsystem. The simulation problem includes forecasting of the reinforcement bead shape, as well as of the probability of development of defects of the type of burns-through and lacks-of-penetration. Studies of the staff members of Tula State University (Russia) lead by Prof. V.A. Sudnik [1] and of the E.O. Paton Electric Welding Institute [2] are known in this field. The developed mathematical models allow for the thermal, thermodynamic and hydrodynamic processes, proceeding in the weld pool. This work is of a rather theoretical nature, and real-time application is limited in view of the model complexity.

In practice the data on penetration depth from the reverse side of the weld pool obtained with TVD are used for forecasting the welded joint quality [3].

The purpose of this work is consideration of the problems in construction of the system of monitoring the technological process of arc welding for pipe-welding mills.

The E.O. Paton Electric Welding Institute developed a system of welding process monitoring in pipe production, which includes three subsystems, namely penetration control from the reverse side of the weld pool, monitoring of pipe weld formation and butt following.

Subsystem of penetration monitoring from the weld pool reverse side. In this subsystem the area, width and length of the metal liquid phase are used as the monitored parameters. The above parameters allow detecting the possibility of formation of a large number of weld joint defects, namely lacks-of-penetration, burns-through, deviations from the specified geometrical shape. Penetration shape can be determined proceeding from the area of the metal liquid phase from the weld pool reverse side, and the length and with of the metal liquid phase can be used to assess the specific heat input and make a substantiated selection of the welding speed. The above parameters are highly important, as they allow taking into account the ambient temperature influence on the welding process. Weld pool width from the reverse side and penetration depth are monitored by thermocouples built-into the welding zone or by the acoustic emission method. Both these methods are contact methods, which leads to their limited use in practice.

Specialists of the E.O. Paton Electric Welding Institute suggested using the optical method for measurement of the dimensions of the metal liquid phase from the weld pool reverse side. Figure 1 gives the block-diagram of the subsystem of penetration monitoring in welding.

The above method allows evaluation of the weld pool temperature field from inside of the pipe. The sensor consists of the two main parts, namely the probe and video camera. Videocapturing board is designed for conversion of the videosignal into digital signal.

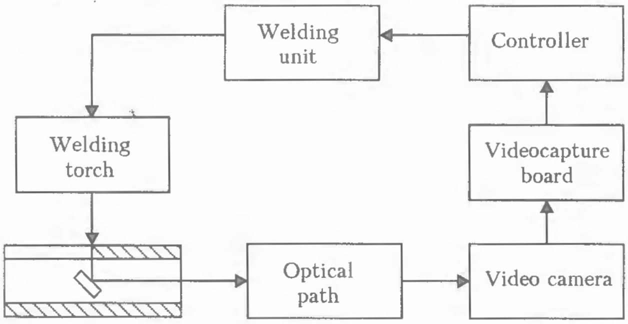

Figure 1. Block-diagram of a subsystem of penetration monitoring in welding

The controller performs real-time videoprocessing which results in determination of «isothermal regions» (Figure 2).

The controller is also used for evaluation of the geometrical parameters (width, length, area) of the region of weld pool image with maximum brightness, which corresponds to the liquid phase. Welding parameters are controlled based on measurement of the weld pool reverse side.

Subsystem for monitoring the pipe weld formation. The most complex task is application of the subsystem for monitoring weld formation in the technological process of tube welding. This is due to the fact that the reinforcement bead formed after welding has a small height (usually less than a millimeter). Application of a precision measurement system in the shop conditions is practically impossible due to vibration. A well-known method of light sections is proposed for monitoring the reinforcement bead width. The TV sensor consists of two blocks, namely optical generator of the light plane and video camera. Light plane is oriented at a certain (triangulation) angle to the axis of video camera vision. At crossing of the light plane with the pipe surface a light band forms, which precisely follows the relief of the surfaces being welded in the zone of weld formation (Figure 3). Video image is transferred to the processing and control block, where the main geometrical parameters of the weld are determined after image filtering.

The developed system is designed for mills for plasma welding of stainless pipes without filler wire (Figure 4). Liquid metal phase forms during plasma welding. Under the conditions of wettability the liquid metal surface conditionally takes on the shape of a plane, distorted by macroroughness, which is the consequence of dynamic processes in the weld pool. The task of video processing includes finding the meeting points (*A* and *B* in Figure 3) of the conditional horizontal plane with the pipe surface, the distance between which corresponds to the reinforcement bead width.

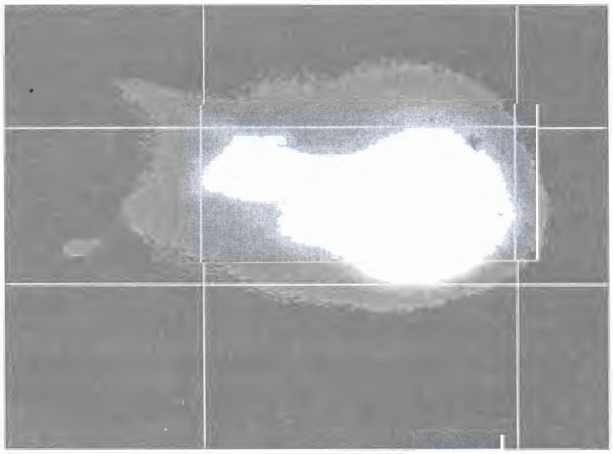

Figure 2. Evaluation of temperature field of weld pool from inside the pipe

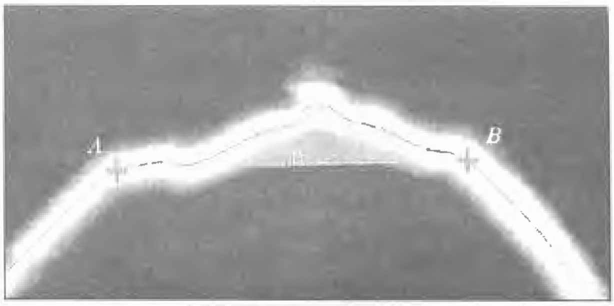

Figure 3. Measurement of reinforcement bead parameters (for explanations *A* and *B* see the text)

The subsystem operates in real time. Working wave length of the light plane optical generator is equal to 630–670 nm. Video camera is fitted with a narrow-band interference and polarization filter, this allowing the influence of the welding arc to be minimized and signal-to-noise ratio to be increased. A feature of the above system is its invariance to different kinds of noise, such as welding spatter, scratches, rust, carbon deposit, burrs, traces of a mill or cutter, arc noise, etc.

Proceeding from the reinforcement bead image, the system automatically determines its area and height, as well as geometrical dimensions of the undercuts.

Butt following subsystem. A following system with feedback was implemented for guiding the welding torch along the butt (Figure 5). Error signal is the difference between the co-ordinates of the butt joint line and welding tool position. Regulator operation is based on a proportional-integral-differential law of control, expressing the directly proportional dependence of the control action value on the sum of

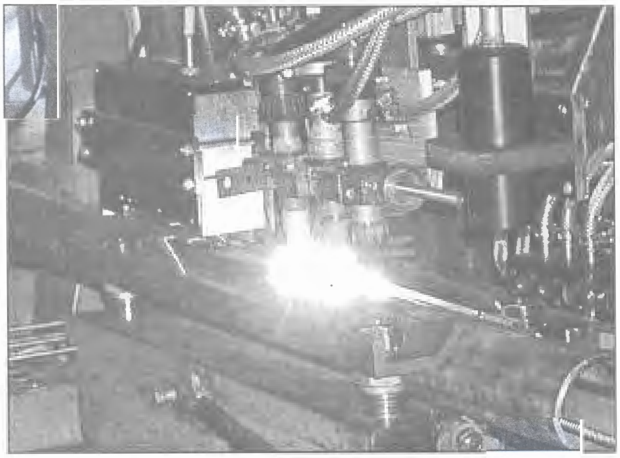

Figure 4. Mock-up of pipe welding mill

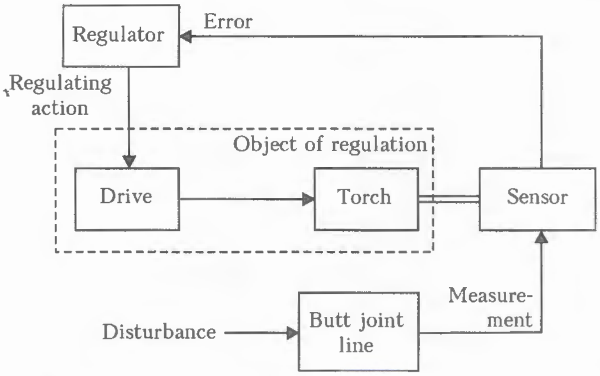

Figure 5. Block-diagram of closed-loop control system

weighted values of deviation, integral and its time derivative.

TVD is used as the feedback sensor for geometrical adaptation. It is based on the TV method of butt following with a gap close to zero [4], based on the light-shade transition appearing at the butt illumination by a diffused light source. The diffused light source is a light-emitting diode (LED) matrix. Uniformity of illumination is achieved due to the LED directional radiation patterns intersecting each other, while the distance from the illuminator to surfaces being welded is much greater than the LED dimensions. The following subsystem incorporates adaptive control of the dissipated light source brightness, depending on the coefficient of illumination of the surfaces being welded. Brightness control is performed using a controller located in the sensor casing. Data exchange between the brightness controller and following system is based on RS 485 interface.

Welding arc is a source of strong optical noise. An interference light filter is used to protect the video camera from optical noise. The light filter working wave length is selected from the following conditions: video camera should have sufficient sensitivity in the wave length range transmitted by interference filter; light radiation of the arc in welding being minimum as far as possible in the working range of the interference light filter.

Spectral characteristics of argon-arc and plasma welding [5] were studied for an intelligent selection of the working range of interference light filters.

The butt illuminated by diffused light, is visible as a narrow dark band in the images. Initial image shown by a massive of numbers to enhance the brightness gradient, is processed by selective matched filtration. Different defects in the form of scratches, rust, scale, mill traces near the butt, are random noise that may lead to considerable errors in determination of the butt co-ordinates. To avoid errors in butt joint detection a mathematical model of detection of the butt joint image was developed, which allows a considerable increase of the probability of finding the butt joint line in images with a high noise level. The model implements a transition from the digital image to object space. Available a priori data are used to take a decision on the object belonging to one of the classes, corresponding to the butt joint or noise (image recognition problem). Objects belonging to the butt joint class are combined into one, and parameters of this object are calculated, and then the object is replaced by an approximating curve (Figures 6 and 7).

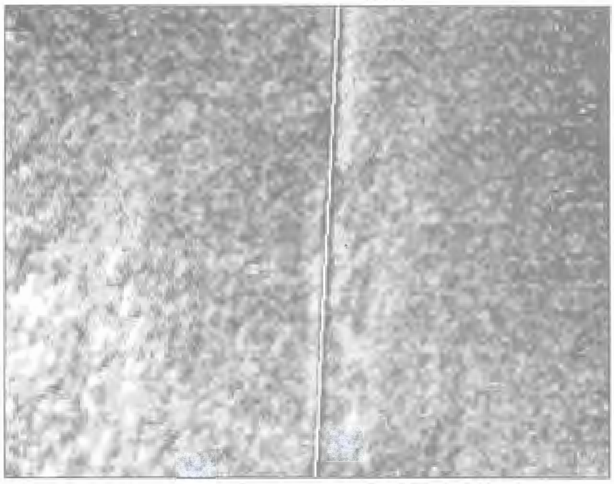

Figure 6. Determination of butt joint line with a gap close to zero

The main advantage of the developed subsystem is a high response (up to 25 frames per second), this allowing following to be performed at the welding speed of up to 100 m/h. As a rule, the butt following systems used in welding fabrication, feature a transport lag. Accumulation of deviations from a specified trajectory occurs in a certain section, located in the video camera field of vision at a given moment. Compensation of the deviations by the welding torch guiding drives is performed with a delay. Delay time is calculated by the following formula:

$$t = \frac{l}{v},$$

where v is the welding speed; l is the distance between the electrode and video camera axis of sight. Therefore, the smaller is l, the higher the accuracy of the following system. The following system is usually positioned so that l values did not exceed 100–150 mm.

In the developed following system it was possible to eliminate the above drawback. If we assume that the trajectory of the butt joint line is rectilinear over distance l, torch deviation from the trajectory can be calculated from the following formula:

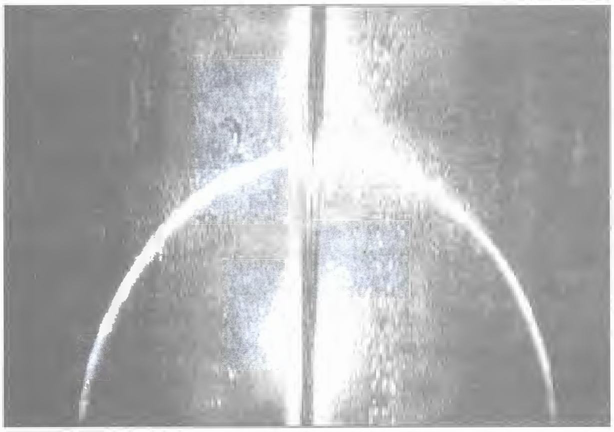

Figure 7. Processing the image of combined TV sensor

$$\Delta = l \operatorname{tg} \alpha + \frac{r}{\cos \alpha},$$

where α is the angle between the approximating curve and straight line, connecting the video camera axis of sight with electrode center; r is the distance from the video camera axis of sight to approximating curve.

This process allows determination of the current deviation of the torch from the butt joint line with 0.1 mm accuracy. For most of the welding processes it is sufficient to guide the welding tool to the butt with the error equal to half of electrode diameter. To avoid the following system transition into an oscillatory mode, limitations on sensitivity to variation of the control object parameters are introduced.

If the technical assignment for the butt following subsystem envisages following the butt joint line by height, the sensor is additionally fitted with light plane optical generator, and the values of the butt height are determined similar to triangulation TVD. The complexity consists in processing the video images (Figure 7), as the dissipated light source creates noise at isolation of the light band. This method was developed by the staff members of the E.O. Paton Electric Welding Institute and is called the combined method.

Experimental verification of the adequacy of the mathematical model of control of arc welding technological process was performed by artificially introducing into the welding mode such disturbances as change of the position and distance to the butt joint line. The control system immediately compensated all the external disturbances, the penetration depth remained constant, and the welding torch center always was above the butt joint line.

Conducted experiments demonstrated the high reliability of the developed automatic system of monitoring the pipe welding mills. The considered systems allow construction of the automatic systems of welding fabrication control and automation of fabrication of welded structures of different classes in the most optimum manner.

1. Sudnik, V.A., Rybakov, A.S., Zajtsev, O.I. (2004) Software and hardware TIGSIM for analysis of TIG welding process. In: *Proc. of 4th All-Union Sci.-Techn. Conf. on Computer Technologies in Joining of Materials* (Tula, 2004). http://comhighech.tsu.tula.ru/weldsim
2. (1986) *Mathematical methods in welding of AS of the Ukr. SSR*. Kiev: PWI.
3. Chen, S.B., Lou, Y.J., Wu, L. et al. (2000) Intelligent method for sensing, modeling and control of pulsed GTAW. Part 1: Bead-on-plate welding. *Welding J.*, **7**, 151–163.
4. Kisilevsky, F.N., Butakov, G.A., Dolinenko, V.V. et al. (2003) Optic sensor for butt following in gap sizes close to zero. *The Paton Welding J.*, **2**, 48–50.
5. Kisilevsky, F.N., Shapovalov, E.V. (2003) Determination of optimum length of an illuminator in technical vision systems for arc welding. *Ibid.*, **8**, 51–53.

RECONDITIONING OF LARGE-SIZED PARTS FOR EQUIPMENT OF ORE MINING AND PROCESSING COMPLEXES BY THE MECHANIZED ARC SURFACING

Yu.M. KUSKOV[1], **V.A. LEBEDEV**[1], **I.A. RYABTSEV**[1], **A.I. PODDUBSKY**[2] and **R.V. SHAPRAN**[2]
[1]E.O. Paton Electric Welding Institute, NASU, Kiev, Ukraine
[2]Company «Alians-Grup», Krovoj Rog, Ukraine

Methods for reconditioning of large-size parts of mining equipment by mechanised arc surfacing are considered. The possibility of an efficient application of semi-automatic surfacing using self-shielding flux-cored wires for the above purposes is shown by an example of treatment of a crushing cone shaft.

Keywords: *arc surfacing, flux-cored wire, semi-automatic surfacing machine, surfacing technology*

Modern ore mining and processing complexes are equipped with powerful crushing equipment processing annually several million tons of ore. Such equipment particularly includes cone-type crushers for coarse crushing of KKD 1500/180 type and the reduction crusher for secondary coarse crushing of KRD 900/100, KRD 700/100 types and others. They are intended for processing (grinding) of ore produced by the open explosion mining of lumps 400–1200 mm in size. The appearance of reduction crusher is shown in Figure 1. The working surfaces of the crusher parts (cross members, crushing cones, bowls, frames) are exposed mainly to abrasive and impact-abrasive wear in the course of operation.

Replaceable armor linings usually produced from steel 110G13L are used for protection of the most loaded and worn surfaces. Service life of crushes is several decades. For this period of time not only working parts are worn out but also less loaded parts, for example crushing cone shafts. The crushing cone is not in the direct contact with ore being crushed. The wear (to 10–12 mm) proceeds in the zone of contact of the upper cylindrical part of the shaft with the bronze sleeve when dust with increased abrasive properties finds its way into the clearance between them. A part of the shaft with the buttress thread on which

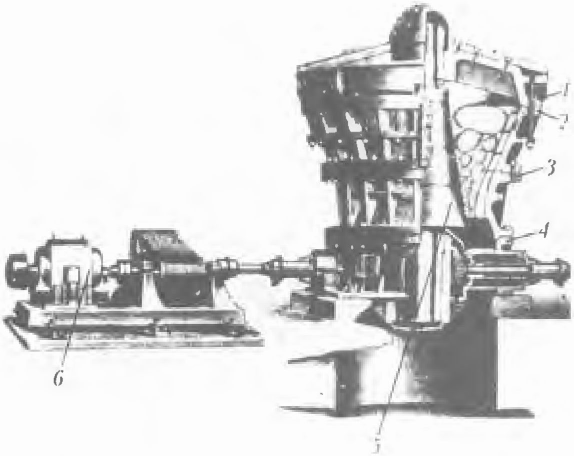

Figure 1. Appearance of reduction crusher: *1* — upper ring of bowl with cross-member; *2, 3* — upper and lower rings of the middle part of bowl, respectively; *4* — frame; *5* — cone; *6* — electric drive

the cone is suspended also fails in operation. The fatigue processes lead to the split-off of separate turns of the thread or local failure of some of its turns. Visual inspection often does not allow detecting the fatigue defects, however under the action of the surfacing thermal cycle they may form and transfer to the deposited metal.

This work features the experience of reconditioning of the worn surfaces of the crushing cone shaft and particular turns of the buttress thread by the mechanized arc surfacing using self-shielded electrode wires. Crusher shafts subject to reconditioning are produced from medium-carbon steels of 40 type or low-alloyed steels of 34KhNM type, which fall under the category of limitedly weldable. For this reason the attempts to restore such parts by the manual arc deposition especially without preheating lead to initiation of cracks in the deposited metal. As it was already mentioned, crack is not permissible in the part operating in the complex stressed condition. It is especially relevant for the part of the cone shaft with the buttress thread, which is a bearing member designed to stand considerable variable loads.

Surfacing technology is developed and equipment for reconditioning of the cylindrical part of the shaft and the buttress thread is selected regarding peculiarities of operation of the crushing cones, weldability of the materials for their production and duration of the surfacing works.

Before surfacing the parts to be restored were exposed to ultrasonic control. In case of fatigue cracks, the latter should be removed by means of machining with abrasive wheels. These works together with machining of the deposited shaft surfaces and the buttress thread were carried out by means of the device fixed directly to the cone. This device was designed and produced at the «Alians Grup» Company (Figure 2). Special cutters allowing long-term and reliable treatment of the deposited sites of the shaft are used for machining.

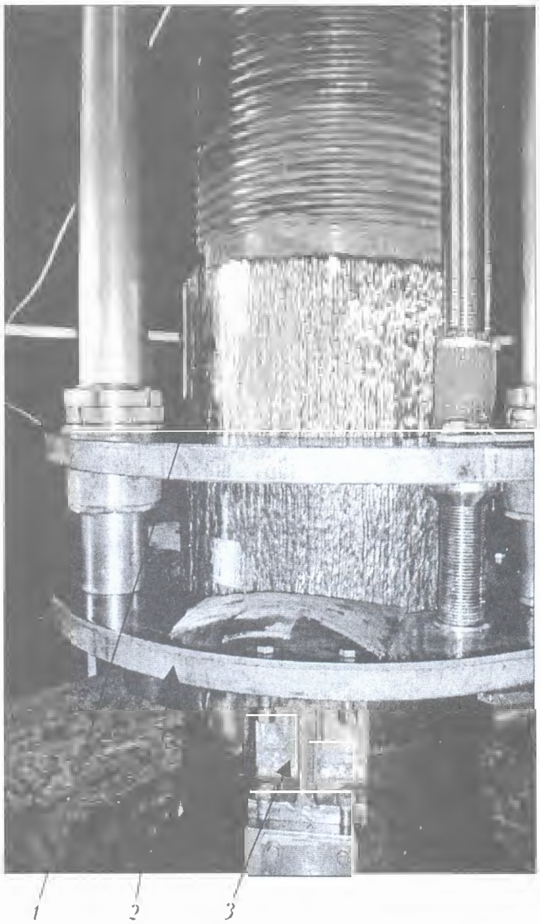

Figure 2. Device for machining of deposited surfaces of cone shaft: *1* — crushing cone shaft; *2* — chuck; *3* — cutter holder

To carry out a cycle of technological operations on reconditioning of the shaft the cone is placed vertically into technological pot-hole used for assembling-dissembling of cones. Operating platform for surfacing workers is mounted around the shaft sites to be reconditioned (Figure 3). The surface to be reconditioned is heated before surfacing by the gas torch of large power. Several torches combined into a single structure are used simultaneously to increase the productivity of the process. Temperature of preheating of the shaft depends on the material from which it is produced.

Self-shielded flux-cored wires of PP-AN198 and PP-AN202 grades developed at the E.O. Paton Elec-

Mechanical properties of deposited metal

Flux-cored wire grade	Yield point $\sigma_{0.2}$, MPa	Tensile strength σ_t, MPa	Relative elongation δ_5, %	Reduction in area ψ, %	Impact toughness *KCU*, J/cm^2
PP-AN198	385	590	24.5	21.8	40
PP-AN202	433	667	18.5	22.1	25

Figure 3. Site for reconditioning of the cone shafts: *1* — cone before reconditioning; *2* — platform for surfacing; *3* — semi-automatic machine PSh 107V; *4* — cone after reconditioning of the shaft

tric Welding Institute were used for surfacing. These wires provide producing the deposited metal with high mechanical properties (Table).

Semi-automatic arc surfacing allowed increasing the labor productivity 1.5–2 times on the average as compared to the manual arc surfacing. In this case the formation of the deposited bead considerably improved, which facilitated and accelerated the machining of the deposited surfaces. Hardness of the deposited metal was not more than *HRC* 30, which provided its easy machining. After machining the quality of the deposited metal was determined by the ultrasonic control method, then the metallic rolls were used for knurling of the deposited surface.

Surfacing technology employed for reconditioning of the shafts specifies the following requirements to the semi-automatic machines:

- duty cycle of the semi-automatic machine is 100 %, which excludes or decrease a probability for drop of the temperature for preheating of the shaft being surfaced;
- provision of the stability of arc starting and arcing in different spatial positions;
- guarantee of a high level of reliability and repairability;

Figure 4. Surfacing of shaft with semi-automatic machine PSh 107V; *1* — unit for autonomous power supply; *2* — semi-automatic machine; *3* — deposited surface of crushing cone shaft

- possibility to work both in the indoor shop conditions and in the outdoor sites with a sharp ambient temperature differential.

The unit-module semi-automatic machine PSh 107V developed at the E.O. Paton Electric Welding Institute most of all meets these requirements [1]. Semi-automatic machines of this type have feedbacks stabilizing the rotation frequency of the electric drive motor shaft (feed rate of electrode wire) and technological process of surfacing. In this case it is also possible to establish different correlations in the action of the feedbacks [2].

The semi-automatic machines of PSh 107V type are adapted to continuous operating due to reinforcing of some components of the structure (roll unit for wire feed, current-carrying tips, power supply and control units). Welding source is selected with the required storage of the power.

The modernized semi-automatic machines PSh 107V provides a considerable increase of the surfacing productivity and higher quality of the deposited metal as compared to the manual surfacing or surfacing by the semi-automatic machines of other types. Surfacing of the crushing cone shaft by the semi-automatic machine PSh 107V on the working site and the appearance of the deposited surface are shown in Figure 4.

Currently the developed technology has been used for reconditioning of some crushing cone shafts. Some of them are successfully operating on the ore mining and processing complexes in Krivoj Rog, Ukraine. Cost of reconditioning of shafts did not exceed 30 % of the value of new crushing cones, while the service life of the reconditioned shafts was not smaller than the standard service life of new articles.

1. Lebedev, V.A., Moshkin, V.F., Pichak, V.G. (1998) Semi-automatic machines of block-module design for welding, surfacing and cutting. *Svarochn. Proizvodstvo*, **1**, 24–28.
2. Lebedev, V.A., Pichak, V.G. (1998) Semi-automatic machines of PSh 107 type for welding and surfacing. *Avtomatich. Svarka*, 7, 38–42.

FORTHCOMING BOOK INFORMATION

Vladimir I. Makhnenko, Viktor E. Pochynok. STRENGTH CALCULATION OF WELDED JOINTS WITH CRACK-LIKE IMPERFECTIONS.

Approx. 300 pp., 165×235 mm, hardback. November 2005. US$ 90

In this manuscript, the idea of the fitness-for-purpose concept is used to improve strength calculations of welded joints with crack-like imperfections caused by structural or technological factors. These include welded joints with fillet, spot, slot and butt welds having sharp fissures brought by geometry of the elements welded and limited sizes of the weld sections. Such joints are widely encountered in modern general-purpose welded structures used in civil building, shipbuilding, automobile industries, etc.

The welded joints just mentioned do not usually cause problems for structures of relatively ductile materials with small-to-medium thicknesses of component sections, and operating under predominantly static loading. However, the use of new structural materials, especially high-strength steels and aluminum alloys, etc., large cross sections of structural elements, and loading with alternate loads, requires a certain caution to be taken. Nonetheless, the technological advantages that these joints produce attract an interest in their use, of course, when it does not cause any harm to the structure safety and its residual service life.

Performing strength calculations based on the fitness-for-purpose criterion for the joints encountered in general-purpose structures, allows ensuring the requirements concerning the service life-time. However, there is a difficulty of implementing such calculations in wide engineering practice. As shown by the authors, a successful implementation of the mentioned concept for general-purpose welded joints and for wide range of users is possible only when it is based on the use of corresponding computer systems with friendly user interface, which do not require a user to have a special knowledge in fracture mechanics, deformation mechanics, numerical methods, etc. Such systems are to be portable and efficient, i.e. calculations of appropriate section sizes or verification of strength of specific joints should be done promptly. In turn, it requires development of numerical procedures and creation of specialized databases that simplify and accelerate calculations.

Viktor Ya. Kononenko. TECHNOLOGIES OF UNDERWATER WET WELDING AND CUTTING.

Approx. 140 pp., 140×200 mm, softback. December 2005. US$ 40

The book deals with the features of arcing, metal transfer and joint formation in consumable-electrode wet underwater welding. Principles of development of coated electrodes and self-shielded flux-cored wires for underwater welding and cutting are established. Characteristics of welding consumables and mechanical properties of weld metal are given. Some types of joints, procedure of preparation and fit-up for welding, possible defects of the joints and methods to prevent their formation are described.

Information on characteristic damage to the underwater metal structures is generalized, and technological solutions are given, which have been implemented during restoration of their performance, using wet processes of underwater welding and cutting. The book gives the characteristics of the equipment for implementation of underwater arc welding process.

The main processes of thermal underwater cutting are presented, and characteristics of consumable materials and equipment for its implementation are described. Examples of work performance using underwater cutting are given.

The book is designed for scientific and engineering-technical personnel, qualified welders-divers involved in design, fabrication and repair of underwater constructions.

The book is written by a specialist, who is developing electrode materials and technologies and has a vast experience of practical work under the water.

ADVANCE BOOK INFORMATION

TITANIUM: Titanium and its alloys. Technologies. Equipment. Production. Electrometallurgy. Welding

Approx. 180 pp., 200×290 mm, softback. December 2005. US$ 50

The collection presents papers on electrometallurgy and welding of titanium and its alloys published between 2002 and 2005 in «Advances in Electrometallurgy» and «The Paton Welding Journal» journals. The authors of the papers are scientists and specialists in the field of titanium and its production, known in Ukraine and abroad. The collection is designed for a broad range of readers dealing with the problems of production, processing and use of titanium.

ORDER RORM

Please return to:

International Association «Welding»,
11, Bozhenko str., Kiev, 03680, Ukraine
Tel.: (38044) 287 6757, 287 6049, 529 2623
Fax: (38044) 287 4677
E-mail: journal@paton.kiev.ua; tomik@mac.relc.com

Please send me:

☐ Vladimir I. Makhnenko, Viktor E. Pochynok «Strength Calculation of Welded Joints with Crack-Like Imperfections».
US$ 90, postage included

☐ Viktor Ya. Kononenko «Technologies of Underwater Wet Welding and Cutting».
US$ 40, postage included

☐ «Titanium». Collection of Scientific Paper.
US$ 50, postage included

How to Pay and Payment Details

☐ By bank transfer (or mail a cheque) into our account
№ 2600801283433
UKREXIMBANK, Kiev, Ukraine
S.W.I.F.T.: EXBSUAUX
CORR. ACC. #04-094-227
Bankers Trust Company,
New York, U.S.A.
S.W.I.F.T.: BKTR US 33

☐ Please Invoice

☐ Your Details
Name ____________________

Organization ____________________

Address ____________________

Signed ____________________ Date ____________________